CAPITAL UNIVERSITY OF SCIENCE AND TECHNOLOGY, ISLAMABAD

An Investigation of a Chemically Reactive Maxwell Viscous Hybrid Nanofluid Flow over a Porous Stretching Surface

by

Asma Shafiq

A thesis submitted in partial fulfillment for the degree of Master of Philosophy

in the

Faculty of Computing
Department of Mathematics

2025

*I dedicate this thesis to my beloved **parents** and **husband**, whose unconditional love, steadfast support, and belief in my potential have been the foundation of my academic journey. The constant support, sacrifices, and motivation from those in my life have inspired me to pursue a path of excellence. I am truly appreciative of the values and insights they have provided, which have greatly contributed to the development of my character and aspirations. This composition is a recognition of their dedicated service and the substantial role they have played in shaping my life. I consider myself fortunate to have remarkable parents and a supportive husband who have consistently provided me with persistent attention and support.*

CERTIFICATE OF APPROVAL

An Investigation of a Chemically Reactive Maxwell Viscous Hybrid Nanofluid Flow over a Porous Stretching Surface

by

Asma Shafiq

(MMT233012)

THESIS EXAMINING COMMITTEE

S No	Examiner	Name	Organization
(a)	External Examiner	Dr. Maryiam Javed	IST, Islamabad
(b)	Internal Examiner	Dr. M. Sabeel Khan	CUST, Islamabad
(c)	Supervisor	Dr. Muhammad Sagheer	CUST, Islamabad

Dr. Muhammad Sagheer
Thesis Supervisor
April, 2025

Dr. Muhammad Sagheer
Head
Department of Mathematics
April, 2025

Dr. M. Abdul Qadir
Dean
Faculty of Computing
April, 2025

Author's Declaration

I, **Asma Shafiq** hereby state that my MPhil thesis titled "**An Investigation of a Chemically Reactive Maxwell Viscous Hybrid Nanofluid Flow over a Porous Stretching Surface**" is my own work and has not been submitted previously by me for taking any degree from Capital University of Science and Technology, Islamabad or anywhere else in the country/abroad.

At any time if my statement is found to be incorrect even after my graduation, the University has the right to withdraw my MPhil Degree.

Asma Shafiq

Registration No: MMT233012

Plagiarism Undertaking

I solemnly declare that research work presented in this thesis titled "**An Investigation of a Chemically Reactive Maxwell Viscous Hybrid Nanofluid Flow over a Porous Stretching Surface**" is solely my research work with no significant contribution from any other person. Small contribution/help wherever taken has been duly acknowledged and that complete thesis has been written by me.

I understand the zero tolerance policy of the HEC and Capital University of Science and Technology towards plagiarism. Therefore, I as an author of the above titled thesis declare that no portion of my thesis has been plagiarized and any material used as reference is properly referred/cited.

I undertake that if I am found guilty of any formal plagiarism in the above titled thesis even after award of MPhil Degree, the University reserves the right to withdraw/revoke my MPhil degree and that HEC and the University have the right to publish my name on the HEC/University website on which names of students are placed who submitted plagiarized work.

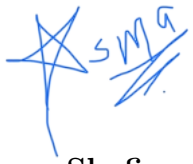

Asma Shafiq

Registration No: MMT233012

Acknowledgement

I am deeply thankful and appreciative of all those who have supported the successful completion of this thesis.

I wish to extend my heartfelt thanks to my supervisor, **Dr. Muhammad Sagheer**, for his unwavering support, encouragement, and guidance throughout the entirety of this research project. His knowledge and insightful contributions have played a crucial role in guiding the focus and enhancing the quality of this work.

I would like to convey my sincere appreciation to my **parents** and **husband**, whose endless love and support have formed the foundation of my academic pursuits. Their steadfast faith in my abilities has been a significant motivator for my accomplishments, and I am eternally thankful for their guidance and insight.

I am also sincerely thankful to my **siblings**, **in-laws** and **friends** for their constant affection, encouragement and confidence in my abilities. The unwavering support and comprehension they have provided is a vital source of strength throughout the difficult phases of this academic journey. The encouragement and sacrifices offered by them have been essential in keeping my motivation and focus intact.

In summary, the successful completion of this thesis is attributable to the collaborative contributions of all those as mentioned above.

Asma Shafiq

Registration No: MMT233012

Abstract

This research has contributed significantly to the understanding of hybrid nanofluid dynamics in the context of a stretching or shrinking sheet, particularly under the influence of a constant magnetic field and the processes of suction and injection. The focus of this investigation is a two-dimensional steady boundary layer flow problem, which incorporates the Maxwell and Cattaneo-Christov heat flux models. This study also incorporates some crucial physical processes such as thermophoresis, thermal slip, Brownian motion, porous medium, chemical reactions, heat source, Joule heating and viscous dissipation. Similarity transformations have been utilized to transform the nonlinear partial differential equations into a corresponding set of ordinary differential equations. Afterwards, the numerical technique, the shooting method, effectively managed to solve the system of ordinary differential equations. Tables and graphs are included to demonstrate how various parameters substantially influence the velocity, temperature, and concentration profiles, along with their respective rates of change. Notably, the higher magnetic field contributes to an increase in the temperature distribution and decrease in the velocity profile. An increase in the Maxwell parameter is observed to decrease the velocity profile. Furthermore, by increasing the Cattaneo-Christov heat flux parameter leads to an elevation in the temperature profile. The concentration profile is found to increase with the amplification of Brownian motion and chemical reaction parameter.

Contents

List of Figures

List of Tables

Abbreviations

BCs	Boundary conditions
hnf	Hybrid nanofluid
IVPs	Initial value problems
MHD	Magnetohydrodynamics
nf	Nanofluid
ODEs	Ordinary differential equations
PDEs	Partial differential equations
RK-4	Runge-Kutta method of order four

Symbols

u, v	Velocity components
v_0	Suction velocity
μ	Viscosity
ν	Kinematic viscosity
ρ	Density
M	Magnetic field parameter
B_0	Magnetic field strength
S	Suction/injection parameter
T	Temperature of nanoparticles
γ	Thermal slip parameter
A	Spatial slip constant
K	Thermal conductivity
$\rho\, c_p$	Heat capacity
T_w	Wall constant temperature
T_∞	Ambient temperature of fluid
C	Concentration
C_w	Nanoparticles concentration at the stretching surface
C_∞	Ambient concentration
q_r	Radiative heat flux
σ^*	Stefan Boltzmann constant
k^*	Absorption coefficient
η	Similarity variable
$f(\eta)$	Dimensionless velocity
$\theta(\eta)$	Dimensionless temperature

$\phi(\eta)$	Dimensionless concentration
Q	Heat source
K_1	Porosity parameter
h_f	Cofficient of heat transfer
δ	Cattaneo-Christov parameter
β	Maxwell's parameter
Pr	Prandtl number
Ec	Eckert number
Q_0	Heat source
D_B	Brownian motion
D_T	Thermophoresis diffusion coefficient
Nb	Brownian motion parameter
Nt	Thermophoresis motion parameter
Γ	Chemical reaction parameter
Le	Lewis number
Re	Reynolds number
Re_x	Local Reynolds number
Cf	Skin friction coefficient
Nu	Nusselt number
Sh_x	Local Sherwood number
Nu_x	Local Nusselt number

Subscripts

p	Nanoparticle
nf	Nanofluid
hnf	Hybrid nanofluid

Chapter 1

Introduction

In this chapter, the literature relevant to the current study is discussed briefly. The chapter is concluded with the layout of the thesis.

1.1 Background

The exploration of Joule heating and Viscous-Enhanced convection concerning flow formation and heat transfer has attracted considerable attention from the research community, primarily due to its advantageous applications in the development of electric ovens, electric heaters, and other high-temperature apparatus. The theoretical framework established by Brinkman [1] is regarded as the earliest investigation of heat resulting from viscous dissipation. Viscous dissipation is a fundamental factor influencing convective heat transfer, particularly in situations involving high-velocity flows, high fluid viscosities, and specific ranges of Prandtl number.

Joule heating, or Ohmic heating, refers to the generation of heat due to resistance when an electric current is conducted through a material. Tassaddiq et al. [2] analyzed the couple stress magneto-hydrodynamic nanofluid thin film flow over an exponentially stretching sheet, addressing the implications of Joule heating and viscous dissipation in their study. Meanwhile, Kumar [3] examines the interplay

between melting heat transfer and viscous dissipation in the context of magnetohydrodynamic (MHD) hybrid nanofluid flow. Recently, Asghar et al. [4] introduced a mixed convection heat transfer model that incorporates slip conditions along with mechanisms for heat generation and absorption. Numerous additional studies have also played a role in examining this model across various contexts, as cited in the referenced articles, Zafar et al. [5], Ouyang et al. [6], Ullah et al. [7] and Khedher et al. [8].

Choi and Eastman [9] coined the term "nanofluids" to describe fluids that consist of nanoparticles, that are measured to be less than 100 nanometers in diameter, dispersed in conventional fluids to augment their heat transfer efficiency. In his work, Buongiorno [10] developed a non-homogeneous equilibrium model, which highlights the influence of Brownian motion and thermophoretic diffusion on the enhancement of heat transfer. According to Tiwari and Das [11], a number of essential models and applications have been established for the exploration of nanofluids. Hayat et al. [12] conducted an indepth analysis of flow and heat transfer characteristics in a nanofluid composed of carbon nanotubes and water, specifically focusing on its behavior over a thin, moving needle. Karim et al. [13] performed a numerical simulation to analyze the flow behavior in a tall permeable cavity featuring two walls that are partially cooled. The primary objective of nanofluids is to attain maximum thermal conductivity with the minimal concentration of nanoparticles.

The use of hybrid nanofluids is an emerging concept that has recently captured the attention of researchers. A hybrid nanofluid can be described as a uniform mixture of two or more types of nanoparticles, which creates new and unique physical and chemical bonding phenomena. The main concept behind hybrid nanofluids is to realize a significant enhancement in thermophysical, hydrodynamic, and heat transfer characteristics in comparison to the mono nanofluids. Numerous experimental research studies have been presented focusing on the concept of hybrid nanofluids. In an experimental study, Momin [14] explored mixed convection with the hybrid nanofluid Al_2O_3–Cu/H_2O, specifically targeting laminar flow within an inclined tube. Sidik et al. [15] highlighted some crucial applications of hybrid nanofluids. Meanwhile, Waini et al. [16] analyzed an unsteady flow and heat

transfer dynamics of a hybrid nanofluid through a sheet that experiences either stretching or shrinking. Mahabaleshwar et al. [17] explores the flow dynamics of hybrid nanofluids in relation to a stretching or shrinking sheet, considering the significant factors of thermal radiation and mass transpiration in the process. The equations obtained were addressed through the shooting method in conjunction with the Runge-Kutta fourth order (RK-4) technique. Likewise further explore the diverse functionalities and behaviors of hybrid nanofluids [18–21].

The review of existing literature indicates that a considerable number of research studies have been carried out on the dynamics of flows through porous medium. One can define porous medium as a material that contain a series of interconnected pores, which are occupied by fluids that may be in liquid or gaseous states. Intergranular and intercrystalline porosities exemplify the concept, characterized by their distinct molecular and cavern interstices. Al-Hadhrami et al. [22] suggest a novel model for viscous-enhanced convection in porous medium. Bhukta et al. [23] conducted an investigation into the mass and heat transfer mechanisms present in the magnetohydrodynamic viscoelastic fluid flow through porous media over a shrinking sheet. Sheikholeslami et al. [24] examined the properties of nanofluids in porous media, with a specific focus on the implications of magnetohydrodynamic transport.

The properties of elasticity and viscosity are inherent in Maxwell fluids. Jordan et al. [25] analyzed Stokes' first problem within the framework of Maxwell fluids, achieving the formulation of new exact solutions. Prominent studies on Maxwell fluids involve the contributions of several key researchers Zierep and Fetecau [26], Jamil et al. [27], Sohail et al. [28], Vieru and Zafar [29].

The process of heat transfer is a natural occurrence that results from the temperature fluctuations within the system. Fourier introduced the widely recognized law of heat conduction, which offers a framework for analyzing heat transfer processes. Cattaneo [30] suggested a modified interpretation of Fourier's law that includes the element of relaxation time. Cattaneo proposed a new model because Fourier's law has limitations, e.g it has a limitless rate of heat transfer. Following this, Christov [31] enhanced the Cattaneo model by integrating Oldroyd's upper convected derivative, which allowed for the retention of frame-indifferent formulations. The

Cattaneo-Christov model has been the focus of many of the recent research, works having applications in multiple fluid flow environments. Numerous researchers are engaged in the investigation of this model across various contexts, as cited in the referenced articles [32–35].

A detailed literature review reveals that a combination of Maxwall's parameter, Cattaneo–Christov heat flux model, heat source, chemical reactions, thermophoresis parameter, Brownian motion and porosity medium in the research of hybrid nanofluids incorporating the concentration profile has not been explored, yet. The purpose of this research is to tackle this deficiency, providing innovative and valuable insights that enrich the current body of knowledge in the field. In this study, similarity transformations are employed to transform non-linear partial differential equations (PDEs) into the dimensionless ordinary differential equations (ODEs), while the shooting method is applied in order to derive the results. Numerical findings are obtained and subsequently visualized in graphical format using MATLAB. The tables and graphs provide a clear representation of how significant parameters affect the velocity $f'(\eta)$, temperature $\theta(\eta)$, and concentration profile $\phi(\eta)$.

1.2 Thesis Structure

Chapter 1 describes the literature relevant to the current study.

Chapter 2 acts as an introductory framework for the thesis, delineating important definitions and terminologies that are essential for a thorough understanding of the concepts that will be addressed in the chapters that follow. This chapter is designed to establish a core understanding of the significant terms and concepts that will be applied in the thesis.

In **Chapter 3**, a detailed numerical investigation is conducted based on the effects of Joule heating and viscous dissipation on the heat transfer characteristics of a hybrid nanofluid with thermal slip, as it interacts with a stretching or shrinking sheet within the Cartesian coordinate framework of x and y. The designed numerical model incorporates the principles of heat and mass transfer that take place on the stretching or shrinking sheet. To achieve the numerical outcomes or results

of the governing flow equations, the shooting method is applied. This chapter explores the characteristics of fluid flow and the performance of heat transfer in $TiO_2 - Fe_3O_4/H_2O$ hybrid nanofluid under different operational conditions.

Following the model outlined in **Chapter 3**, **Chapter 4** further explores the topic by examining a water-based hybrid nanofluid consisting of TiO_2 and Fe_3O_4. This chapter presents an examination of the affect of Maxwell's parameter and the porosity medium parameter on the momentum equation, while also considering some additional factors such as the Cattaneo–Christov heat flux and the heat source parameter within the energy equation of the proposed model. Moreover, the proposed model features the concentration equation of the hybrid nanofluid, which accounts for the Brownian motion, the thermophoresis parameter, and the influence of chemical reactions. Similarity transformations are utilized to transform the partial differential equations (PDEs) into a system of ordinary differential equations (ODEs), which are then addressed through numerical methods.

In **Chapter 5**, a concluding discussion is conducted, highlighting the major findings that have been revealed through the research conducted in this thesis. The main goal of this chapter is to present a thorough synthesis of the key results and contributions of the research.

The section titled **Bibliography** comprises a thorough compilation of all references and sources that have been utilized throughout the thesis.

Chapter 2

Preliminaries

In this chapter, we will elucidate fundamental definitions, essential laws, terminologies and key concepts necessary for the analysis of the partial and ordinary differential equations governing the flow problem. These foundational elements are crucial for comprehending the subsequent chapters of this thesis and will provide a solid framework for the development of a comprehending understanding.

2.1 Foundational Concepts

2.1.1 Fluid

"A fluid is a substance which deforms continuously when subjected to external shearing force." [36]
A fluid posseses the following properties:

- It is shapeless in nature, conforming to the dimensions of the vessel that encases it.
- A liquid or fluid will undergo deformation when subjected to a shear force, with the deformation continuing for the duration of the applied force.

2.1.2 Fluid Mechanics

"Fluid mechanics is that branch of science which deals with the behavior of fluid (liquids or gases) at rest as well as in motion." [37]

2.1.3 Fluid Dynamics

"Fluid dynamics is the study of motion of liquids, gases and plasma from one place to another." [37]

2.1.4 Viscosity

"Viscosity is defined as the property of fluid which offers resistance to the movement of one layer of fluids over another adjacent layer.
Mathematically,

$$\tau \propto \frac{du}{dy} \quad \text{or} \quad \tau = \mu \frac{du}{dy}$$

where μ is a viscosity coefficient, τ is a shear stress and $\frac{\partial u}{\partial y}$ represents the velocity gradient or rate of shear strain." [37]

2.1.5 Kinematic Viscosity

"Kinematic viscosity is defined as the ratio between the dynamic viscosity and density of fluid. It is denoted by the Greek symbol ν, thus mathematically,

$$\nu = \frac{viscosity}{density} = \frac{\mu}{\rho}$$

where the unit of kinematic viscosity is m^2/sec ." [37]

2.2 Classification of Fluid

2.2.1 Ideal Fluid

"A fluid which is incompressible and has no viscosity is known as an ideal fluid. Ideal fluid is only an imaginary fluid as all the fluids, which exists, have some viscosity." [37]

2.2.2 Real Fluid

"A fluid, which possesses viscosity, is known as a real fluid. All the fluids, in actual practice, are real fluid." [37]

2.2.3 Newtonian Fluid

"A real fluid, in which shear stress is directly proportional to the rate of shear strain (or viscosity gradient), is known as a Newtonian fluid." [37]

2.2.4 Non-Newtonian Fluid

"A real fluid, in which shear stress is proportional to the rate of shear strain (or viscosity gradient), is known as a Non-Newtonian fluid." [37]

2.2.5 Ideal Plastic Fluid

"A real fluid, in which shear stress is more than the yield value and shear stress is proportional to the rate of shear strain (or viscosity gradient), is known as ideal plastic fluid." [37]

2.3 Modes of Heat Transfer

2.3.1 Conduction

"The mechanism of heat transfer due to a temperature gradient in a stationary medium is called conduction. The medium may solid or a fluid. The Fourier heat conduction law states that the heat flow is proportional to the temperature gradient." [38]

Common examples of heat conduction include the ironing process, melting of chocolate in one's hand and the heating of a metal spoon when dipped into hot tea.

2.3.2 Convection

"The mode by which heat is transferred between a solid surface and the adjacent fluid in motion when there is a temperature difference between the two, is known as convection heat transfer. The temperature of the fluid stream refers either to its bulk or free stream temperature." [38]

Convection is exemplified by the boiling of water, a process in which heat energy

is transferred through the circulation of water molecules.

2.3.3 Forced Convection

"In forced convection, the fluid is forced to flow over a solid surface by external means such as fan, pump or atmospheric wind." [38]

2.3.4 Free Convection

"When the fluid motion is caused by buoyancy forces that are induced by density differences due to the variation in temperature or species concentration (in case of multicomponent systems) in the fluid, the convection is called natural (or free) convection." [38]

2.3.5 Radiation

"Any substance at a finite temperature emits energy in the form of electromagnetic waves in all directions and at all wavelengths (from a very low one to a very high one). The energy emitted within a specific band of wavelength $(0.1 - 100\mu m)$ is termed as thermal radiation." [38]
Examples of electromagnetic radiation include microwave energy emitted by ovens, X-rays produced by X-ray tubes and ultraviolet radiation from the sun.

2.4 Different Flow Classifications

2.4.1 Steady and Unsteady Flows

"Steady flow is defined as that type of flow in which the fluid characteristics like velocity, pressure, density etc, at a point do not change with time. Thus for steady flow, mathematically we have:

$$\left(\frac{\partial V}{\partial t}\right)_{(x_0,y_0,z_0)} = 0, \quad \left(\frac{\partial p}{\partial t}\right)_{(x_0,y_0,z_0)} = 0, \quad \left(\frac{\partial \rho}{\partial t}\right)_{(x_0,y_0,z_0)} = 0,$$

where (x_0, y_0, z_0) is fixed point in fluid field." [36]
"Unsteady flow is that type of flow, in which the velocity, pressure, density etc, at a point changes with respect to time. Thus for unsteady flow, mathematically we

have:

$$\left(\frac{\partial V}{\partial t}\right)_{(x_0,y_0,z_0)} \neq 0, \quad \left(\frac{\partial p}{\partial t}\right)_{(x_0,y_0,z_0)} \neq 0, \quad \left(\frac{\partial \rho}{\partial t}\right)_{(x_0,y_0,z_0)} \neq 0,$$

where (x_0, y_0, z_0) is fixed point in fluid field." [36]

2.4.2 Uniform and Non-uniform flow

"Uniform flow is defined as that type of flow in which the velocity at any given time does not change with respect to space (i.e., length of direction of the flow). Mathematically, for the uniform flow:

$$\left(\frac{\partial V}{\partial s}\right)_{r=c} = 0,$$

where ∂V=change of velocity and c is constant." [36]

"Non-uniform flow is the type of flow in which the velocity at any given time changes with respect to space. Mathematically for nonuniform flow:

$$\left(\frac{\partial V}{\partial s}\right)_{r=c} \neq 0."[36]$$

2.4.3 Laminar Flow

"Laminar flow is defined as that type of flow in which the fluid particles move along well-defined paths or stream lines and all the stream lines are straight and parallel. Thus the particles move in lamines or layers gliding smoothly over the adjacent layer. This type of flow is called stream-line flow or viscous flow." [36]

2.4.4 Turbulent Flow

"Turbulent flow is that type of flow in which the fluid particles move in a zig-zag way. Due to the movement of fluid particles in a zig-zag way, the eddies formulation takes place which are responsible for high energy loss." [36]

2.4.5 Compressible and Incompressible Flows

"Compressible flow is that type of flow in which the density for the fluid changes from point to point or in other words the density (ρ) is not constant for the fluid.

Incompressible flow is that type of flow in which the density is constant for the fluid flow. Liquids are generally incompressible while gases are compressible." [36]

2.4.6 Inviscous Flow

"A flow in which viscosity of the fluid is equal to zero is known as inviscous (inviscid) flow." [36]

2.5 Porous Material

"A solid containing holes or voids, either connected or non-connected, dispersed within it in either a regular or random manner, is known as a porous material provided that holes occur relatively frequently within the solid.
Pores are either interconnected or non-interconnected. A fluid can flow through a porous material only if at least some of the pores are interconnected. Some natural porous materials are beach sand, limestone, sandstone, wood, loaf of bread and human lung etc." [36]

2.5.1 Porosity

"The porosity of a porous material is the fraction of the bulk volume of the material occupied by voids. The symbol usually employed for this parameter is ϕ. Thus

$$\phi = \frac{V_P}{V_B} = \frac{\text{volume of porous}}{\text{bulk volume}}$$

Bulk volume, is a dimensionless quantity. Since that portion of the bulk volume not occupied by pores is occupied by the solid grains or matrix of the material, it follows that:

$$1 - \phi = \frac{V_S}{V_B} = \frac{\text{volume of solids}}{\text{bulk volume}}.$$" [36]

2.5.2 Permeability

"Permeability is the property of a porous material which characterizes the ease with which a fluid may be made to flow through the material by an applied pressure gradient. Permeability is the fluid conductivity of the porous material.

If horizontal linear row of an incompressible fluid is established through a sample of porous material of length L in the direction of flow, and cross sectional area A, then the permeability K of the material is defined as:

$$K = \frac{q\mu}{A\left(\frac{\delta P}{L}\right)}$$

Here q is the fluid flow rate in volume per unit time, μ is the viscosity of the fluid and δP is the applied pressure difference across the length of the specimen." [36]

2.6 Conservation Laws

2.6.1 Law of Conservation of Mass

"The principle of conservation of mass states that the time rate of change of mass in a fixed volume is equal to the net rate of mass across the surface. The mathematical statement of the principle results in the following equation, known as the continuity (of mass) equation,

$$\frac{\partial \rho}{\partial t} + \delta.(\rho V) = 0, \tag{2.1}$$

where ρ is the density (kg/m^3) of the medium, V is the velocity vector (ms^{-1}) and δ is the nabla or del operator.
For steady-state conditions the continuity equation becomes:

$$\delta.(\rho V) = 0. \tag{2.2}$$

When the density changes following a fluid particle are negligible, the continuum is termed incompressible. The continuity equation (2.2) then becomes:

$$(\delta.V) = 0. \tag{2.3}$$

which is often referred to as the incompressibility condition or incompressibility constraint." [39]

2.6.2 Equation of Momentum

"The principle of conservation of linear momentum (or Newton's Second Law of motion) states that the time rate of change of linear momentum of a given set of particles is equal to the vector sum of all the external forces acting on the particles of the set, provided Newton's Third Law of action and reaction governs the internal forces. Newton's Second Law can be written as:

$$\frac{\partial}{\partial t}(\rho V) + \delta(\rho V \otimes V) = \delta.\sigma + \rho f, \tag{2.4}$$

where $\otimes$ is the tensor (or dyadic) product of two vectors, σ is the Cauchy stress tensor (N/m^2) and f is the body force vector, measured per unit mass and normally taken to be the gravity vector. Equation (2.4) describes the motion of a continuous medium, and in fluid mechanics they are also known as the Navier equations. The form of the momentum equation shown in (2.4) is the conservation (divergence) form that is most often utilized for compressible flows. This equation may be simplified to a form more commonly used with incompressible flows. Expanding the first two derivatives and collecting terms,

$$\rho\left(\frac{\partial V}{\partial t} + V\delta.V\right) + V\left(\frac{\partial \rho}{\partial t} + \delta.\rho V\right) = \delta.\sigma + \rho f \tag{2.5}$$

The second term in parentheses is the continuity equation (2.1) and neglecting this term allows (2.5) to reduce to the non-conservation (advective) form:

$$\rho\frac{DV}{Dt} = \delta.\sigma + \rho f \tag{2.6}$$

where the material derivative (2.2) has been employed. The principle of conservation of angular momentum can be stated as the time rate of change of the total moment of momentum of a given set of particles is equal to the vector sum of the moments of the external forces acting on the system. In the absence of distributed couples, the principle leads to the symmetry of the stress tensor

$$\sigma = \sigma^T, \tag{2.7}$$

where the superscript T denotes the transpose of the enclosed quantity." [39]

2.6.3 Law of Conservation of Energy

"The law of conservation of energy (or the First Law of Thermodynamics) states that the time rate of change of the total energy is equal to the sum of the rate of work done by applied forces and the change of heat content per unit time. In the general case, the First Law of Thermodynamics can be expressed in conservation form as

$$\frac{\partial \rho e^t}{\partial t} + \delta.\rho\nu e^t = -\delta.q + \delta.(\sigma.V) + Q + \rho f.\nu, \tag{2.8}$$

where $e^t = e + 1/2\nu.\nu$ is the total energy (J/m^3) , e is the internal energy, q is he heat flux vector (W/m^2) and Q is the internal heat generation (W/m^3)." [39]

2.6.4 Newton's Law of Viscosity

"It states that the shear stress (τ) on a fluid element layer is proportional to the rate of shear strain. The constant of proportionally is called coefficient of viscosity. Mathematically, it is expressed as:

$$\tau = \mu \frac{\partial u}{\partial y}." \text{ [39]}$$

2.7 Dimensionless Parameters

2.7.1 Reynolds Number (Re)

"It is the most significant dimensionless number which is used to identify the different flow behaviors like laminar or turbulent flow. Mathematically, it is expressed as:

$$Re = \frac{LU}{\nu},$$

where U denotes the free stream velocity, L is the characteristic length and ν stands for kinematic viscosity." [40]

2.7.2 Nusselt Number (Nu)

"It is the relationship between the convective to the conductive heat transfer

through the boundary of the surface. Mathematically, it is defined as:

$$Nu = \frac{hL}{k},$$

where h stands for convective heat transfer, L stands for characteristic length and k stands for thermal conductivity." [40]

2.7.3 Prandtl Number (Pr)

"The ratio of kinematic diffusivity to heat the diffusivity is said to be Prandtl number. It is denoted by Pr. Mathematically, it can be written as:

$$\begin{aligned} Pr &= \frac{\nu}{\alpha}, \\ &= \frac{\mu c_\rho}{\rho k}, \end{aligned}$$

where μ and α denote the momentum diffusivity or kinetic diffusivity and thermal diffusivity respectively." [40]

2.7.4 Skin Friction Coefficient (Cf_x)

"It is a non-dimensional quantity that represents the ratio of wall shear stress to the dynamic pressure of the fluid flow. Mathematically,

$$Cf = \frac{2\tau_w}{\rho U_w^2},$$

where τ_w is the local wall shear stress, ρ is the fluid density and U_w is the free stream velocity (usually taken outside the boundary layer or at the inlet)." [40]

2.7.5 Sherwood Number (Sh_x)

"It is a non-dimensional quantity which describes the ratio of the mass transport by convection to the transfer of mass by diffusion. Mathematically,

$$Sh = \frac{kL}{D},$$

here L is characteristics length, D is the mass diffusivity and k is the mass transfer coefficient." [40]

2.7.6 Thermophoresis Parameter

"In a temperature gradient, small particles are pushed towards the lower temperature because of the asymmetry of molecular impacts." [40]

2.7.7 Eckert Number

"It is a dimensionless number used in continuum mechanics. It describes the relation between flows and the boundary layer enthalpy difference and it is used for characterized heat dissipation. Mathematically,

$$Ec = \frac{u^2}{c_\rho \delta T}." \text{ [40]}$$

2.8 Shooting Method

To elaborate the shooting method, take into account the subsequent nonlinear boundary value problem:

$$\left.\begin{aligned} &\widetilde{E''}(\widetilde{\eta}) - \widetilde{E}(\widetilde{\eta}) + \widetilde{E}^2(\widetilde{\eta}) = 0, \\ &\widetilde{E}(0) = 0, \quad \widetilde{E}(b) = 0. \end{aligned}\right\} \tag{2.9}$$

To reduce the order of the above BVP, introduce the following notations:

$$\widetilde{E}(\widetilde{\eta}) = \widetilde{y}_1, \quad \widetilde{E'}(\widetilde{\eta}) = \widetilde{y}_1' = \widetilde{y}_2. \tag{2.10}$$

The system of first order ordinary differential equations (ODEs) that results from the conversion of (2.9) is as follows:

$$\left.\begin{aligned} \widetilde{y}_1' &= \widetilde{y}_2, & \widetilde{y}_1(0) &= 0, \\ \widetilde{y}_2' &= \widetilde{y}_1^2 - \widetilde{y}_1, & \widetilde{y}_2(0) &= s_1, \end{aligned}\right\} \tag{2.11}$$

where s_1 is the initial condition which will be guessed. The $RK4$ method will be used to numerically solve the above IVP. Choose missing condition s_1 in such a way that:

$$\widetilde{y}_1(b, s_1) = 0. \tag{2.12}$$

The above equation can effectively be solved through the application of Newton's method with the following iterative scheme:

$$s_1^{(m+1)} = s_1^{(m)} - \frac{(\widetilde{y}_1(b, s_1))^m}{\left(\frac{\partial \widetilde{y}_1(b, s_1)}{\partial s_1}\right)^m}. \tag{2.13}$$

Further, introduce the following notations:

$$\frac{\partial \widetilde{y}_1}{\partial s_1} = \widetilde{y}_3, \quad \frac{\partial \widetilde{y}_2}{\partial s_1} = \widetilde{y}_4. \tag{2.14}$$

As a result of these new notations, the Newton's iterative scheme, will then get the form:

$$s_1^{(m+1)} = s_1^{(m)} - \frac{(\widetilde{y}_1(b, s_1))^{(m)}}{(\widetilde{y}_3(b, s_1))^{(m)}}. \tag{2.15}$$

Now differentiating the system of a pair of first order ODEs (2.11) with respect to s_1, we get another new system of ODEs, as follows:

$$\left.\begin{aligned} \widetilde{y}_3' &= \widetilde{y}_4, & \widetilde{y}_3(0) &= 0, \\ \widetilde{y}_4' &= 2\widetilde{y}_1\widetilde{y}_3 - \widetilde{y}_3, & \widetilde{y}_4(0) &= 1. \end{aligned}\right\} \tag{2.16}$$

Now, writing (2.11) and (2.16) together, the following IVP can be written:

$$\begin{aligned} \widetilde{y}_1' &= \widetilde{y}_2, & \widetilde{y}_1(0) &= 0, \\ \widetilde{y}_2' &= \widetilde{y}_1^2 - \widetilde{y}_1, & \widetilde{y}_2(0) &= s_1, \\ \widetilde{y}_3' &= \widetilde{y}_4, & \widetilde{y}_3(0) &= 0, \\ \widetilde{y}_4' &= 2\widetilde{y}_1\widetilde{y}_3 - \widetilde{y}_3, & \widetilde{y}_4(0) &= 1. \end{aligned}$$

The above system together will be systematically solved by $RK-4$ method. The stopping criteria for the Newton's technique is:

$$|\widetilde{y}_1(b, s_1)| < \epsilon,$$

where $\epsilon > 0$ is an arbitrarily small positive number.

Chapter 3

Thermal Performance of Hybrid Nanofluids with Joule Heating and Viscous-Enhanced Convection

3.1 Introduction

This chapter examines the thermal performance of hybrid nanofluids with Joule heating and viscous-enhanced convection numerically. Using appropriate transformations, we address this by converting the governing nonlinear partial differential equations into a collection of dimensionless ordinary differential equations. Thereafter, the shooting method is applied in MATLAB to achieve the numerical solution of these equations. We discuss and analyze the computational solution of ODEs for a number of parameters, particularly the velocity profile $f'(\eta)$ and the temperature profile $\theta(\eta)$ for the system. To display the numerical results, tables and graphs are utilized. This chapter offers a thorough analysis of [41].

3.2 Physical Model

This study investigates the laminar, incompressible, and two-dimensional (2D) fluid flow of a viscous hybrid nanofluid across a stretching/shrinking sheet. The verticle y-axis is normal to the sheet, and the sheet is positioned along the x-axis. In the y-direction, a constant magnetic field with a strength of B_0 is applied. Assume that the sheet is stretching/shrinking with the fluid velocity of $u_w(x) = ax$, where $a > 0$ is a constant and $v_0 = -\sqrt{a\nu_f}S$, where S is a constant, represents the constant mass flux velocity. Both the surface of the temperature T_w, and the ambient temperature T_∞ are held constant. The following equations (3.1)-(3.3) and the boundary conditions (3.4) control the steady two-dimensional flow of hybrid nanofluid.

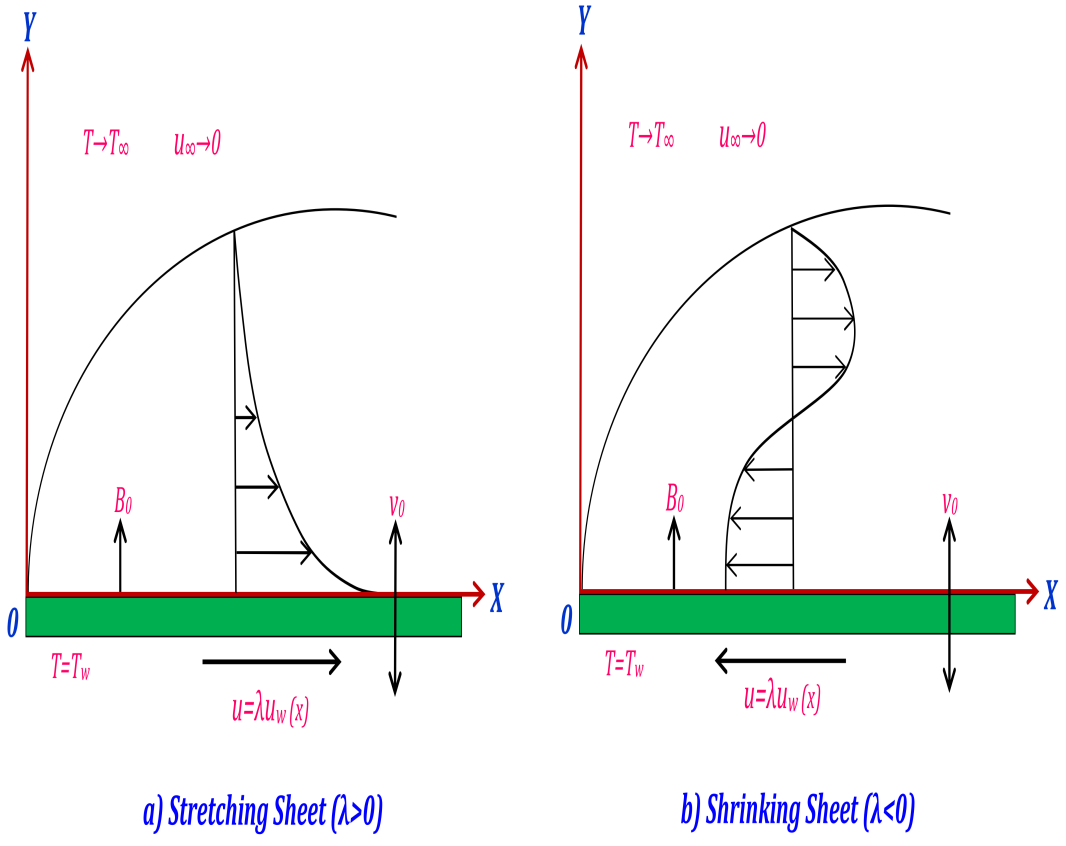

FIGURE 3.1: Flow Configuration

$$\frac{\partial u}{\partial x} + \frac{\partial v}{\partial y} = 0, \tag{3.1}$$

$$u\frac{\partial u}{\partial x}+v\frac{\partial u}{\partial y}=\nu_{hnf}\frac{\partial^2 u}{\partial^2 y}-\frac{\sigma_{hnf}}{rho_{hnf}}B_0^2 u, \tag{3.2}$$

$$u\frac{\partial T}{\partial x}+v\frac{\partial T}{\partial y}=\frac{k_{hnf}}{(\rho C_p)_{hnf}}\frac{\partial^2\, T}{\partial y^2}-\frac{1}{(\rho C_p)_{hnf}}\frac{\partial q_r}{\partial y}+\frac{\sigma_{hnf}}{(\rho C_P)_{hnf}}B_0^2u^2+\frac{\mu_{hnf}}{(\rho C_P)_{hnf}}\left(\frac{\partial u}{\partial y}\right)^2. \tag{3.3}$$

Boundary condition:

$$\left.\begin{aligned} &v=v_0,\quad u=\lambda u_w(x),\quad T=A\frac{\partial T}{\partial y}+T_w\quad at\quad y=0,\\ &u\longrightarrow 0,\quad T\longrightarrow T_\infty\quad \text{as}\quad y\longrightarrow\infty. \end{aligned}\right\} \tag{3.4}$$

3.2.1 Formulation and Thermo-physical Characteristics

For the purpose of establishing a clear and well defined comparison, the important thermo-physical characteristics of both HNF and NF are illustrated in the table 3.1.

TABLE 3.1: Thermo-physical properties of water and nanoparticles.

Physical Properties	$\rho(kg/m^{-3})$	$C_p(J/kgK)$	$k(W/mK)$	$\sigma(s/m)$
Water	997.1	4179	0.613	5.5×10⁻6
TiO_2	4250	686.2	8.9538	2.38×10^6
Fe_3O_4	5810	670	6	2.5×10^4

The detailed physical properties of both nanofluids and hybrid nanofluids are comprehensively summarized in tables table 3.2 and table 3.3 respectively.

3.3 Similarity Transformation and Non-dimensionalization of Mathematical Model

This section focuses on the non-dimensionalization process relevant to the mathematical model that describes the behavior of our hybrid nanofluid. The procedure entails the

introduction of dimensionless variables and parameters, which serve to simplify the original equations. The applications of dimensionless quantities not only deepens our insight to the physical phenomena but also enhances the analysis tractability. The mathematical model will be converted into a system of ordinary differential equations through the following similarity transformations:

$$\left.\begin{aligned} &\eta = \sqrt{\frac{a}{\nu_f}}\, y, \quad \Psi = \sqrt{a\nu_f}\, x f(\eta), \quad \theta(\eta) = \frac{T - T_\infty}{T_w - T_\infty}, \\ &u = a x f'(\eta), \quad v = -\sqrt{a\nu_f}\, f(\eta). \end{aligned}\right\} \tag{3.5}$$

The derivatives listed below are required for satisfying the mass conservation equation (3.1).

$$\begin{aligned} u &= \frac{\partial \Psi}{\partial y} \\ &= \sqrt{a\nu_f}\, x f'(\eta) \sqrt{\frac{a}{\nu_f}} \\ &= a x f'(\eta). \end{aligned} \tag{3.6}$$

$$\begin{aligned} v &= -\frac{\partial \Psi}{\partial x} \\ &= -\sqrt{a\nu_f}\, f(\eta). \end{aligned} \tag{3.7}$$

$$\begin{aligned} \frac{\partial u}{\partial x} &= \frac{\partial}{\partial x}\left(a x f'(\eta)\right) \\ &= a f'(\eta). \end{aligned} \tag{3.8}$$

$$\begin{aligned} \frac{\partial v}{\partial y} &= \frac{\partial}{\partial y}\left(-\sqrt{a\nu_f}\, f(\eta)\right) \\ &= -\sqrt{a\nu_f}\, f'(\eta) \left(\sqrt{\frac{a}{\nu_f}}\right) \\ &= -a f'(\eta). \end{aligned} \tag{3.9}$$

Using (3.8) and (3.9) in (3.1), we get:

$$\frac{\partial u}{\partial x} + \frac{\partial v}{\partial y} = a f'(\eta) - a f'(\eta) = 0.$$

Hence the continuity equation (3.1) is satisfied identically. The following expression, denoted by P_i $(i = 1, 2, 3, 4, 5)$ incorporate various thermo-physical properties. These notations will simplify the dimensionless model to be achieved in the upcoming sections.

- $P_1 = \dfrac{\mu_{hnf}}{\mu_{nf}}$

- $P_2 = \dfrac{\rho_{hnf}}{\rho_f}$
- $P_3 = \dfrac{\sigma_{hnf}}{\sigma_f}$
- $P_4 = \dfrac{(\rho C_p)_{hnf}}{(\rho C_p)_f}$
- $P_5 = \dfrac{k_{hnf}}{k_f}$

TABLE 3.2: Thermo-physical properties of the nanofluids. [41]

Properties	**Nanofluid**
Density	$\rho_{nf} = (1-\phi_1)\rho_f + \phi_1\rho_{n1}$
Dynamic viscosity	$\mu_{nf} = \frac{\mu_f}{(1-\Phi_1)^{2.5}}$
Thermal conductivity	$\frac{k_{nf}}{k_f} = \frac{k_{n1}+2k_f-2\phi_1(k_f-k_{n1})}{k_{n1}+2k_f+\phi_1(k_f-k_{n1})}$
Heat capacity	$(\rho C_p)_{nf} = (1-\phi_1)(\rho C_p)_f + \phi_1(\rho C_p)_{n1}$
Electrical conductivity	$\frac{\sigma_{nf}}{\sigma_f} = 1 + \frac{3\left(\frac{\sigma_{n1}}{\sigma_f}-1\right)\phi_1}{\frac{\sigma_{n1}}{\sigma_f}+2-\left(\frac{\sigma_{n1}}{\sigma_f}-1\right)\phi_1}$

TABLE 3.3: Thermo-physical properties of hybridnanofluids. [41]

Properties	**Hybrid Nanofluid**
Density	$\rho_{hnf} = (1-\phi_2)[(1-\phi_1)\rho_f + \phi_1\rho_{n1}] + \phi_2\rho_{n2}$
Dynamic viscosity	$\mu_{hnf} = \frac{\mu_f}{(1-\Phi_1)^{2.5}(1-\Phi_2)^{2.5}}$
Thermal conductivity	$\frac{k_{hnf}}{k_{nf}} = \frac{k_{n2}+2k_{nf}-2\phi_2(k_{nf}-k_{n2})}{k_{n2}+2k_{nf}+\phi_2(k_{nf}-k_{n2})}$
Heat capacity	$(\rho C_p)_{hnf} = (1-\phi_2)\left[(1-\phi_1)(\rho C_p)_f + \phi_2(\rho C_p)_{n1}\right] + \phi_2(\rho C_p)_{n2}$
Electrical conductivity	$\frac{\sigma_{hnf}}{\sigma_{nf}} = 1 + \frac{3\left(\frac{\sigma_{n2}}{\sigma_{nf}}-1\right)\phi_2}{\frac{\sigma_{n2}}{\sigma_{nf}}+2-\left(\frac{\sigma_{n2}}{\sigma_{nf}}-1\right)\phi_2}$ where $\sigma_{nf} = \sigma_f\left[1 + \frac{3\left(\frac{\sigma_{n1}}{\sigma_f}-1\right)\phi_1}{\frac{\sigma_{n1}}{\sigma_f}+2-\left(\frac{\sigma_{n1}}{\sigma_f}-1\right)\phi_1}\right]$

3.3.1 Non-dimensionalization of Momentum Equation

The following derivatives are considered essential for the non-dimensionalization of the momentum equation (3.2):

$$\Rightarrow \quad \frac{\partial u}{\partial y} = axf''(\eta)\sqrt{\frac{a}{\nu_f}}. \tag{3.10}$$

$$\Rightarrow \quad \frac{\partial^2 u}{\partial y^2} = \frac{a^2 x f'''(\eta)}{\nu_f}. \tag{3.11}$$

Using (3.6), (3.7), (3.8) , (3.9) , (3.10) , (3.11) in equation (3.2) , then we get:

$$\left(axf'(\eta)\right)\left(af'(\eta)\right) + \left(-\sqrt{a\nu_f}f(\eta)\right)\left(axf''(\eta)\sqrt{\frac{a}{\nu_f}}\right) = \nu_{hnf}\left(\frac{a^2 x f'''(\eta)}{\nu_f}\right) - \frac{\sigma_{hnf}}{\rho_{hnf}}B_0^2\left(axf'(\eta)\right).$$

$$\Rightarrow \quad a^2 x f'^2(\eta) - \sqrt{a\nu_f}f(\eta)axf''(\eta)\sqrt{\frac{a}{\nu_f}} = \nu_{hnf}\left(\frac{a^2 x f'''(\eta)}{\nu_f}\right) - \frac{\sigma_{hnf}}{\rho_{hnf}}B_0^2 axf'(\eta).$$

$$\Rightarrow \quad a^2 x f'^2(\eta) - a^2 x f''(\eta)f(\eta) = \nu_{hnf}\left(\frac{a^2 x f'''(\eta)}{\nu_f}\right) - \frac{\sigma_{hnf}}{\rho_{hnf}}B_0^2 axf'(\eta).$$

$$\Rightarrow \quad a^2 x\left[f'^2(\eta) - f''(\eta)f(\eta)\right] = a^2 x\left[\nu_{hnf}\left(\frac{f'''(\eta)}{\nu_f}\right) - \frac{\sigma_{hnf}}{\rho_{hnf}}\frac{B_0^2 f'(\eta)}{a}\right].$$

$$\Rightarrow \quad f'^2(\eta) - f''(\eta)f(\eta) = \nu_{hnf}\left(\frac{f'''(\eta)}{\nu_f}\right) - \frac{\sigma_{hnf}}{\rho_{hnf}}\frac{B_0^2 f'(\eta)}{a}.$$

$$\Rightarrow \quad \frac{\nu_{hnf}}{\nu_f}f'''(\eta) + f''(\eta)f(\eta) - f'^2(\eta) - \frac{\sigma_{hnf}}{\rho_{hnf}}\frac{B_0^2 f'(\eta)}{a} = 0.$$

$$\Rightarrow \quad \frac{\frac{\mu_{hnf}}{\mu_f}}{\frac{\rho_{hnf}}{\rho_f}}f'''(\eta) + f''(\eta)f(\eta) - f'^2(\eta) - \frac{\frac{\sigma_{hnf}}{\sigma_f}}{\frac{\rho_{hnf}}{\rho_f}}Mf' = 0.$$

$$\Rightarrow \quad \frac{P_1}{P_2}f''' + ff'' - f'^2 - \frac{P_3}{P_2}Mf' = 0, \tag{3.12}$$

where,

$$M = \frac{\sigma_f B_0^2}{\rho_f a}.$$

3.3.2 Non-dimensionalization of Energy Equation

This section addresses the process of non-dimensionalizing the energy equation (3.3) for our hybrid nanofluid model.

$$\theta(\eta) = \frac{T - T_\infty}{T_w - T_\infty}$$

$$\Rightarrow \quad T = \theta(\eta)\,(T_w - T_\infty) + T_\infty. \tag{3.13}$$

$$\Rightarrow \quad \frac{\partial T}{\partial x} = 0. \tag{3.14}$$

$$\begin{aligned}\Rightarrow \quad \frac{\partial T}{\partial y} &= \frac{\partial}{\partial y}\left[\theta(\eta)\,(T_w - T_\infty) + T_\infty\right]. \\ &= \frac{\partial}{\partial y}\left[\theta(\eta)\,(T_w - T_\infty)\right] + \frac{\partial}{\partial y}\,(T_\infty). \\ &= \theta'(\eta)\sqrt{\frac{a}{\nu_f}}\,(T_w - T_\infty). \end{aligned} \tag{3.15}$$

$$\begin{aligned}\Rightarrow \quad \frac{\partial^2 T}{\partial y^2} &= \frac{\partial}{\partial y}\left[\theta'(\eta)\sqrt{\frac{a}{\nu_f}}\,(T_w - T_\infty)\right]. \\ &= \theta''(\eta)\left(\frac{a}{\nu_f}\right)(T_w - T_\infty). \end{aligned} \tag{3.16}$$

$$\begin{aligned}\Rightarrow \quad \left(\frac{\partial u}{\partial y}\right)^2 &= \left(axf''(\eta)\sqrt{\frac{a}{\nu_f}}\right)^2 \\ &= a^2 x f''^2(\eta)\left(\frac{a}{\nu_f}\right). \\ &= \frac{a^3 x}{\nu_f} f''^2(\eta). \end{aligned} \tag{3.17}$$

The radiation heat flux q_r can be expressed as:

$$q_r = -\frac{4\sigma^*}{3k^*}\frac{\partial T^4}{\partial y}. \tag{3.18}$$

The Stefan-Boltzmann constant is expressed as σ^*, and the absorption coefficient is represented by k^*. In instances where the temperature difference is minimal, the Taylor series expansion can be employed to represent the temperature T^4 around the point T_∞, as follows:

$$T^4 = T_\infty^4 + 4T_\infty^3\big(T - T_\infty\big) + 6T_\infty^2\big(T - T_\infty\big)^2 + ...$$

The higher-order terms are neglected, we obtain the expression presented below:

$$\begin{aligned} T^4 &= T_\infty^4 + 4T_\infty^3\big(T - T_\infty\big), \\ &= 4T_\infty^3 T - 3T_\infty^4. \end{aligned}$$

Substituting the above expression into equation (3.18), we obtain,

$$q_r = -\frac{4\sigma^*}{3k^*}\frac{\partial}{\partial y}\left[4T_\infty^3 T - 3T_\infty^4\right]$$

$$= -\frac{4\sigma^*}{3k^*}\left[4T_\infty^3\frac{\partial T}{\partial y}\right]$$

$$= -\frac{16\sigma^*}{3k^*}T_\infty^3\frac{\partial T}{\partial y}. \tag{3.19}$$

$$\Rightarrow \quad \frac{\partial q_r}{\partial y} = -\frac{16\sigma^*}{3k^*}T_\infty^3\frac{\partial^2 T}{\partial y^2}$$
$$= -\frac{16\sigma^*}{3k^*}T_\infty^3\left[\theta''(\eta)\left(\frac{a}{\nu_f}\right)(T_w - T_\infty)\right]. \tag{3.20}$$

Using (3.6), (3.7), (3.14), (3.15), (3.16), (3.17), (3.19) in equation (3.3), we have:

$$-\sqrt{a\nu_f}f(\eta)\left[\theta'(\eta)\sqrt{\frac{a}{\nu_f}}(T_w - T_\infty)\right] = \frac{k_{hnf}}{(\rho C_p)_{hnf}}\left[\theta''(\eta)\left(\frac{a}{\nu_f}\right)(T_w - T_\infty)\right]$$
$$-\frac{1}{(\rho C_p)_{hnf}}\left[-\frac{16\sigma^*}{3k^*}T_\infty^3\left(\theta''(\eta)\left(\frac{a}{\nu_f}\right)(T_w - T_\infty)\right)\right]$$
$$+\frac{\sigma_{hnf}}{(\rho C_P)_{hnf}}B_0^2(a^2x^2f'^2(\eta)) + \frac{\mu_{hnf}}{(\rho C_P)_{hnf}}\left(\frac{a^3x^2f''^2(\eta)}{\nu_f}\right).$$

$$\Rightarrow \quad -af(\eta)\theta'(\eta)(T_w - T_\infty) = \frac{k_{hnf}}{(\rho C_p)_{hnf}}\theta''(\eta)\frac{a}{\nu_f}(T_w - T_\infty)$$
$$+\frac{1}{(\rho C_p)_{hnf}}\frac{16\sigma^*}{3k^*}T_\infty^3\theta''(\eta)\left(\frac{a}{\nu_f}\right)(T_w - T_\infty)$$
$$+\frac{\sigma_{hnf}}{(\rho C_P)_{hnf}}B_0^2a^2x^2f'^2(\eta) + \frac{\mu_{hnf}}{(\rho C_P)_{hnf}}\frac{a^3x^2f''^2(\eta)}{\nu_f}.$$

$$\Rightarrow \quad -af(\eta)\theta'(\eta)(T_w - T_\infty) = (T_w - T_\infty)\,a\left[\frac{k_{hnf}}{(\rho C_p)_{hnf}}\frac{\theta''(\eta)}{\nu_f} + \frac{1}{(\rho C_p)_{hnf}}\frac{16\sigma^*}{3k^*}T_\infty^3\frac{\theta''(\eta)}{\nu_f}\right.$$
$$\left.+\frac{\sigma_{hnf}}{(\rho C_P)_{hnf}}\frac{B_0^2ax^2f'^2(\eta)}{(T_w - T_\infty)} + \frac{\mu_{hnf}}{(\rho C_P)_{hnf}}\frac{a^2x^2f''^2(\eta)}{\nu_f(T_w - T_\infty)}\right].$$

$$\Rightarrow \quad -f(\eta)\theta'(\eta) = \frac{k_{hnf}}{(\rho C_p)_{hnf}}\frac{\theta''(\eta)}{\nu_f} + \frac{1}{(\rho C_p)_{hnf}}\frac{16\sigma^*}{3k^*}T_\infty^3\frac{\theta''(\eta)}{\nu_f} + \frac{\sigma_{hnf}}{(\rho C_P)_{hnf}}\frac{B_0^2ax^2f'^2(\eta)}{(T_w - T_\infty)}$$
$$+\frac{\mu_{hnf}}{(\rho C_P)_{hnf}}\frac{a^2x^2f''^2(\eta)}{\nu_f(T_w - T_\infty)}.$$

$$\Rightarrow \quad f(\eta)\theta'(\eta) + \frac{k_{hnf}}{(\rho C_p)_{hnf}}\frac{\theta''(\eta)}{\nu_f} + \frac{1}{(\rho C_p)_{hnf}}\frac{16\sigma^*}{3k^*}T_\infty^3\frac{\theta''(\eta)}{\nu_f} + \frac{\sigma_{hnf}}{(\rho C_P)_{hnf}}\frac{B_0^2ax^2f'^2(\eta)}{(T_w - T_\infty)}$$
$$+\frac{\mu_{hnf}}{(\rho C_P)_{hnf}}\frac{a^2x^2f''^2(\eta)}{\nu_f(T_w - T_\infty)} = 0.$$

$$\Rightarrow \quad f(\eta)\theta'(\eta) + \frac{k_f(\frac{k_{hnf}}{k_f})}{(\rho C_p)_f(\frac{(\rho C_p)_{hnf}}{(\rho C_p)_f})}\frac{\theta''(\eta)}{\nu_f} + \frac{1}{(\rho C_p)_{hnf}}\frac{16\sigma^*}{3k^*}T_\infty^3\frac{\theta''(\eta)}{\nu_f}$$
$$+\frac{\sigma_f(\frac{\sigma_{hnf}}{\sigma_f})}{(\rho C_p)_f(\frac{(\rho C_p)_{hnf}}{(\rho C_p)_f})}\frac{B_0^2a^2x^2f'^2(\eta)}{a(T_w - T_\infty)} + \frac{\mu_{hnf}}{(\rho C_P)_{hnf}}\frac{a^2x^2f''^2(\eta)}{\nu_f(T_w - T_\infty)} = 0.$$

$$\Rightarrow \quad \frac{1}{P_r}\frac{1}{\frac{(\rho C_p)_{hnf}}{(\rho C_p)_f}}\left(\frac{k_{hnf}}{k_f}+\frac{4}{3}R\right)\theta''(\eta)+f(\eta)\theta'(\eta)+\frac{\frac{\sigma_{hnf}}{\sigma_f}}{\frac{(\rho C_p)_{hnf}}{(\rho C_p)_f}}ME_cf'^2(\eta)$$
$$+\frac{\frac{\mu_{hnf}}{\mu_f}}{\frac{(\rho C_p)_{hnf}}{(\rho C_p)_f}}Ecf''^2(\eta)=0.$$

$$\Rightarrow \quad \frac{1}{P_rP_4}\left(\frac{k_{hnf}}{k_f}+\frac{4}{3}R\right)\theta''+f\theta'+\frac{P_3}{P_4}ME_cf'^2+\frac{P_1}{P_4}Ecf''^2=0, \tag{3.21}$$

where

$$P_r=\frac{\nu_f(\rho C_p)_f}{k_f},\ R=\frac{4\sigma^*T_\infty^3}{3k^*} \ \text{ and } \ E_c=\frac{a^2x^2}{(C_\rho)_f(T_w-T_\infty)}.$$

3.3.3 Non-dimensionalization of Boundary Condition

The following procedure has facilitated the transformation of the associated boundary conditions (BCs) into the non-dimensional framework.

- $u=\lambda u_w(x), \qquad at \quad y=0.$

  $\Rightarrow \ axf'(\eta)=\lambda ax, \qquad at \quad \eta=0.$

  $\Rightarrow \ f(\eta)=\lambda, \qquad at \quad \eta=0.$

  $\Rightarrow \ f(0)=\lambda.$

- $v=v_0, \qquad at \quad y=0.$

  $\Rightarrow \ -\sqrt{a\nu_f}f(\eta)=-\sqrt{a\nu_f}S, \qquad at \quad \eta=0.$

  $\Rightarrow \ f(\eta)=S, \qquad at \quad \eta=0.$

  $\Rightarrow \ f(0)=S.$

- $T=T_w+A\dfrac{\partial T}{\partial y}, \qquad at \quad y=0.$

  $\Rightarrow \quad \theta(\eta)\big(T_w-T_\infty\big)+T_\infty=T_w+A\left(\theta'(\eta)\sqrt{\dfrac{a}{\nu_f}}(T_w-T_\infty)\right), \qquad at \quad \eta=0.$

  $\Rightarrow \quad \theta(\eta)\big(T_w-T_\infty\big)+T_\infty=T_w+A\theta'(\eta)\sqrt{\dfrac{a}{\nu_f}}(T_w-T_\infty), \qquad at \quad \eta=0.$

  $\Rightarrow \quad \theta(\eta)\big(T_w-T_\infty\big)=(T_w-T_\infty)+A\theta'(\eta)\sqrt{\dfrac{a}{\nu_f}}(T_w-T_\infty), \qquad at \quad \eta=0.$

  $\Rightarrow \quad \theta(\eta)=\dfrac{(T_w-T_\infty)}{(T_w-T_\infty)}+A\theta'(\eta)\sqrt{\dfrac{a}{\nu_f}}\dfrac{(T_w-T_\infty)}{(T_w-T_\infty)}, \qquad at \quad \eta=0.$

  $\Rightarrow \quad \theta(\eta)=1+A\theta'(\eta)\sqrt{\dfrac{a}{\nu_f}}, \qquad at \quad \eta=0.$

  $\Rightarrow \quad \theta(\eta)=1+\gamma\ \theta'(\eta), \qquad at \quad \eta=0.$

$$\Rightarrow \quad \theta(0) = 1 + \gamma\ \theta'(0).$$

- $u \longrightarrow 0, \qquad as\ y \longrightarrow \infty.$

$\Rightarrow\ axf'(\eta) \longrightarrow 0, \qquad as\ \eta \longrightarrow \infty.$

$\Rightarrow\ f'(\eta) \longrightarrow 0, \qquad as\ \eta \longrightarrow \infty.$

- $T \longrightarrow T_\infty, \qquad as\ \eta \longrightarrow \infty.$

$\Rightarrow\ \theta(\eta)\big(T_w - T_\infty\big) + T_\infty \longrightarrow T_\infty, \qquad as\ \eta \longrightarrow \infty.$

$\Rightarrow\ \theta(\eta) \longrightarrow 0, \qquad as\ \eta \longrightarrow \infty.$

3.3.4 Non-dimensionalization of Physical Quantities

The sub-section is dedicated to conversion of the physical quantities, the skin fraction and the Nusselt number into the dimensionless form.

Skin friction:

$$\begin{aligned}
C_f &= \frac{\tau_w}{\rho_f u_w^2}, \qquad \left(\tau_w = \mu_{hnf}\left(\frac{\partial u}{\partial y}\right)_{y=0}\right)\\
&= \frac{\mu_{hnf}}{\rho_f u_w^2}\left(\frac{\partial u}{\partial y}\right)_{y=0}\\
&= \frac{\mu_{hnf}}{\rho_f a^2 x^2}\left(axf''(\eta)\sqrt{\frac{a}{\nu_f}}\right)_{\eta=0}, \left(Re_x = \frac{u_e x}{\nu_f}\right)\\
&= \frac{\mu_{hnf}}{\rho_f a x} f''(0)\sqrt{\frac{a}{\nu_f}},\\
&= \frac{\mu_{hnf}}{\rho_f a^{\frac{1}{2}} x \nu_f^{\frac{1}{2}}} f''(0)\\
&= \frac{\mu_{hnf}.\mu_f}{\mu_f \rho_f a^{\frac{1}{2}} x \nu_f^{\frac{1}{2}}} f''(0)\\
&= \frac{\mu_{hnf}.\nu_f}{\mu_f a^{\frac{1}{2}} x \nu_f^{\frac{1}{2}}} f''(0)\\
&= \frac{\mu_{hnf}.\nu_f^{\frac{1}{2}}}{\mu_f a^{\frac{1}{2}} x} f''(0)\\
\sqrt{\frac{a}{\nu_f}} x C_f &= \frac{\mu_{hnf}}{\mu_f} f''(0)\\
\Rightarrow \quad Re_x^{\frac{1}{2}} C_f &= \frac{\mu_{hnf}}{\mu_f} f''(0). \qquad \left(Re_x^{1/2} = x\sqrt{\frac{a}{\nu_f}}\right)
\end{aligned} \tag{3.22}$$

Nusselt number:

$$Nu_x = \frac{x}{k_f(T_w - T_\infty)}\left\{(-q_r)_{y=0} + q_w\right\}$$

$$= \frac{x}{k_f(T_w - T_\infty)} \left\{ (-q_r)_{y=0} - k_{hnf} \left(\frac{\partial T}{\partial y} \right)_{y=0} \right\}, \quad \text{because} \quad q_w = -k_{hnf} \left(\frac{\partial T}{\partial y} \right)_{y=0}$$

$$= -\frac{x}{k_f(T_w - T_\infty)} \left\{ k_{hnf} \left[\theta'(0) \sqrt{\frac{a}{\nu_f}} (T_w - T_\infty) - \frac{16\sigma^*}{3k^*} T_\infty^3 \theta'(0)(T_w - T_\infty) \right] \right\}$$

$$= -\frac{x(T_w - T_\infty)}{k_f(T_w - T_\infty)} \left[k_{hnf} \theta'(0) \sqrt{\frac{a}{\nu_f}} - \frac{16\sigma^*}{3k^*} T_\infty^3 \theta'(0) \right]$$

$$= -\frac{x}{k_f} \left[k_{hnf} \theta'(0) \sqrt{\frac{a}{\nu_f}} - \frac{16\sigma^*}{3k^*} T_\infty^3 \theta'(0) \right]$$

$$= -x \sqrt{\frac{a}{\nu_f}} \left(\frac{k_{hnf}}{k_f} + \frac{16\sigma^*}{3k^*} T_\infty^3 \right) \theta'(0)$$

$$\Rightarrow \quad Re_x^{-1/2} Nu_x = -\left(\frac{k_{hnf}}{k_f} + \frac{4}{3} R \right) \theta'(0). \tag{3.23}$$

3.4 Solution Framework

The shooting method has been used for solving the ODE (3.12). Let us use the following notations:

$$f(\eta) = \widetilde{M}_1,$$
$$f'(\eta) = \widetilde{M}_1' = \widetilde{M}_2,$$
$$f''(\eta) = \widetilde{M}_2' = \widetilde{M}_3.$$

The following collection of first order ordinary differential equations (ODEs) has been generated to replace the existing momentum equation.

$$\left.\begin{aligned} \widetilde{M}_1' &= \widetilde{M}_2, & \widetilde{M}_1(0) &= S, \\ \widetilde{M}_2' &= \widetilde{M}_3, & \widetilde{M}_2(0) &= \lambda, \\ \widetilde{M}_3' &= -\frac{P_2}{P_1} \left[\widetilde{M}_1 \widetilde{M}_3 - \widetilde{M}_2' - \frac{P_3}{P_2} M \widetilde{M}_2 \right], & \widetilde{M}_3(0) &= h_1. \end{aligned}\right\} \tag{3.24}$$

To address the initial value problem described above, we will identify the missing initial condition for its numerical solution through the application of Runge-Kutta Method of order four ($RK4$). The condition labeled as h_1 must be selected to ensure that:

$$\widetilde{M}_2(\eta_\infty, h_1) = 0.$$

Additionally, Newton's Method is employed for the selection of h_1, utilizing the following iterative scheme:

$$h_1^{(n+1)} = h_1^{(n)} - \frac{\widetilde{M}_2(\eta_\infty, h_1^{(n)})}{\left(\frac{\partial}{\partial h_1} \widetilde{M}_2(\eta_\infty, h_1) \right)^{(n)}}.$$

We further introduce the following notations:

$$\frac{\partial \widetilde{M}_1}{\partial h_1} = \widetilde{M}_4,$$

$$\frac{\partial \widetilde{M_2}}{\partial h_1} = \widetilde{M_5},$$
$$\frac{\partial \widetilde{M_3}}{\partial h_1} = \widetilde{M_6}.$$

Due to the new scheme, Newtons iterative scheme gets this form:

$$h_1^{(n+1)} = h_1^{(n)} - \frac{\widetilde{M_2}(\eta_\infty, h_1^{(n)})}{\widetilde{M_5}(\eta_\infty, h_1^{(n)})}.$$

Now differentiating (3.24) with respect to the missing initial condition h_1, we get another system of ODEs:

$$\left.\begin{aligned}
\widetilde{M_4'} &= \widetilde{M_5}, & \widetilde{M_4}(0) &= 0,\\
\widetilde{M_5'} &= \widetilde{M_6}, & \widetilde{M_5}(0) &= 0,\\
\widetilde{M_6'} &= -\frac{P_2}{P_1}\left[\widetilde{M_1}\widetilde{M_6} + \widetilde{M_3}\widetilde{M_4} - 2\widetilde{M_2}\widetilde{M_5} - \frac{P_3}{P_2}M\widetilde{M_5}\right], & \widetilde{M_6}(0) &= 1.
\end{aligned}\right\} \tag{3.25}$$

From (3.24) and (3.25), the following IVP can be written:

$$\left.\begin{aligned}
\widetilde{M_1'} &= \widetilde{M_2}, & \widetilde{M_1}(0) &= S,\\
\widetilde{M_2'} &= \widetilde{M_3}, & \widetilde{M_2}(0) &= \lambda,\\
\widetilde{M_3'} &= -\frac{P_2}{P_1}\left[\widetilde{M_1}\widetilde{M_3} - \widetilde{M_2'} - \frac{P_3}{P_2}M\widetilde{M_2}\right], & \widetilde{M_3}(0) &= h_1,\\
\widetilde{M_4'} &= \widetilde{M_5}, & \widetilde{M_4}(0) &= 0,\\
\widetilde{M_5'} &= \widetilde{M_6}, & \widetilde{M_5}(0) &= 0,\\
\widetilde{M_6'} &= -\frac{P_2}{P_1}\left[\widetilde{M_1}\widetilde{M_6} + \widetilde{M_3}\widetilde{M_4} - 2\widetilde{M_2}\widetilde{M_5} - \frac{P_3}{P_2}M\widetilde{M_5}\right], & \widetilde{M_6}(0) &= 1.
\end{aligned}\right\} \tag{3.26}$$

The IVP (3.26), will be solved numerically by $RK4$ method. The establised stopping criteria for the Newton's technique is:

$$\left|\widetilde{M_2}\left(\eta_\infty, h_1\right) - 0\right| < \epsilon,$$

where $\epsilon > 0$ is an arbitrarily small positive number. From this point onward, ϵ has been consistently taken as 10^{-9}. Treating f, f' and f'' as known, we apply the shooting method to solve the energy equation (3.21). To implement the shooting method, the subsequent notations are utilized:

$$\theta(\eta) = \widetilde{N_1},$$
$$\theta'(\eta) = \widetilde{N_1'} = \widetilde{N_2}.$$

The initial value problem for the energy equation is given as:

$$\left.\begin{aligned}
\widetilde{N_1'} &= \widetilde{N_2}, & \widetilde{N_1}(0) &= 1 + \gamma k_1,\\
\widetilde{N_2'} &= -\frac{P_r P_4}{(P5 + \frac{4}{3}R)}\left[f\widetilde{N_2} + \frac{P_3}{P_4}ME_c f'^2 + \frac{P_2}{P_4}E_c f''^2(\eta)\right], & \widetilde{N_2}(0) &= k_1.
\end{aligned}\right\} \tag{3.27}$$

To utilize the $RK4$ method for the numerical solution of above IVP the missing condition k_1 within the system of equations need to be carefully chosen. The missing condition k_1 needs to be appropriately chosen in such a manner that:

$$\widetilde{N_2}(\eta_\infty, k_1) = 0.$$

Newton's method will be employed for the updation of k_1, utilizing the following iterative scheme:

$$k_1^{(n+1)} = k_1^{(n)} - \frac{\widetilde{N_2}(\eta_\infty, k_1^{(n)})}{\left(\frac{\partial}{\partial k_1}\widetilde{N_2}(\eta_\infty, k_1)\right)^{(n)}}.$$

We further introduce the following notations;

$$\frac{\partial \widetilde{N_1}}{\partial k_1} = \widetilde{N_3},$$
$$\frac{\partial \widetilde{N_2}}{\partial k_1} = \widetilde{N_4}.$$

Due to the new notations, the Newtons iterative scheme takes the following form:

$$k_1^{(n+1)} = k_1^{(n)} - \frac{\widetilde{N_2}(\eta_\infty, k_1^{(n)})}{\widetilde{N_4}(\eta_\infty, k_1)}. \tag{3.28}$$

Now differentiating (3.26) with respect to k_1, we get another system of ODEs as follows:

$$\left.\begin{aligned} \widetilde{N_3'} &= \widetilde{N_4}, & \widetilde{N_3}(0) &= \gamma, \\ \widetilde{N_4'} &= -\frac{P_r P_4}{(P5 + \frac{4}{3}R)}\left[f\widetilde{N_4}\right], & \widetilde{N_4}(0) &= 1. \end{aligned}\right\} \tag{3.29}$$

Now, writing (3.26) and (3.28) together, the following IVP can be written:

$$\left.\begin{aligned} \widetilde{N_1'} &= \widetilde{N_2}, & \widetilde{N_1}(0) &= 1 + \gamma k_1, \\ \widetilde{N_2'} &= -\frac{P_r P_4}{(P5 + \frac{4}{3}R)}\left[f\widetilde{N_2} + \frac{P_3}{P_4}ME_c f'^2 + \frac{P_2}{P_4}E_c f''^2(\eta)\right], & \widetilde{N_2}(0) &= k_1, \\ \widetilde{N_3'} &= \widetilde{N_4}, & \widetilde{N_3}(0) &= \gamma, \\ \widetilde{N_4'} &= -\frac{P_r P_4}{(P5 + \frac{4}{3}R)}\left[f\widetilde{N_4}\right], & \widetilde{N_4}(0) &= 1. \end{aligned}\right\} \tag{3.30}$$

The specified stopping criteria for the Newton's technique is:

$$\left|\widetilde{N_2}\left(\eta_\infty, k_1\right) - 0\right| < \epsilon. \tag{3.31}$$

Choose missing condition k_1 in (3.26) and apply Runge-Kutta method of order four to solve the above IVP numerically. Choose an $\epsilon > 0$. If (3.30) is satisfied then it will be our solution. Otherwise solve (3.28) and compute the next guess for missing condition by using (3.27). Use this new guess in (3.29) and repeat the same process until the (3.30) is met.

3.5 Results Interpretation

The primary objective of this section is to conduct an indepth analysis of the physical properties of velocity and energy profiles in relation to the changes in several key physical parameters, which include magnetic field strength (M), the stretching/shrinking parameter (λ), Prandtl number (Pr), volume fractions (ϕ_1, ϕ_2), the suction/injection parameter (S), radiation parameter (R), Eckert number (E_c), and thermal slip parameter (γ). This analysis is carried out using the graphical representations of both velocity and temperature profiles. Furthermore, by making adjustment to the values of the dimensionless parameters, the impact of these parameters on various physical quantities such as skin friction and Nusselt number is investigated and presented in a tabular format. The graphical representations of velocity and temperature profiles provide significant insights into the system's behavior as the physical parameters are altered. By analyzing the trends observed in these profiles, a clear understanding of the system's physical properties and energy distribution can be achieved. These visual tools facilitate the exploration of how variations in parameters like M, λ, R, Pr, γ, Ec and S influence the velocity and energy profiles.

3.5.1 Analysis of Computational Results

The results concerning the skin friction coefficient for the hybrid nanofluid comprising of TiO_2 and Fe_3O_4 with H_2O as the base fluid are presented in Table 3.4, which takes into account various inputs of M, ϕ_1, ϕ_2, λ, and S. In this table MC_1 denotes the intervals associated with the first missing condition h_1. This table effectively highlights the effects of the magnetic field as well as the volume fractions of nanoparticles (ϕ_1, ϕ_2) in the context of suction ($S = 0.5$) on the skin friction coefficient at $\lambda = 1.0$. The analysis reveals that an increase in values of M leads to higher absolute local skin friction coefficient. Increasing the volume friction parameters ϕ_1 and ϕ_2 results in a decrease in skin friction.

In Table 3.5, the influences of magnetic field and nanoparticle volume fractions (ϕ_1, ϕ_2) under injection condition ($S = -0.5$) on the skin friction coefficient of hybrid nanofluid, with $\lambda = 1.0$, are depicted. The findings reveal that skin friction coefficient reduces as the values of magnetic field parameter (M) increase. Increasing the volume friction parameters ϕ_1 and ϕ_2 results in a decrease in the skin friction. In addition, Table 3.6 details the value of the Nusselt number for the different values of parameters with $\lambda = 1.0$. The results indicate a decline in the Nusselt number with increasing values of M, E_c and γ. Conversely, an increase in the Nusselt number is noted with higher values of R.

Table 3.7 presents the values of the Nusselt number under conditions of a suction/injection parameter ($S = 2.0$) and a Prandtl number ($Pr = 6.2$) with a parameter value of ($\lambda = -1.0$).

The findings reveal that the Nusselt number decreases as the values of M, E_c, and γ increase. Additionally, an increase in the Nusselt number is observed with higher values of R.

TABLE 3.4: The results of $C_f\sqrt{Re_x}$ based on the values of the parameters M , ϕ_1 and ϕ_2 when $\lambda = 1.0$ and $S = 0.5$.

M	ϕ_1	ϕ_2	$C_f\sqrt{Re_x}$	MC_1
0.1	0.1	0.1	-2.296432	[-1.4 , 1.2]
0.4			-2.471043	[-0.9 , 0.7]
0.8			-2.682779	[-0.9 , 0.3]
1.2			-2.876153	[-0.9 ,-0.2]
	0.01		-1.907263	[-1.5 , 1.0]
	0.04		-2.030454	[-1.4 , 1.0]
	0.07		-2.159921	[-1.4 , 1.1]
		0.01	-1.786730	[-1.4 , 1.2]
		0.04	-1.949697	[-1.4 , 1.2]
		0.07	-2.119242	[-1.4 , 1.2]

TABLE 3.5: The results of $C_f\sqrt{Re_x}$ based on the values of M , ϕ_1 and ϕ_2 when $\lambda = 1.0$ and $S = -0.5$.

M	ϕ_1	ϕ_2	$C_f\sqrt{Re_x}$	MC_1
0.1	0.1	0.1	-1.408362	[-0.8 , -0.1]
0.4			-1.582903	[-0.9 , -0.3]
0.8			-1.794629	[-0.9 , -0.6]
1.2			-1.988002	[-0.9 , -0.6]
	0.01		-1.151283	[-0.8 , -0.2]
	0.04		-1.230441	[-0.8 , -0.2]
	0.07		-1.315878	[-0.8 , -0.1]
		0.01	-1.101176	[-0.8 , -0.1]
		0.04	-1.196636	[-0.8 , -0.1]
		0.07	-1.298675	[-0.8 , -0.1]

TABLE 3.6: The results of $\frac{Nu_x}{\sqrt{Re_x}}$ for the values of M, E_c, λ , R and γ when $\phi_1 = 0.1 = \phi_2$, $P_r = 6.2$ and $S = 2.0$.

λ	M	Ec	R	γ	$\frac{Nu_x}{\sqrt{Re_x}}$
1.0	0.1	0.1	0.1	0.1	6.462312
	0.2				6.445297
	0.3				6.428588
		0.2			5.726414
		0.3			4.990516
			0.3		6.887392
			0.5		7.253394
				0.2	4.526821
				0.5	2.384403

TABLE 3.7: The results of $\frac{Nu_x}{\sqrt{Re_x}}$ for the values of M, λ , E_c, R and γ when $\phi_1 = 0.1 = \phi_2$, $P_r = 6.2$ and $S = 2.0$.

λ	M	Ec	R	γ	$\frac{Nu_x}{\sqrt{Re_x}}$
-1.0	0.1	0.1	0.1	0.1	6.326590
	0.2				6.240653
	0.3				6.037435
		0.2			5.965945
		0.3			5.605300
			0.3		6.627460
			0.5		6.857546
				0.2	4.528018
				0.5	2.443795

3.5.2 Velocity Profile

Figures 3.2 to 3.4 illustrate the characteristics of the velocity profile, represented as $f'(\eta)$, in relation to various physical parameters including the magnetic field parameter M, volume fractions (ϕ_1 and ϕ_2), and the suction/injection parameter S.

Figure 3.2 illustrates the influence of the suction/injection parameter (S) on the velocity profile $f'(\eta)$ for magnetic parameters $M = 0.1$ and $M = 1.0$. It can be observed that the suction/injection parameter (S) leads to a reduction in the velocity profile. Additionally, it is noted that the elevated values of the magnetic parameter (M) diminish the velocity of hybrid nanofluid throughout the flow domain. This reduction is attributed to the Lorentz force, which acts perpendicular to the applied magnetic field and opposes the fluid's motion.

Figure 3.3 demonstrates a compelling result of velocity profile for the stretching/shrinking sheet scenarios. The observations indicate that by positively varying the titanium dioxide volume fraction (ϕ_1), the velocity distribution decreases for the shrinking sheet ($\lambda = -1.0$), whereas it behaves the other way round for the stretching sheet ($\lambda = 1.0$).

Figure 3.4 illustrates the velocity distribution as a function of the volume fraction of iron oxide (ϕ_2). By comparing figures 3.3 and 3.4, it can be observed that the velocity distribution is significantly affected in the same manner by changes in volume fraction of both the titanium dioxide (ϕ_1) and iron oxide (ϕ_2).

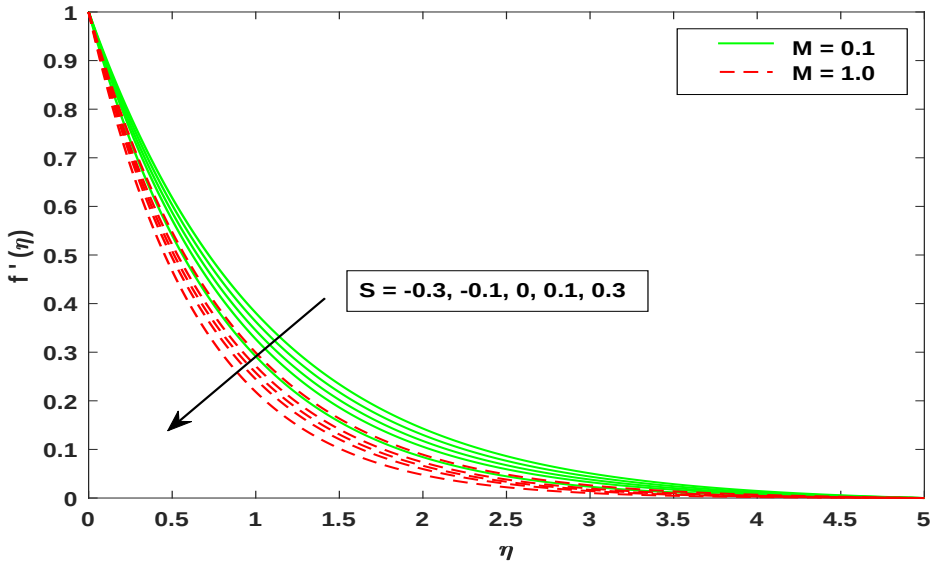

FIGURE 3.2: The distribution of velocity across S when $M = 0.1$ and $M = 1.0$, $\phi_1 = \phi_2 = 0.1$, S $= 2.0$, $\lambda = 1.0$.

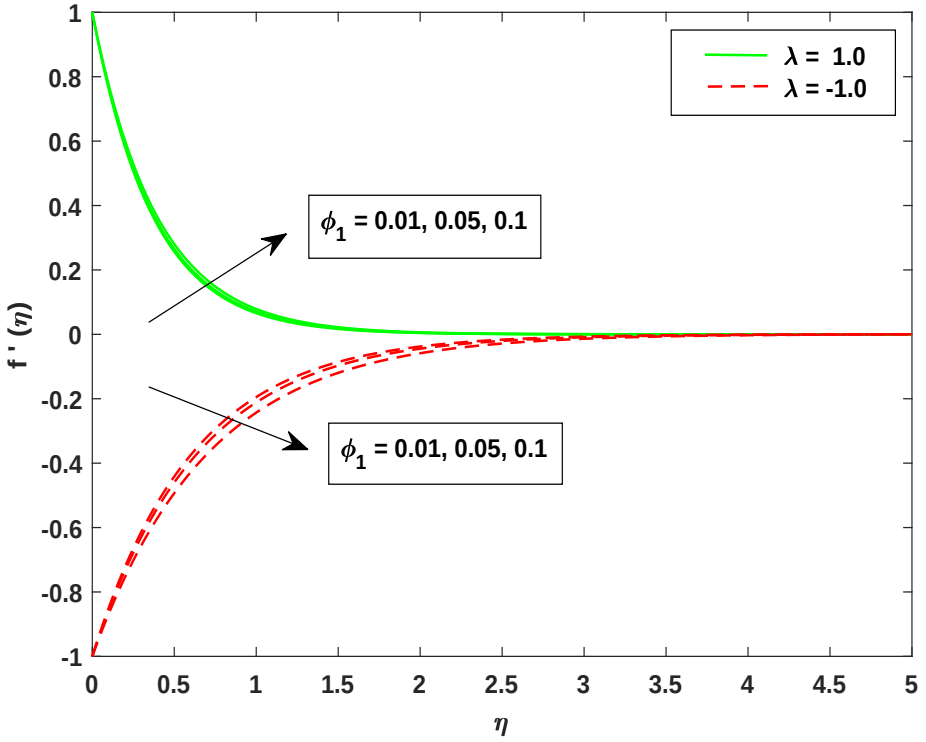

FIGURE 3.3: The distribution of velocity across ϕ_1 when $\lambda = 1.0$ and $\lambda = -1.0$, $\phi_2 = 0.1$, S $= 2.0$, $M = 0.1$.

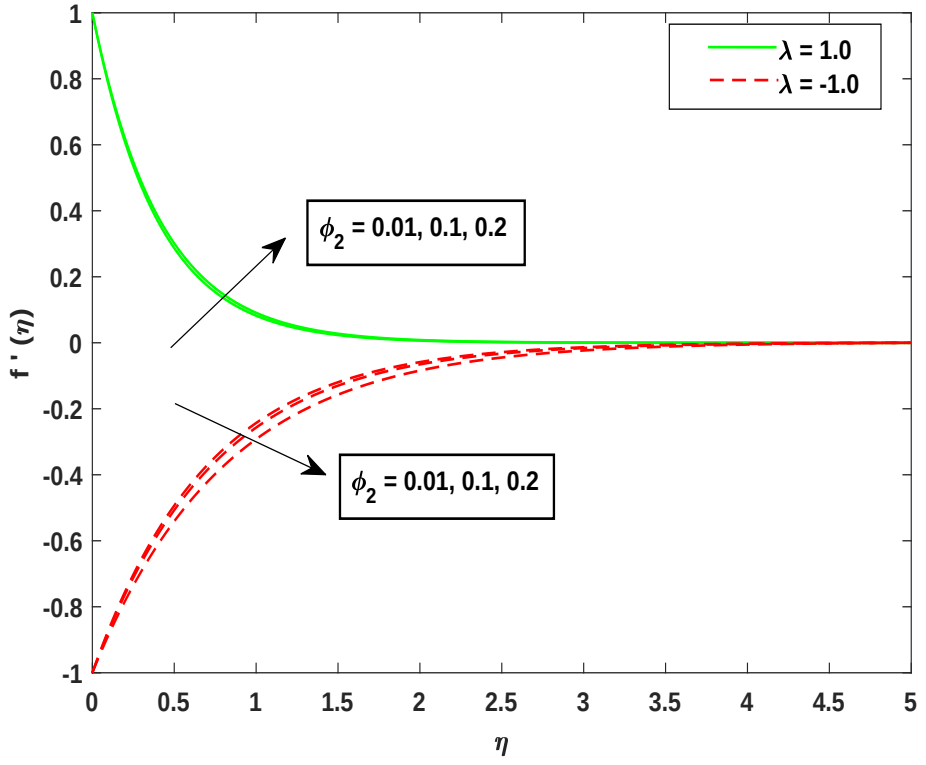

FIGURE 3.4: The distribution of velocity across ϕ_2 when $\lambda = 1.0$ and $\lambda = -1.0$, $\phi_1 = 0.1$, S $= 2.0$, M $= 0.1$.

3.5.3 Temperature Profile

The temperature distribution $\theta(\eta)$ is presented in the Figures 3.5 to 3.9, reflecting the influence of various thermophysical parameters, including the Prandtl number (Pr), radiation parameter (R), Eckert number (Ec), magnetic parameter (M), volume fractions (ϕ_1, ϕ_2), thermal slip parameter (γ), and the suction/injection parameter (S). A frequent phenomenon is observed in the thermal transport across the flow field, that is, the asymptotic variation that enables the system to reach the free stream state.

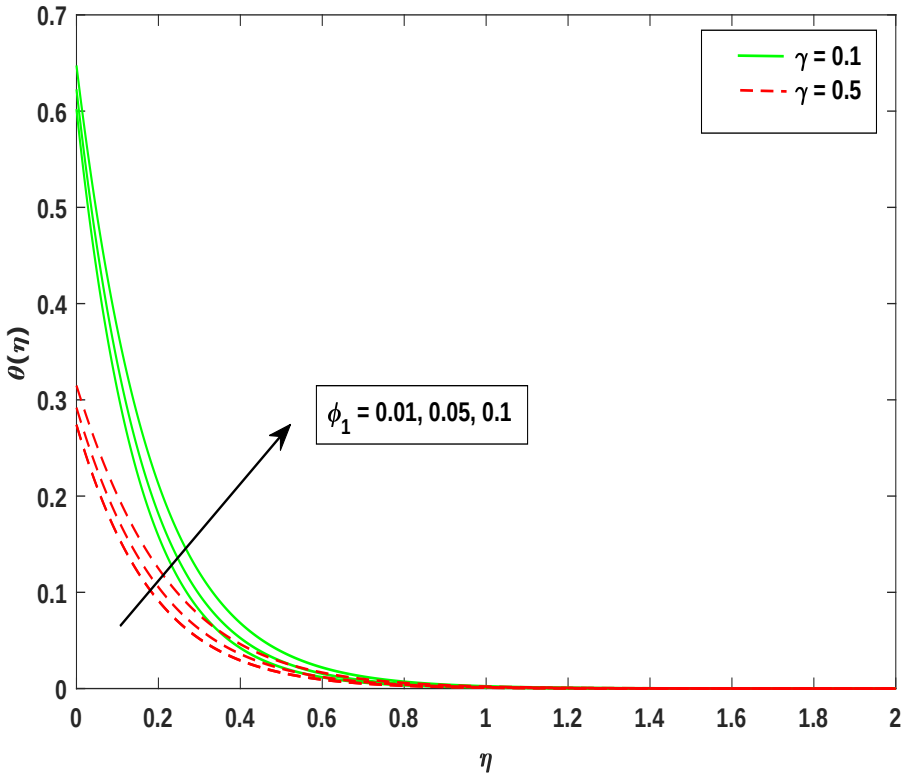

FIGURE 3.5: The distribution of temperature across ϕ_1 when $\gamma = 0.1$ and $\gamma = 0.5$, $\lambda = 1.0$, $E_c = \phi_2 = \mathrm{M} = 0.1$, $\mathrm{R} = 0.3$, $S = 2.0$, $P_r = 6.2$.

The findings depicted in Figure 3.5 suggest that a greater thermal slip results in lower temperatures, while a higher volume fraction contributes to the increased temperatures. This illustrates that an enhanced thermal slip significantly improves the transport of thermal power, especially as the volume fraction of the medium increases. The slip factor, whether concerning velocity or temperature, results from the fluid's thinness. Thus, an increment in the volume of nanoparticles, which signifies a greater concentration, leads to a rise in temperature associated with higher values of (ϕ_1), whereas it decreases in response to the thermal slip parameter γ.

The data presented in Figure 3.6 demonstrates that enhancing the thermal slip the temperature decreases. The temperature reduces for the different values of thermal slip and ϕ_2. It is depicted in Figure 3.7 that there is a notable increase in temperature corresponding to higher values of the magnetic parameter (M). Additionally, the temperature continues to rise with elevated values of E_c, which serves as an indicator of frictional heat and the heat contributed by viscous dissipation.

Figure 3.8 demonstrates that a contracting bounding surface results in an elevated temperature at all measured points as compared with that for a stretching surface ($\lambda > 0$). The transport of thermal energy in fluid layers is further improved with rising values of the radiation parameter R. Therefore, it is ultimately concluded that a shrinking surface ($\lambda < 0$) with increased thermal radiation effectively enhances this energy transport. Figure 3.9 illustrates a consistent decrease in temperature throughout the flow field, with an increased suction observed at the plate

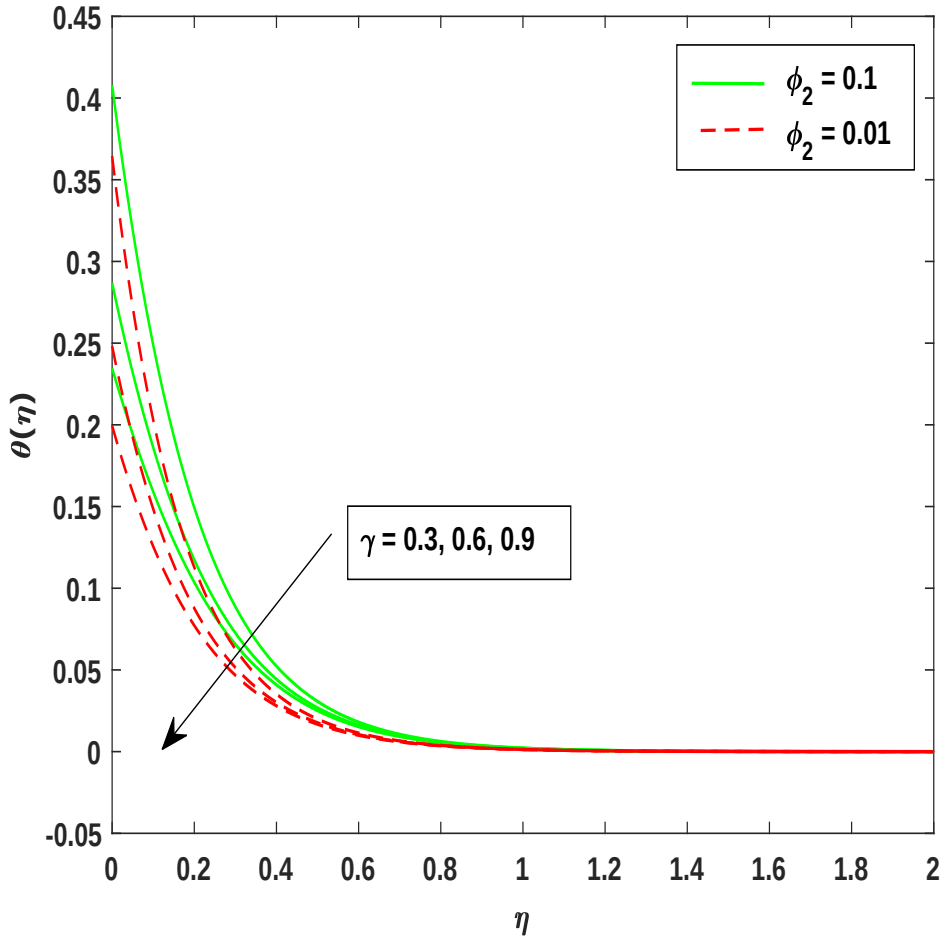

FIGURE 3.6: The distribution of temperature across γ when $\phi_2 = 0.1$ and $\phi_2 = 0.01$, $\phi_1 = 0.1$, M = Ec = 0.1, $\lambda = 1.0$, R = 0.3, Pr = 6.2, S = 2.0.

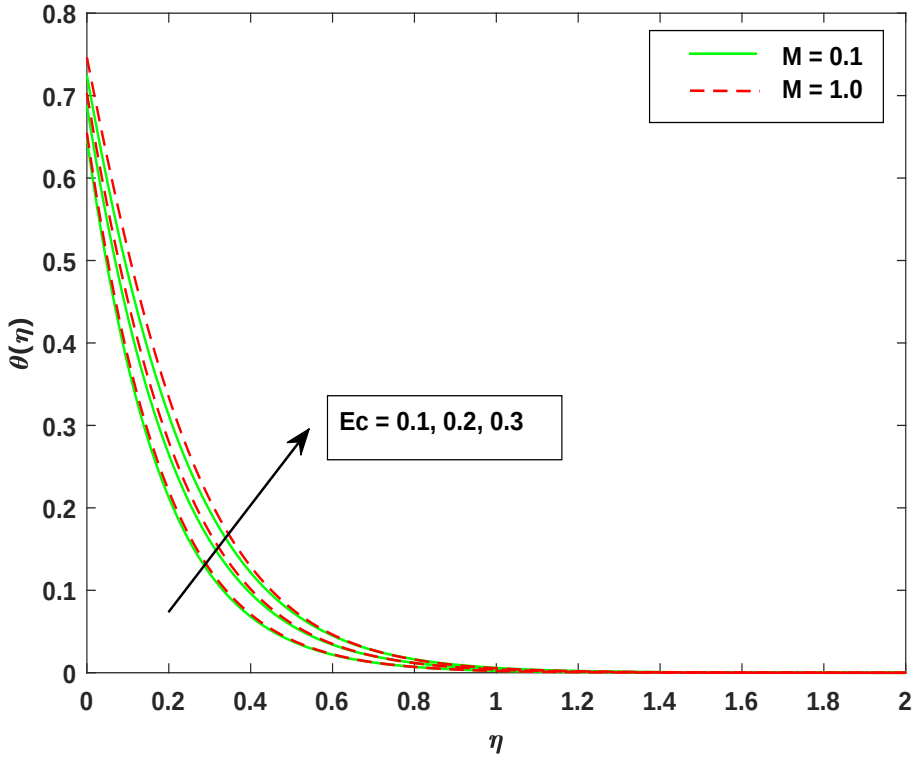

FIGURE 3.7: The distribution of temperature across Ec when M = 0.1 and M= 1.0, $\gamma = \phi_1 = \phi_2 = 0.1$, $\lambda = 1.0$, R = 0.3, Pr = 6.2, S = 2.0.

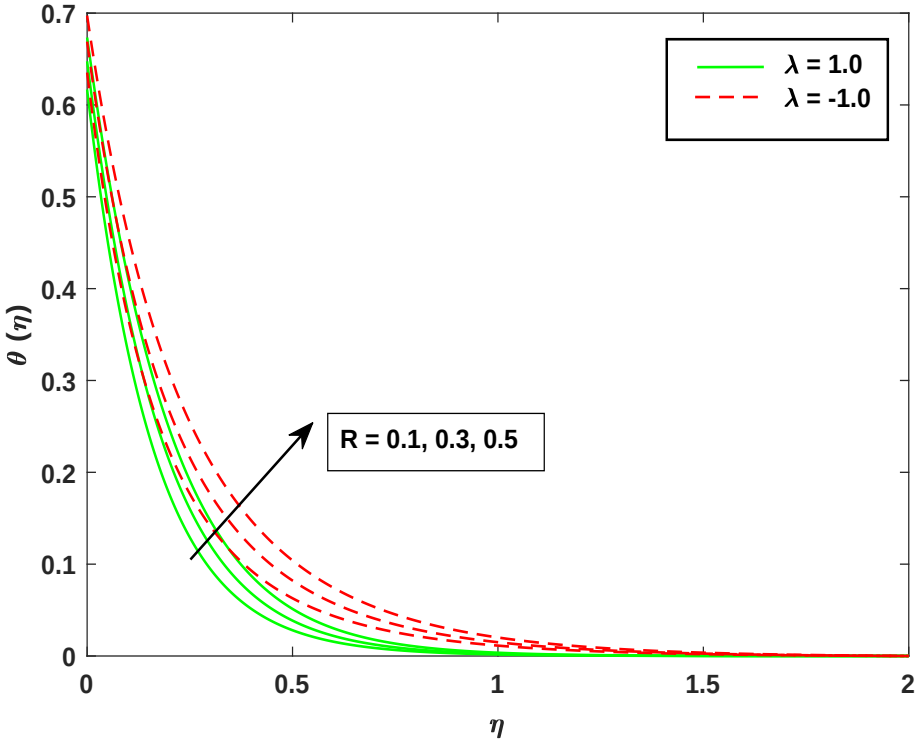

FIGURE 3.8: The distribution of temperature across R when $\lambda = 1.0$ and $\lambda = -1.0$, M = Ec = $\gamma = \phi_1 = \phi_2 = 0.1$, Pr = 6.2, S = 2.0.

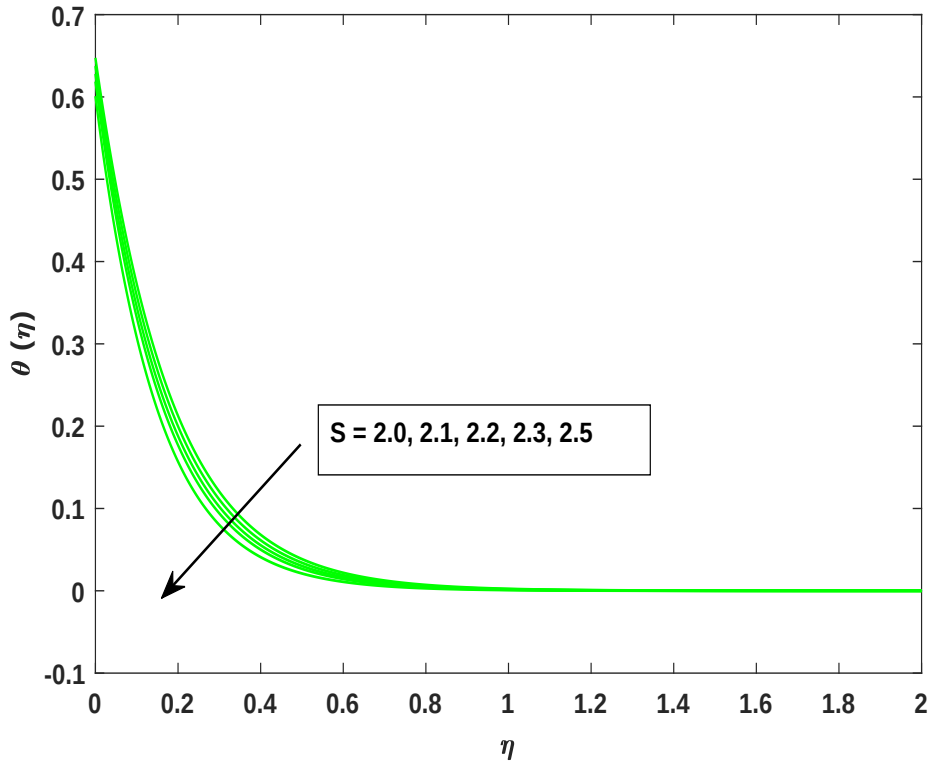

FIGURE 3.9: The distribution of temperature across S when $\phi_1 = 0.1$ and $\phi_1 = 0.2$, M $= \phi_2 =$ Ec $= \gamma = 0.1$, $\lambda = 1.0$, R $= 0.3$, Pr $= 6.2$.

Chapter 4

An Investigation Involving Maxwell's Parameter, Cattaneo-Christov Model and Concentration equation.

4.1 Introduction

In this chapter, a discussion on the flow behavior and thermal performance of hybrid nanofluid $(TiO_2 + Fe_3O_4)/H_2O$ with Joule heating and viscous-enhanced convection, previously presented in Chapter 3, has been extended. This expansion involves the incorporation of Maxwell's parameter and the porosity medium parameter into the momentum equation. Additionally, the Cattaneo-Christov model and the effects of heat source have also been integrated into the energy equation. Moreover, the concentration equation pertaining to the mentioned hybrid nanofluid has been introduced. This introduction enables the investigation of the interactive effects of these hybrid nanofluids on the flow behavior of the fluid across a stretchable or shrinking permeable sheet. Through detailed numerical simulations and analysis, the study investigates the complex interactions of these effects and their joint influence on the overall flow behavior. The results provide critical insights into the behavior of hybrid nanofluid under a range of physical conditions, thereby advancing the understanding of fluid flow in these contexts.

4.2 Mathematical Modeling

In the current chapter, it has been aimed to examine a viscous, incompressible and two-dimensional hybrid nanofluid flow in a laminar manner across a stretching/shrinking sheet. The y-axis is normal to the sheet, and the sheet is positioned along the x-axis. In the y-direction, a magnetic field with a strength B_0 is applied. Assume that the sheet is stretching/shrinking with the velocity $u_w(x) = ax$, where $a > 0$ is a constant and $v_0 = -\sqrt{a\nu_f}S$, where S is a constant, represents the constant mass flux velocity. The impact of Cattaneo-Christov model, Maxwell's parameter, heat source effect, porosity medium parameter, thermophoresis parameter, Brownian motion and chemical reaction of the flow has been studied under several key assumptions. In this context, T_w and C_w refer to the surface temperature and concentration, whereas T_∞ and C_∞ signify the constant ambient temperature and concentration associated with the hybrid nanofluid.

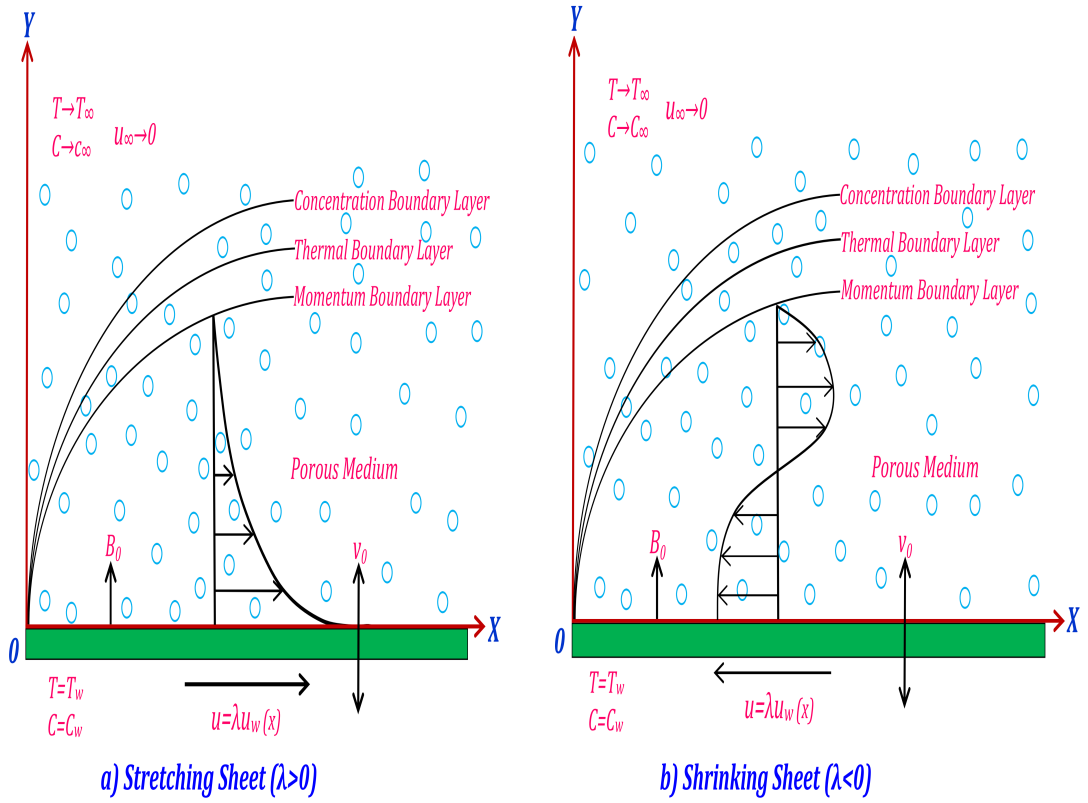

FIGURE 4.1: Flow Configuration

According to the above-mentioned assumptions and geometrical setting, the governing mathematical model in the dimensional form, comprises of the following equations:

$$\frac{\partial u}{\partial x} + \frac{\partial v}{\partial y} = 0, \tag{4.1}$$

$$\begin{aligned} u\frac{\partial u}{\partial x}+v\frac{\partial u}{\partial y} =&\nu_{hnf}\frac{\partial^2 u}{\partial^2 y}-\frac{\sigma_{hnf}}{rho_{hnf}}B_0^2u-\lambda_1\left(u^2\frac{\partial^2 u}{\partial x^2}+v^2\frac{\partial^2 u}{\partial y^2}+2uv\frac{\partial^2 u}{\partial x\partial y}\right)\\ &-\frac{\nu_{hnf}}{K_{p*}}u, \end{aligned} \tag{4.2}$$

$$\begin{aligned} u\frac{\partial T}{\partial x}+v\frac{\partial T}{\partial y}+&\lambda_2\left(u\frac{\partial u}{\partial x}\frac{\partial T}{\partial x}+v\frac{\partial v}{\partial y}\frac{\partial T}{\partial y}+v\frac{\partial u}{\partial y}\frac{\partial T}{\partial x}+2uv\frac{\partial^2 T}{\partial x\partial y}+u^2\frac{\partial T}{\partial x^2}+v^2\frac{\partial^2 T}{\partial y^2}\right)\\ &=\frac{k_{hnf}}{(\rho C_p)_{hnf}}\frac{\partial^2\ T}{\partial y^2}-\frac{1}{(\rho C_p)_{hnf}}\frac{\partial q_r}{\partial y}+\frac{\sigma_{hnf}}{(\rho C_P)_{hnf}}B_0^2u^2\\ &+\frac{\mu_{hnf}}{(\rho C_P)_{hnf}}\left(\frac{\partial u}{\partial y}\right)^2+\frac{Q_0}{(\rho C_p)_{hnf}}(T-T_\infty), \end{aligned} \tag{4.3}$$

$$v\frac{\partial C}{\partial y}+u\frac{\partial C}{\partial x}=\frac{\partial^2 C}{\partial y^2}D_B+\left(\frac{\partial^2 T}{\partial y^2}\right)\frac{D_T}{T_\infty}+K_r(C_\infty-C). \tag{4.4}$$

The following boundary conditions have been assumed for the current fluidic problem [41]:

$$\left.\begin{aligned} &v=v_0,\quad u=\lambda u_w(x),\quad T=A\frac{\partial T}{\partial y}+T_w,\quad C_w=C\quad at\quad y=0,\\ &u\longrightarrow 0,\quad T\longrightarrow T_\infty,\quad C\longrightarrow C_\infty\quad \text{as}\quad y\longrightarrow\infty. \end{aligned}\right\} \tag{4.5}$$

4.3 Similarity Transformation and Non-dimensionalization of Mathematical Model

In this section, we provide a detailed description of the non-dimensionalization approach applied to the mathematical model governing the behavior of our hybrid nanofluid. This process entails the introduction of dimensionless variables and parameters, allowing for the simplification of the original equations. The application of dimensionless quantities enhances our understanding of physical phenomena and facilitates a more manageable analysis. The mathematical model will be reformulated into a system of ordinary differential equations (ODEs) through the implementation of the subsequent similarity transformations:

$$\left.\begin{aligned} &\eta=\sqrt{\frac{a}{\nu_f}}y,\quad \Psi=\sqrt{a\nu_f}xf(\eta),\quad u=axf'(\eta),\quad v=-\sqrt{a\nu_f}f(\eta),\\ &\theta(\eta)=\frac{T-T_\infty}{T_w-T_\infty},\quad \phi(\eta)=\frac{C-C_\infty}{C_w-C_\infty}. \end{aligned}\right\} \tag{4.6}$$

The notation η is used to represent the similarity variable. The velocity components along the x-direction and y-direction are specifically denoted by u and v, respectively. Moreover, $\theta(\eta)$ and $\phi(\eta)$ illustrate the dimensionless temperature and concentration profiles. A list of various parameters that will be used in the upcoming ordinary differential equations (ODEs) and their corresponding boundary conditions (BCs) is presented in TABLE 4.1.

TABLE 4.1: Different dimensionless parameters.

Symbols	**Name**	**Appearance**
M	Magnetic field	$M = \frac{\sigma_f B_o^2}{\rho_f a}$
R	Radiation parameter	$R = \frac{4\sigma^* T_\infty^3}{3kk^*}$
K_1	Porosity medium	$K_1 = \frac{\nu_f}{ak^p*}$
β	Maxwell's parameter	$\beta = \lambda_1 a$
Nb	Brownian motion parameter	$Nb = \frac{D_B\left(C_w - C_\infty\right)\tau}{\nu_f}$
Pr	Prandtl number	$Pr = \frac{(\mu C_p)_f}{k_f}$
Ec	Eckert number	$Ec = \frac{a^2x^2}{\left(C_p\right)_f\left(T_w - T_\infty\right)}$
γ	Thermal slip parameter	$\gamma = A\sqrt{\frac{a}{\nu_f}}$
Le	Lewis number	$Le = \frac{\nu_f}{D_B}$
Q	Heat source	$Q = \frac{Q_o}{a\left(\rho C_p\right)_f}$
δ	Cattaneo-Christov parameter	$\delta = \lambda_2 a$
Nt	Thermophoresis parameter	$Nt = \frac{\tau\left(T_w - T_\infty\right)D_\tau}{T_\infty \nu_f}$
Γ	Chemical reaction	$\Gamma = \frac{K_r}{a}$

4.3.1 Non-dimensionalization of Momentum Equation

In this section, we convert the governing momentum equation (4.2) into a non-dimensional format. The non-dimensionalization of most of the terms is already carried out in Chapter 3. Some additional terms have been non-dimensionalized through the following process:

$$\begin{aligned} &\frac{\partial u}{\partial x} = af'(\eta) \qquad . \\ \Rightarrow \quad &\frac{\partial^2 u}{\partial x^2} = 0. \end{aligned} \tag{4.7}$$

$$\Rightarrow \quad \frac{\partial^2 u}{\partial x \partial y} = \frac{\partial}{\partial x}\left(\frac{\partial u}{\partial y}\right)$$
$$= \frac{\partial}{\partial x}\left(axf''(\eta)\sqrt{\frac{a}{\nu_f}}\right)$$
$$= af''(\eta)\sqrt{\frac{a}{\nu_f}}. \tag{4.8}$$

Substituting (3.6), (3.7), (3.8), (3.9), (3.10), (3.11), (4.7) and (4.8) in equation (4.2), we get:

$$a^2xf'^2(\eta) + (-a^2xf(\eta)f''(\eta)) = \nu_{hnf}\left(\frac{a^2xf'''(\eta)}{\nu_f}\right) - \frac{\sigma_{hnf}}{\rho_{hnf}}B_0^2\left(axf'(\eta)\right)$$
$$- \lambda_1\left[a\nu_f f^2(\eta)\left(\frac{a^2xf'''(\eta)}{\nu_f}\right) + 2(axf'(\eta))(-\sqrt{a\nu_f}f(\eta))\left(af''(\eta)\sqrt{\frac{a}{\nu_f}}\right)\right]$$
$$- \frac{\nu_{hnf}}{K_{p^*}}\left(axf'(\eta)\right).$$

$$\Rightarrow \quad a^2xf'^2(\eta) - a^2xf''(\eta)f(\eta) = \nu_{hnf}\frac{a^2xf'''(\eta)}{\nu_f} - \frac{\sigma_{hnf}}{\rho_{hnf}}B_0^2axf'(\eta) - \lambda_1a^3xf^2(\eta)f'''(\eta)$$
$$+ 2\lambda_1a^3xf(\eta)f'(\eta)f''(\eta) - \frac{\nu_{hnf}}{K_{p^*}}axf'(\eta).$$

$$\Rightarrow \quad a^2x\left[f'^2(\eta) - f''(\eta)f(\eta)\right] = a^2x\left[\nu_{hnf}\frac{f'''(\eta)}{\nu_f} - \frac{\sigma_{hnf}}{\rho_{hnf}}\frac{B_0^2}{a}f'(\eta) - \lambda_1af^2(\eta)f'''(\eta)\right.$$
$$\left. + 2\lambda_1af(\eta)f'(\eta)f''(\eta) - \frac{\nu_{hnf}}{K_{p^*}}\frac{f'(\eta)}{a}\right].$$

$$\Rightarrow \quad f'^2(\eta) - f''(\eta)f(\eta) = \nu_{hnf}\frac{f'''(\eta)}{\nu_f} - \frac{\sigma_{hnf}}{\rho_{hnf}}\frac{B_0^2}{a}f'(\eta) - \lambda_1af^2(\eta)f'''(\eta) +$$
$$2\lambda_1af(\eta)f'(\eta)f''(\eta) - \frac{\nu_{hnf}}{K_{p^*}}\frac{f'(\eta)}{a}.$$

$$\Rightarrow \quad -f'^2(\eta) + f''(\eta)f(\eta) + \nu_{hnf}\frac{f'''(\eta)}{\nu_f} - \frac{\sigma_{hnf}}{\rho_{hnf}}\frac{B_0^2}{a}f'(\eta) - \lambda_1af^2(\eta)f'''(\eta)$$
$$+ 2\lambda_1af(\eta)f'(\eta)f''(\eta) - \frac{\nu_{hnf}}{K_{p^*}}\frac{f'(\eta)}{a} = 0.$$

$$\Rightarrow \quad -f'^2(\eta) + f''(\eta)f(\eta) + \frac{\frac{\mu_{hnf}}{\mu_f}}{\frac{\rho_{hnf}}{\rho_f}}f'''(\eta) - \frac{\sigma_f(\frac{\sigma_{hnf}}{\sigma_f})}{\rho_f(\frac{\rho_{hnf}}{\rho_f})}\frac{B_0^2}{a}f'(\eta)$$
$$+ \lambda_1a\left(2f(\eta)f'(\eta)f''(\eta) - f^2(\eta)f'''(\eta)\right) - \frac{\frac{\mu_{hnf}}{\mu_f}}{\frac{\rho_{hnf}}{\rho_f}}\frac{\nu_f}{aK_{p^*}}f'(\eta) = 0.$$

$$\Rightarrow \quad \frac{\frac{\mu_{hnf}}{\mu_f}}{\frac{\rho_{hnf}}{\rho_f}}f'''(\eta) + f''(\eta)f(\eta) - f'^2(\eta) - \frac{\frac{\sigma_{hnf}}{\sigma_f}}{\frac{\rho_{hnf}}{\rho_f}}Mf'(\eta)$$
$$+ \beta\left(2f(\eta)f'(\eta)f''(\eta) - f^2(\eta)f'''(\eta)\right) - \frac{\frac{\mu_{hnf}}{\mu_f}}{\frac{\rho_{hnf}}{\rho_f}}K_1f'(\eta) = 0.$$

$$\Rightarrow \quad \frac{P_1}{P_2}f''' + f''f - f'^2 - \frac{P_3}{P_2}Mf' + \beta\left(2ff'f'' - f^2f'''\right) - \frac{P_1}{P_2}K_1f' = 0. \tag{4.9}$$

4.3.2 Non-dimensionalization of Energy Equation

In this section, we conduct the non-dimensionalization of the energy equation (4.3). In addition to those discussed in Chapter 3, the subsequent derivatives are essential for this conversion:

$$\frac{\partial^2 T}{\partial x \partial y} = \frac{\partial}{\partial x}\left(\frac{\partial T}{\partial y}\right) \tag{4.10}$$

$$\begin{aligned} \Rightarrow \quad \frac{\partial^2 T}{\partial y^2} &= \frac{\partial}{\partial y}\left[\theta'(\eta)\sqrt{\frac{a}{\nu_f}}\,(T_w - T_\infty)\right] \\ &= \theta''(\eta)\frac{a}{\nu_f}\,(T_w - T_\infty)\,. \end{aligned} \tag{4.11}$$

Substituting partial derivatives (3.6), (3.7), (3.14), (3.15), (3.16), (3.17), (3.20), (4.10) and (4.11) in (4.3), we get:

$$\begin{aligned} &-\sqrt{a\nu_f}f(\eta)\left(\theta'(\eta)\sqrt{\frac{a}{\nu_f}}(T_w - T_\infty)\right) + \lambda_2\Bigg[-\sqrt{a\nu_f}f(\eta)(-af'(\eta))\left(\theta'(\eta)\sqrt{\frac{a}{\nu_f}}\right) \\ &+ (a\nu_f f^2(\eta))\left(\theta''(\eta)\left(\frac{a}{\nu_f}\right)(T_w - T_\infty)\right)\Bigg] = \frac{k_{hnf}}{(\rho C_p)_{hnf}}\left[\theta''(\eta)\left(\frac{a}{\nu_f}\right)\right. \\ &\left.(T_w - T_\infty)\right] - \frac{1}{(\rho C_p)_{hnf}}\left[-\frac{16\sigma^*}{3k^*}T_\infty^3\left(\theta''(\eta)\left(\frac{a}{\nu_f}\right)(T_w - T_\infty)\right)\right] \\ &+ \frac{\sigma_{hnf}}{(\rho C_P)_{hnf}}B_0^2(a^2x^2f'^2(\eta)) + \frac{\mu_{hnf}}{(\rho C_P)_{hnf}}\left(\frac{a^3x^2f''^2(\eta)}{\nu_f}\right) \\ &+ \frac{Q_0}{(\rho C_p)_{hnf}}\Big[\theta(\eta)(T_w - T_\infty) + T_\infty - T_\infty\Big]. \end{aligned}$$

$$\begin{aligned} \Rightarrow \quad &-af(\eta)\theta'(\eta)(T_w - T_\infty) + \lambda_2\Big[a^2f(\eta)\theta'(\eta)f'(\eta)(T_w - T_\infty) + a^2f^2(\eta)\theta''(\eta) \\ &(T_w - T_\infty)\Big] = \frac{k_{hnf}}{(\rho C_p)_{hnf}}\theta''(\eta)\left(\frac{a}{\nu_f}\right)(T_w - T_\infty) + \frac{1}{(\rho C_p)_{hnf}}\frac{16\sigma^*}{3k^*}T_\infty^3\theta''(\eta) \\ &\left(\frac{a}{\nu_f}\right)(T_w - T_\infty) + \frac{\sigma_{hnf}}{(\rho C_P)_{hnf}}B_0^2a^2x^2f'^2(\eta) + \frac{\mu_{hnf}}{(\rho C_P)_{hnf}}\frac{a^3x^2f''^2(\eta)}{\nu_f} \\ &+ \frac{Q_0}{(\rho C_p)_{hnf}}\Big(\theta(\eta)(T_w - T_\infty)\Big). \end{aligned}$$

$$\begin{aligned} \Rightarrow \quad &-af(\eta)\theta'(\eta)(T_w - T_\infty) + \lambda_2a^2f(\eta)\theta'(\eta)f'(\eta)(T_w - T_\infty) + \lambda_2a^2f^2(\eta)\theta''(\eta) \\ &(T_w - T_\infty) = \frac{k_{hnf}}{(\rho C_p)_{hnf}}\theta''(\eta)\left(\frac{a}{\nu_f}\right)(T_w - T_\infty) + \frac{1}{(\rho C_p)_{hnf}}\frac{16\sigma^*}{3k^*}T_\infty^3\theta''(\eta) \\ &\left(\frac{a}{\nu_f}\right)(T_w - T_\infty) + \frac{\sigma_{hnf}}{(\rho C_P)_{hnf}}B_0^2a^2x^2f'^2(\eta) + \frac{\mu_{hnf}}{(\rho C_P)_{hnf}}\frac{a^3x^2f''^2(\eta)}{\nu_f} \\ &+ \frac{Q_0}{(\rho C_p)_{hnf}}\theta(\eta)(T_w - T_\infty). \end{aligned}$$

$$\Rightarrow \quad -a\Big(T_w - T_\infty\Big)\Big[-f(\eta)\theta'(\eta)+\lambda_2 a f(\eta)\theta'(\eta)f'(\eta)+\lambda_2 a f^2(\eta)\theta''(\eta)\Big]$$
$$= a\Big(T_w - T\infty\Big)\Big[\frac{k_{hnf}}{(\rho C_p)_{hnf}}\frac{\theta''(\eta)}{\nu_f}+\frac{1}{(\rho C_p)_{hnf}}\frac{16\sigma^*}{3k^*}T_\infty^3\left(\frac{\theta''(\eta)}{\nu_f}\right)$$
$$+\frac{\sigma_{hnf}}{(\rho C_P)_{hnf}}\left(\frac{B_0^2 a x^2}{(T_w-T_\infty)}\right)f'^2(\eta)+\frac{\mu_{hnf}}{(\rho C_P)_{hnf}}\frac{a^2x^2f''^2(\eta)}{\nu_f(T_w-T_\infty)}$$
$$+\frac{Q_0}{(\rho C_p)_{hnf}}\frac{\theta(\eta)}{a}\Big].$$

$$\Rightarrow \quad -f(\eta)\theta'(\eta)+\lambda_2 a f(\eta)\theta'(\eta)f'(\eta)+\lambda_2 a f^2(\eta)\theta''(\eta)=\frac{k_{hnf}}{(\rho C_p)_{hnf}}\frac{\theta''(\eta)}{\nu_f}$$
$$+\frac{1}{(\rho C_p)_{hnf}}\frac{16\sigma^*}{3k^*}T_\infty^3\left(\frac{\theta''(\eta)}{\nu_f}\right)+\frac{\sigma_{hnf}}{(\rho C_P)_{hnf}}\left(\frac{B_0^2 a x^2}{(T_w-T_\infty)}\right)f'^2(\eta)$$
$$+\frac{\mu_{hnf}}{(\rho C_P)_{hnf}}\frac{a^2x^2f''^2(\eta)}{\nu_f(T_w-T_\infty)}+\frac{Q_0}{(\rho C_p)_{hnf}}\frac{\theta(\eta)}{a}.$$

$$\Rightarrow \quad f(\eta)\theta'(\eta)-\lambda_2 a f(\eta)\theta'(\eta)f'(\eta)-\lambda_2 a f^2(\eta)\theta''(\eta)+\frac{k_{hnf}}{(\rho C_p)_{hnf}}\frac{\theta''(\eta)}{\nu_f}$$
$$+\frac{1}{(\rho C_p)_{hnf}}\frac{16\sigma^*}{3k^*}T_\infty^3\left(\frac{\theta''(\eta)}{\nu_f}\right)+\frac{\sigma_{hnf}}{(\rho C_P)_{hnf}}\left(\frac{B_0^2 a x^2}{(T_w-T_\infty)}\right)f'^2(\eta)$$
$$+\frac{\mu_{hnf}}{(\rho C_P)_{hnf}}\frac{a^2x^2f''^2(\eta)}{\nu_f(T_w-T_\infty)}+\frac{Q_0}{(\rho C_p)_{hnf}}\frac{\theta(\eta)}{a}=0.$$

$$\Rightarrow \quad f(\eta)\theta'(\eta)-\lambda_2 a\Big(f(\eta)\theta'(\eta)f'(\eta)+f^2(\eta)\theta''(\eta)\Big)+\frac{k_f\left(\frac{k_{hnf}}{k_f}\right)}{(\rho C_p)_f\left(\frac{(\rho C_p)_{hnf}}{(\rho C_p)f}\right)}\frac{\theta''(\eta)}{\nu_f}$$
$$+\frac{1}{(\rho C_p)_{hnf}}\frac{16\sigma^*}{3k^*}T_\infty^3\left(\frac{\theta''(\eta)}{\nu_f}\right)+\frac{\sigma_f\left(\frac{\sigma_{hnf}}{\sigma_f}\right)}{(\rho C_p)_f\left(\frac{(\rho C_p)_{hnf}}{(\rho C_p)_f}\right)}\left(\frac{B_0^2a^2x^2}{a(T_w-T_\infty)}\right)f'^2(\eta)$$
$$+\frac{\mu_f\left(\frac{\mu_{hnf}}{\mu_f}\right)}{(\rho C_p)_f\left(\frac{(\rho C_p)_{hnf}}{(\rho C_p)_f}\right)}\frac{a^2x^2f''^2(\eta)}{\nu_f(T_w-T_\infty)}+\frac{Q_0}{(\rho C_p)_f\left(\frac{(\rho C_p)_{hnf}}{(\rho C_p)_f}\right)}\frac{\theta(\eta)}{a}=0.$$

$$\Rightarrow \quad f(\eta)\theta'(\eta)-\delta\Big(f(\eta)\theta'(\eta)f'(\eta)+f^2(\eta)\theta''(\eta)\Big)+\frac{1}{P_r}\frac{1}{\frac{(\rho C_p)_{hnf}}{(\rho C_p)_p}}\left(\frac{k_{hnf}}{k_f}+\frac{4}{3}R\right)\theta''(\eta)$$
$$+\frac{\frac{\sigma_{hnf}}{\sigma_f}}{\frac{(\rho C_p)_{hnf}}{(\rho C_p)_f}}ME_cf'^2(\eta)+\frac{\frac{\mu_{hnf}}{\mu_f}}{\frac{(\rho C_p)_{hnf}}{(\rho C_p)_f}}E_cf''^2(\eta)+\frac{1}{\frac{(\rho C_p)_h nf}{(\rho C_p)_f}}Q\theta(\eta)=0.$$

$$\Rightarrow \quad \frac{1}{P_r}\frac{1}{\frac{(\rho C_p)_{hnf}}{(\rho C_p)_p}}\left(\frac{k_{hnf}}{k_f}+\frac{4}{3}R\right)\theta''(\eta)+\theta'(\eta)f(\eta)+\frac{\frac{\sigma_{hnf}}{\sigma_f}}{\frac{(\rho C_p)_{hnf}}{(\rho C_p)_f}}ME_cf'^2(\eta)$$
$$+\frac{\frac{\mu_{hnf}}{\mu_f}}{\frac{(\rho C_p)_{hnf}}{(\rho C_p)_f}}E_cf''^2(\eta)-\delta\Big(f(\eta)f'(\eta)\theta'(\eta)+f^2(\eta)\theta''(\eta)\Big)+\frac{1}{\frac{(\rho C_p)_h nf}{(\rho C_p)_f}}Q\theta(\eta)=0.$$

$$\Rightarrow \quad \frac{1}{P_rP_4}\left(\frac{k_{hnf}}{k_f}+\frac{4}{3}R\right)\theta''+f\theta'+\frac{P_3}{P_4}ME_cf'^2$$
$$+\frac{P_1}{P_4}E_cf''^2-\delta\Big(f\theta'f'+f^2\theta''\Big)+\frac{1}{P_4}Q\theta=0. \tag{4.12}$$

4.3.3 Non-dimensionalization of Concentration Equation

Here, we examine the non-dimensionalization procedure for the concentration equation (4.4) in our hybrid nanofluid model. The subsequent derivatives are required for this purpose:

$$\phi(\eta) = \frac{C - C_\infty}{C_w - C_\infty}$$

$$\Rightarrow \quad C = \phi(\eta)(C_w - C_\infty) + C_\infty. \tag{4.13}$$

$$\Rightarrow \quad \frac{\partial C}{\partial y} = \phi'(\eta)\sqrt{\frac{a}{\nu_f}}(C_w - C_\infty). \tag{4.14}$$

$$\begin{aligned} \Rightarrow \quad \frac{\partial^2 C}{\partial y^2} &= \frac{\partial}{\partial y}\left(\frac{\partial C}{\partial y}\right) \\ &= \frac{\partial}{\partial y}\left(\phi'(\eta)\sqrt{\frac{a}{\nu_f}}(C_w - C_\infty)\right). \\ &= \phi''(\eta)\frac{a}{\nu_f}(C_w - C_\infty). \end{aligned} \tag{4.15}$$

Using (4.13), we have:

$$\frac{\partial C}{\partial x} = 0. \tag{4.16}$$

Now, substituting the partial derivatives (4.13), (4.14), (4.15) and (4.16) in equation (4.4), we get:

$$\begin{aligned} -\sqrt{a\nu_f} f(\eta)\left(\phi'(\eta)\sqrt{\frac{a}{\nu_f}}(C_w - C_\infty)\right) &= \left(\phi''(\eta)\left(\frac{a}{\nu_f}\right)(C_w - C_\infty)\right) D_B \\ &+ \left(\theta''(\eta)\left(\frac{a}{\nu_f}\right)(T_w - T_\infty)\right)\frac{D_T}{T_\infty} + K_r\Big(C_\infty - (\phi(\eta)(C_w - C_\infty) + C_\infty)\Big). \end{aligned}$$

$$\begin{aligned} \Rightarrow \quad -af(\eta)\phi'(\eta)(C_w - C_\infty) &= \phi''(\eta)\left(\frac{a}{\nu_f}\right)(C_w - C_\infty)D_B \\ &+ \theta''(\eta)\left(\frac{a}{\nu_f}\right)(T_w - T_\infty)\frac{D_T}{T_\infty} + K_r C_\infty - K_r\phi(\eta)(C_w - C_\infty) - K_r C_\infty. \end{aligned}$$

$$\begin{aligned} \Rightarrow \quad -af(\eta)\phi'(\eta)(C_w - C_\infty) &= \phi''(\eta)\left(\frac{a}{\nu_f}\right)(C_w - C_\infty)D_B \\ &+ \theta''(\eta)\left(\frac{a}{\nu_f}\right)(T_w - T_\infty)\frac{D_T}{T_\infty} - K_r\phi(\eta)(C_w - C_\infty). \end{aligned}$$

$$\begin{aligned} \Rightarrow \quad -a\Big(C_w - C_\infty\Big)f(\eta)\phi'(\eta) = &a\Big(C_w - C_\infty\Big)\left[\frac{\phi''(\eta)}{\nu_f}D_B + \frac{\theta''(\eta)}{\nu_f}\frac{(T_w - T_\infty)}{(C_w - C_\infty)}\frac{D_T}{T_\infty}\right. \\ &\left. - \frac{K_r\phi(\eta)}{a}\right]. \end{aligned}$$

$$\Rightarrow \quad -f(\eta)\phi'(\eta) = \frac{\phi''(\eta)}{\nu_f}D_B + \frac{\theta''(\eta)}{\nu_f}\frac{(T_w - T_\infty)}{(C_w - C_\infty)}\frac{D_T}{T_\infty} - \frac{K_r\phi(\eta)}{a}.$$

$$\Rightarrow \quad -f(\eta)\phi'(\eta) = \frac{D_B}{\nu_f}\left[\phi''(\eta) + \frac{\theta''(\eta)}{D_B}\frac{(T_w - T_\infty)}{(C_w - C_\infty)}\frac{D_T}{T_\infty} - \frac{K_r\phi(\eta)}{a}\frac{\nu_f}{D_B}\right].$$

$$\Rightarrow \quad -\frac{\nu_f f(\eta)\phi'(\eta)}{D_B} = \phi''(\eta) + \frac{\theta''(\eta)}{D_B}\frac{(T_w - T_\infty)}{(C_w - C_\infty)}\frac{D_T}{T_\infty} - \frac{K_r\phi(\eta)}{a}\frac{\nu_f}{D_B}.$$

$$\Rightarrow \quad \phi''(\eta) + \frac{\nu_f f(\eta)\phi'(\eta)}{D_B} + \frac{\theta''(\eta)}{D_B}\frac{(T_w - T_\infty)}{(C_w - C_\infty)}\frac{D_T}{T_\infty} - \frac{K_r\phi(\eta)}{a}\frac{\nu_f}{D_B} = 0.$$

$$\Rightarrow \quad \phi'' + Le\phi' f' + \frac{N_t}{N_b}\theta'' - \Gamma\phi = 0. \tag{4.17}$$

4.3.4 Dimensionless form of Boundary Conditions

To transform the BCs into non-dimensional form, the following detailed procedure has been systematically carried out:

- $u = \lambda u_w(x), \qquad at \quad y = 0.$

  $\Rightarrow \; axf'(\eta) = \lambda ax, \qquad at \quad \eta = 0.$

  $\Rightarrow \; f(\eta) = \lambda, \qquad at \quad \eta = 0.$

  $\Rightarrow \; f(0) = \lambda.$

- $v = v_0, \qquad at \quad y = 0.$

  $\Rightarrow \; -\sqrt{a\nu_f}f(\eta) = -\sqrt{a\nu_f}S, \qquad at \quad \eta = 0.$

  $\Rightarrow \; f(\eta) = S, \qquad at \quad \eta = 0.$

  $\Rightarrow \; f(0) = S.$

- $T = T_w + A\dfrac{\partial T}{\partial y}, \qquad at \quad y = 0.$

  $\Rightarrow \quad \theta(\eta)\big(T_w - T_\infty\big) + T_\infty = T_w + A\left(\theta'(\eta)\sqrt{\dfrac{a}{\nu_f}}(T_w - T_\infty)\right), \qquad at \quad \eta = 0.$

  $\Rightarrow \quad \theta(\eta)\big(T_w - T_\infty\big) + T_\infty = T_w + A\theta'(\eta)\sqrt{\dfrac{a}{\nu_f}}(T_w - T_\infty), \qquad at \quad \eta = 0.$

  $\Rightarrow \quad \theta(\eta)\big(T_w - T_\infty\big) = (T_w - T_\infty) + A\theta'(\eta)\sqrt{\dfrac{a}{\nu_f}}(T_w - T_\infty), \qquad at \quad \eta = 0.$

  $\Rightarrow \quad \theta(\eta) = \dfrac{(T_w - T_\infty)}{(T_w - T_\infty)} + A\theta'(\eta)\sqrt{\dfrac{a}{\nu_f}}\dfrac{(T_w - T_\infty)}{(T_w - T_\infty)}, \qquad at \quad \eta = 0.$

  $\Rightarrow \quad \theta(\eta) = 1 + A\theta'(\eta)\sqrt{\dfrac{a}{\nu_f}}, \qquad at \quad \eta = 0.$

$\Rightarrow \quad \theta(\eta) = 1 + \gamma\ \theta'(\eta), \qquad at \quad \eta = 0.$

$\Rightarrow \quad \theta(0) = 1 + \gamma\ \theta'(0).$

- $C = C_w, \qquad at \quad y = 0.$

$\Rightarrow \quad \phi(\eta)(C_w - C_\infty) + C_\infty = C_w, \qquad at \quad \eta = 0.$

$\Rightarrow \quad \phi(\eta)(C_w - C_\infty) = (C_w - C_\infty), \qquad at \quad \eta = 0.$

$\Rightarrow \quad \phi(\eta) = \dfrac{(C_w - C_\infty)}{(C_w - C_\infty)}, \qquad at \quad \eta = 0.$

$\Rightarrow \quad \phi(\eta) = 1, \qquad at \quad \eta = 0.$

$\Rightarrow \quad \phi(0) = 1.$

- $u \longrightarrow 0, \qquad as\ y \longrightarrow \infty.$

$\Rightarrow \quad axf'(\eta) \longrightarrow 0, \qquad as\ \eta \longrightarrow \infty.$

$\Rightarrow \quad f'(\eta) \longrightarrow 0, \qquad as\ \eta \longrightarrow \infty.$

$\Rightarrow f'(\infty) \longrightarrow 0.$

- $T \longrightarrow T_\infty, \qquad as\ y \longrightarrow \infty.$

$\Rightarrow \quad \theta(\eta)\big(T_w - T_\infty\big) + T_\infty \longrightarrow T_\infty, \qquad as\ \eta \longrightarrow \infty.$

$\Rightarrow \theta(\eta) \longrightarrow 0, \qquad as\ \eta \longrightarrow \infty.$

$\Rightarrow \theta(\infty) \longrightarrow 0.$

- $C \longrightarrow C_\infty, \qquad as\ y \longrightarrow \infty.$

$\Rightarrow \quad \phi(\eta)\big(C_w - C_\infty\big) + C_\infty \longrightarrow C_\infty, \qquad as\ \eta \longrightarrow \infty.$

$\Rightarrow \quad \phi(\eta)\big(C_w - C_\infty\big) \longrightarrow 0, \qquad as\ \eta \longrightarrow \infty.$

$\Rightarrow \phi(\eta) \longrightarrow 0, \qquad as\ \eta \longrightarrow \infty.$

$\Rightarrow \phi(\infty) \longrightarrow 0.$

4.4 Solution Framework

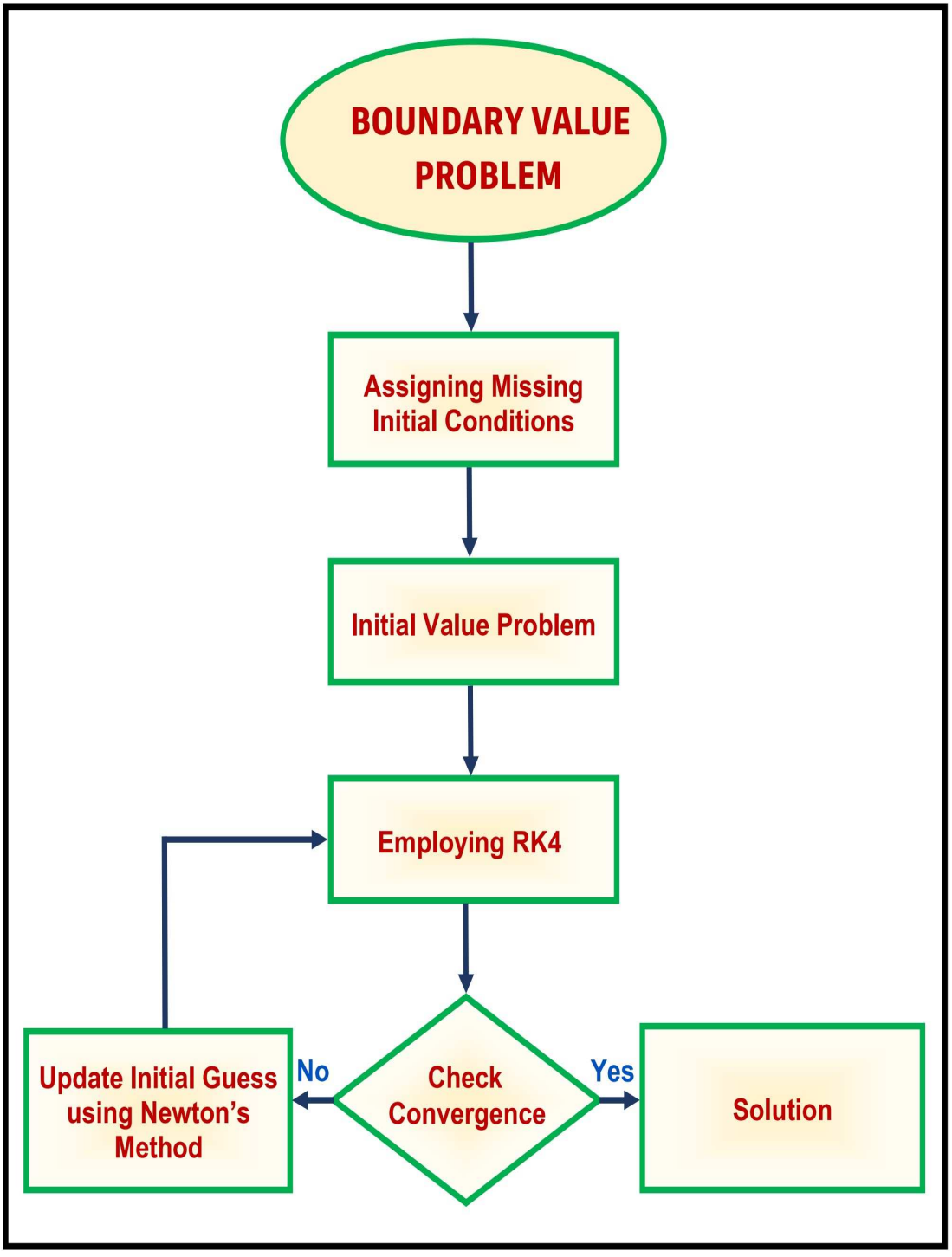

FIGURE 4.2: Shooting method's methodological framework

The numerical solutions are derived through the application of the shooting method Figure 4.2, which incorporates the Runge-Kutta method of order four ($RK4$) technique and the Newton's method. To address the ordinary differential equation (4.9), we introduce the following notations:

$$f(\eta) = \widetilde{M_1},$$
$$f'(\eta) = \widetilde{M_1'} = \widetilde{M_2},$$
$$f''(\eta) = \widetilde{M_2'} = \widetilde{M_3}.$$

The following system of first order ODEs has been obtained to replace the momentum equation:

$$\left.\begin{aligned}
\widetilde{M_1'} &= \widetilde{M_2}, && \widetilde{M_1}(0) = S,\\
\widetilde{M_2'} &= \widetilde{M_3}, && \widetilde{M_2}(0) = \lambda,\\
\widetilde{M_3'} &= -\frac{1}{\left(\frac{P_1}{P_2} - \beta\widetilde{M_1'}^2\right)}\Bigg[\widetilde{M_1'}\widetilde{M_3'} - \widetilde{M_2'}^2 - \frac{P_3}{P_2}M\widetilde{M_2'} && \\
&\quad + 2\beta\widetilde{M_1'}\widetilde{M_2'}\widetilde{M_3'} - \frac{P_1}{P_2}K_1\widetilde{M_2'}\Bigg], && \widetilde{M_3}(0) = \widetilde{q_1}.
\end{aligned}\right\} \quad (4.18)$$

In order to address the initial value problem described above, we will identify the missing initial condition for its numerical solution through the application of Runge-Kutta method of order four ($RK4$). The condition labeled as $\widetilde{q_1}$ must be selected to ensure that:

$$\widetilde{M_2}\big(\eta_\infty, \widetilde{q_1}\big) = 0.$$

Newton's method will be employed for computing the approximate value of $\widetilde{q_1}$, utilizing the following iterative scheme:

$$\widetilde{q_1}^{(n+1)} = \widetilde{q_1}^{(n)} - \frac{\widetilde{M_2}\big(\eta_\infty, \widetilde{q_1}^{(n)}\big)}{\left(\frac{\partial}{\partial\widetilde{q_1}}\widetilde{M_2}\big(\eta_\infty, \widetilde{q_1}\big)\right)^{(n)}}.$$

We further introduce the following notations:

$$\frac{\partial\widetilde{M_1}}{\partial\widetilde{q_1}} = \widetilde{M_4},$$
$$\frac{\partial\widetilde{M_2}}{\partial\widetilde{q_1}} = \widetilde{M_5},$$
$$\frac{\partial\widetilde{M_3}}{\partial\widehat{q_1}} = \widetilde{M_6}.$$

As a consequences of implementing the new scheme, Newtons iterative scheme takes the following form:

$$\widetilde{q_1}^{(n+1)} = \widetilde{q_1}^{(n)} - \frac{\widetilde{M_2}(\eta_\infty, \widetilde{q_1}^{(n)})}{\widetilde{M_5}(\eta_\infty, \widetilde{q_1}^{(n)})}.$$

Differentiating the system (4.18) w.r.t q_1, the following IVP is obtained:

$$\left.\begin{aligned}
\widetilde{M}_4' &= \widetilde{M}_5, && \widetilde{M}_4(0) = 0,\\
\widetilde{M}_5' &= \widetilde{M}_6, && \widetilde{M}_5(0) = 0,\\
\widetilde{M}_6' &= -\frac{1}{\left(\frac{P_1}{P_2} - \beta\widetilde{M}_1{}^2\right)^2}\Bigg[\left(\frac{P_1}{P_2} - \beta\widetilde{M}_1{}^2\right)\left(\widetilde{M}_1\widetilde{M}_6 + \widetilde{M}_3\widetilde{M}_4\right.\\
&\quad - 2\widetilde{M}_2\widetilde{M}_5 - \frac{P_3}{P_2}M\widetilde{M}_5 + 2\beta\widetilde{M}_4\widetilde{M}_2\widetilde{M}_3 + 2\beta\widetilde{M}_1\widetilde{M}_5\widetilde{M}_3\\
&\quad \left. + 2\beta\widetilde{M}_1\widetilde{M}_2\widetilde{M}_6 - \frac{P_1}{P_2}K_1\widetilde{M}_5\right) - \left(\widetilde{M}_1\widetilde{M}_3 - \widetilde{M}_2{}^2 - \frac{P_3}{P_2}M\widetilde{M}_2\right.\\
&\quad \left. + 2\beta\widetilde{M}_1\widetilde{M}_2\widetilde{M}_3 - \frac{P_1}{P_2}K_1\widetilde{M}_2\right)\left(-2\beta\widetilde{M}_1\widetilde{M}_4\right)\Bigg], && \widetilde{M}_6(0) = 1.
\end{aligned}\right\} \tag{4.19}$$

Now, writing together (4.18) and (4.19), the following IVP can be written:

$$\left.\begin{aligned}
\widetilde{M}_1' &= \widetilde{M}_2, && \widetilde{M}_1(0) = S,\\
\widetilde{M}_2' &= \widetilde{M}_3, && \widetilde{M}_2(0) = \lambda,\\
\widetilde{M}_3' &= -\frac{1}{\left(\frac{P_1}{P_2} - \beta\widetilde{M}_1'{}^2\right)}\left[\widetilde{M}_1'\widetilde{M}_3' - \widetilde{M}_2'{}^2 - \frac{P_3}{P_2}M\widetilde{M}_2'\right.\\
&\quad \left. + 2\beta\widetilde{M}_1'\widetilde{M}_2'\widetilde{M}_3' - \frac{P_1}{P_2}K_1\widetilde{M}_2'\right], && \widetilde{M}_3(0) = \widetilde{q}_1.\\
\widetilde{M}_4' &= \widetilde{M}_5, && \widetilde{M}_4(0) = 0,\\
\widetilde{M}_5' &= \widetilde{M}_6, && \widetilde{M}_5(0) = 0,\\
\widetilde{M}_6 &= -\frac{1}{\left(\frac{P_1}{P_2} - \beta\widetilde{M}_1{}^2\right)^2}\Bigg[\left(\frac{P_1}{P_2} - \beta\widetilde{M}_1{}^2\right)\left(\widetilde{M}_1\widetilde{M}_6 + \widetilde{M}_3\widetilde{M}_4\right.\\
&\quad - 2\widetilde{M}_2\widetilde{M}_5 - \frac{P_3}{P_2}M\widetilde{M}_5 + 2\beta\widetilde{M}_4\widetilde{M}_2\widetilde{M}_3 + 2\beta\widetilde{M}_1\widetilde{M}_5\widetilde{M}_3\\
&\quad \left. + 2\beta\widetilde{M}_1\widetilde{M}_2\widetilde{M}_6 - \frac{P_1}{P_2}K_1\widetilde{M}_5\right) - \left(\widetilde{M}_1\widetilde{M}_3 - \widetilde{M}_2{}^2 - \frac{P_3}{P_2}M\widetilde{M}_2\right.\\
&\quad \left. + 2\beta\widetilde{M}_1\widetilde{M}_2\widetilde{M}_3 - \frac{P_1}{P_2}K_1\widetilde{M}_2\right)\left(-2\beta\widetilde{M}_1\widetilde{M}_4\right)\Bigg], && \widetilde{M}_6(0) = 1.
\end{aligned}\right\} \tag{4.20}$$

The above system (4.20), will be solved numerically by the $RK4$ method. The stopping criteria for the Newton's technique is set as:

$$\left|\widetilde{M}_2\left(\eta_\infty, q_1\right) - 0\right| < \epsilon.$$

Now, to solve equation (4.12), treating f, f' and f'' as known, we again apply the

shooting method. To implement the shooting method, the subsequent notations are utilized:

$$\theta(\eta) = \widetilde{N_1},$$
$$\theta'(\eta) = \widetilde{N_1'} = \widetilde{N_2}.$$

The system of equation (4.12), can be expressed in the following form of the first-order ODE:

$$\left.\begin{aligned} \widetilde{N_1'} &= \widetilde{N_2}, && \widetilde{N_1}(0) = 1 + \gamma n_1, \\ \widetilde{N_2'} &= -\frac{1}{\frac{1}{P_r P_4}\left(P_5 + \frac{4}{3}R\right) - \delta f^2(\eta)}\Bigg[f(\eta)\widetilde{N_1} + \frac{P_3}{P_4} M E_c f'^2(\eta) \\ &\quad + \frac{P_1}{P_4} M E_c f''^2(\eta) - \delta f(\eta) f'(\eta)\widetilde{N_2} + \frac{1}{P_4} Q \widetilde{N_1}\Bigg], && \widetilde{N_2}(0) = n_1. \end{aligned}\right\} \quad (4.21)$$

To utilize the RK4 method for the numerical solution of above IVP, the missing condition n_1 within the system of equations needs to be carefully chosen. The missing condition n_1 needs to be selected in such a way that:

$$\widetilde{N_2}\left(\eta_\infty, n_1\right) = 0.$$

Newton's Method will be used for the solution of the above equation for n_1, which has the following iterative scheme:

$$n_1^{(n+1)} = n_1^{(n)} - \frac{\widetilde{N_2}\left(\eta_\infty, n_1^{(n)}\right)}{\left(\frac{\partial}{\partial n_1}\widetilde{N_2}\left(\eta_\infty, n_1\right)\right)^{(n)}}.$$

We further introduce the following notations:

$$\frac{\partial \widetilde{N_1}}{\partial n_1} = \widetilde{N_3}, \quad \frac{\partial \widetilde{N_2}}{\partial n_1} = \widetilde{N_4}.$$

As a consequence of the newly introduced notations, Newtons iterative scheme gets to the following form:

$$n_1^{(n+1)} = n_1^{(n)} - \frac{\widetilde{N_2}(\eta_\infty, n_1^{(n)})}{\widetilde{N_4}(\eta_\infty, n_1^{(n)})}.$$

Now differentiating the system of two first order ODEs (4.21) with respect to n_1, we get another system of ODEs as follows:

$$\left.\begin{aligned} \widetilde{N_3'} &= \widetilde{N_4}, && \widetilde{N_3}(0) = \gamma, \\ \widetilde{N_4'} &= -\frac{1}{\frac{1}{P_r P_4}\left(P_5 + \frac{4}{3}R\right)}\left[f(\eta)\widetilde{N_3} - \delta f(\eta) f'(\eta)\widetilde{N_4} + \frac{1}{P_4} Q \widetilde{N_3}\right], && \widetilde{N_4}(0) = 1. \end{aligned}\right\} \quad (4.22)$$

From (4.21) and (4.22), the following IVP can be written:

$$\left.\begin{aligned}
&\widetilde{N_1'} = \widetilde{N_2}, && \widetilde{N_1}(0) = 1+\gamma n_1,\\
&\widetilde{N_2'} = -\frac{1}{\frac{1}{P_r P_4}\left(P_5+\frac{4}{3}R\right)-\delta f^2(\eta)}\Big[f(\eta)\widetilde{N_1}+\frac{P_3}{P_4}ME_c f'^2(\eta)\\
&\qquad +\frac{P_1}{P_4}ME_c f''^2(\eta)-\delta f(\eta)f'(\eta)\widetilde{N_2}+\frac{1}{P_4}Q\widetilde{N_1}\Big], && \widetilde{N_2}(0) = n_1.\\
&\widetilde{N_3'} = \widetilde{N_4}, && \widetilde{N_3}(0) = \gamma,\\
&\widetilde{N_4'} = -\frac{1}{\frac{1}{P_r P_4}\left(P_5+\frac{4}{3}R\right)}\left[f(\eta)\widetilde{N_3}-\delta f(\eta)f'(\eta)\widetilde{N_4}+\frac{1}{P_4}Q\widetilde{N_3}\right], && \widetilde{N_4}(0) = 1.
\end{aligned}\right\} \tag{4.23}$$

The above system (4.23), will be solved numerically by the $RK4$ method. The predefined stopping criteria for the Newton's technique is:

$$\left|\widetilde{N}_2\left(\eta_\infty, n_1\right)-0\right| < \epsilon.$$

Now to solve (4.17) numerically by using the shooting method, treating f, f', f'', θ and θ' as known functions, the following notations are utilized:

$$\begin{aligned}
\phi(\eta) &= \widetilde{N_5},\\
\phi'(\eta) &= \widetilde{N_5'} = \widetilde{N_6}.
\end{aligned}$$

The system of equation (4.17), can be represented in the form of following first-order ODEs:

$$\left.\begin{aligned}
&\widetilde{N_5'} = \widetilde{N_6}, && \widetilde{N_5}(0) = 1,\\
&\widetilde{N_6'} = -\Big[L_e f\widetilde{N_6}+\frac{N_t}{N_b}\Big(-\frac{1}{\frac{1}{P_r P_4}\left(P_5+\frac{4}{3}R\right)-\delta f^2(\eta)}\Big[f(\eta)\widetilde{N_1}\\
&\qquad +\frac{P_3}{P_4}ME_c f'^2(\eta)+\frac{P_1}{P_4}ME_c f''^2(\eta)-\delta f(\eta)f'(\eta)\widetilde{N_2}\\
&\qquad +\frac{1}{P_4}Q\widetilde{N_1}\Big)\Big]-\Gamma\widetilde{N_5}\Big], && \widetilde{N_6}(0) = p_1.
\end{aligned}\right\} \tag{4.24}$$

In order to address the initial value problem (4.24), we will identify the missing initial condition p_1 for its numerical solution through the application of Runge-Kutta method. The condition labeled as p_1 must be selected to ensure that:

$$\widetilde{N_6}\left(\eta_\infty, p_1\right) = 0.$$

Newton's Method will be employed for the updation of p_1, utilizing the following iterative scheme:

$$p_1^{(n+1)} = p_1^{(n)} - \frac{\widetilde{N_6}\left(\eta_\infty, p_1^{(n)}\right)}{\left(\frac{\partial}{\partial p_1}\widetilde{N_6}\left(\eta_\infty, p_1\right)\right)^{(n)}}.$$

Furthermore, we introduce the following notations:

$$\frac{\partial \widetilde{N_5}}{\partial p_1} = \widetilde{N_7}, \quad \frac{\partial \widetilde{N_6}}{\partial p_1} = \widetilde{N_8}.$$

As a result of newly adopted notations, Newtons iterative scheme takes the form:

$$p_1^{(n+1)} = p_1^{(n)} - \frac{\widetilde{N_6}(\eta_\infty, p_1^{(n)})}{\widetilde{N_8}(\eta_\infty, p_1^{(n)})}. \tag{4.25}$$

Now differentiating (4.24) with respect to p_1, we get another system of ODEs as follows:

$$\left.\begin{aligned} \widetilde{N_7'} &= \widetilde{N_8}, & \widetilde{N_7}(0) &= 0, \\ \widetilde{N_8'} &= -\left[L_e f \widetilde{N_8} - \Gamma \widetilde{N_7}\right], & \widetilde{N_8}(0) &= 1. \end{aligned}\right\} \tag{4.26}$$

Writing together (4.24) and (4.26), the following IVP can be written:

$$\left.\begin{aligned} \widetilde{N_5'} &= \widetilde{N_6}, & \widetilde{N_5}(0) &= 1, \\ \widetilde{N_6'} &= -\Bigg[L_e f \widetilde{N_6} + \frac{N_t}{N_b}\Bigg(- \frac{1}{\frac{1}{P_r P_4}\left(P_5 + \frac{4}{3}R\right) - \delta f^2(\eta)}\Bigg[f(\eta)\widetilde{N_1} \\ &\quad + \frac{P_3}{P_4} M E_c f'^2(\eta) + \frac{P_1}{P_4} M E_c f''^2(\eta) - \delta f(\eta) f'(\eta)\widetilde{N_2} \\ &\quad + \frac{1}{P_4} Q \widetilde{N_1}\Bigg)\Bigg] - \Gamma \widetilde{N_5}\Bigg], & \widetilde{N_6}(0) &= p_1. \\ \widetilde{N_7'} &= \widetilde{N_8}, & \widetilde{N_7}(0) &= 0, \\ \widetilde{N_8'} &= -\left[L_e f \widetilde{N_8} - \Gamma \widetilde{N_7}\right], & \widetilde{N_8}(0) &= 1. \end{aligned}\right\} \tag{4.27}$$

The stopping criteria for the Newton's technique is set as:

$$\left|\widetilde{N_6}\left(\eta_\infty, p_1\right) - 0\right| < \epsilon. \tag{4.28}$$

4.5 Results Interpretation

While transforming the governing partial differential equations (PDEs) related to the modeled fluid flow into a system of ordinary differential equations, several dimensionless parameters become crucial. The significant influence of these physical parameters on the distributions of velocity $f'(\eta)$, temperature $\theta(\eta)$ and nanoparticle concentration $\phi(\eta)$ is extensively explored

through graphical representations. A detailed examination for the significance and interpretations of each parameter's contribution is conducted, and the results of the study are presented in a comprehensive manner.

4.5.1 Analysis of Computational Results

This study examines the significant impact of different physical parameters on the skin friction coefficient, the local Nusselt number, and the local Sherwood number. The numerical findings are collected in Tables 4.2, 4.3 and 4.4. An increment in the magnetic field strength (M) under assumption of suction ($S = 0.5$) leads to a decrease in both the skin friction coefficient and the Nusselt number. Additionally, due to an increase in the Maxwell parameter (β), the skin friction reduces. Furthermore, an increment in the porosity medium also contributes to a reduction in the skin friction.

As the radiation parameter (R) is increased, the Nusselt number also experiences an increase. On the other hand, an increase in the parameter γ leads to a decrease in the Nusselt number. The parameter δ is linked to the Cattaneo-Christov heat flux model. When δ is increased, the temperature profile rises. Conversely, a decrease in δ results in a lower Nusselt number. Moreover, an increase in the heat source causes a decline in the Nusselt number when λ is set to 1.0.

TABLE 4.2: The numerical results of the Skin friction $\left(\sqrt{Re_x}C_f\right)$, when $L = 1.0$ and $S = 0.5$.

ϕ_1	ϕ_2	M	β	K_1	$Re_x^{1/2}C_f$
0.01	0.1	0.1	0.01	0.01	-1.929706
0.02					-1.970605
0.03					-2.012158
0.05					-2.097325
	0.02				-1.487293
	0.03				-1.540478
	0.05				-1.648456
		0			-1.870790
		0.4			-2.094323
		0.8			-2.291834
			0.03		-1.963307
			0.07		-2.031871
			0.1		-2.084508
				0.1	-1.980917
				0.5	-2.191041
				1	-2.423459

An increase in the Lewis number is associated with a corresponding rise in the Sherwood number, transitioning from negative to positive values. In contrast, an increase in the thermophoresis

parameter (Nt) results in a decrease in the Sherwood number. In practical scenarios, as (Nt) increases, the fluid accelerates rapidly, which enhances the kinetic energy and contributes to the expansion of the boundary layer. Furthermore, increasing the parameters related to the Brownian motion (Nb) and chemical reactions (Γ) directly contribute to an increase in the Sherwood number. Physically, as the quantity of Nb rises, the random acceleration diminishes, thereby facilitating a quicker transition of fluid particles from elevated regions to lower areas.

TABLE 4.3: The numerical results of the Nusselt number $\left(Re^{-1/2}Nu_x\right)$, when $\phi_1 = 0.01$ and $\phi_2 = 0.1$, $P_r = 6.2$, $S = 0.5$, $\beta = K_1 = 0.01$.

M	R	λ	δ	γ	E_c	Q	$Re^{-1/2}Nu_x$
0.1	0.1	1.0	0.1	0.1	0.1	0.1	3.148411
0.2							3.108596
0.3							3.070302
0.4							3.033371
	0.4						3.374513
	0.8						3.607351
	1.2						3.788373
		0.2					2.869711
		0.5					3.106624
		0.8					3.178989
			0.03				2.895623
			0.06				2.999971
			0.09				3.110256
				0			4.234791
				0.5			1.553890
				1			0.951517
					0.3		2.242180
					0.5		1.335950
					0.7		0.429719
						0.5	2.710632
						1	1.922679
						1.5	0.451126

TABLE 4.4: The numerical results of the Sherwood number $\left(Re^{-1/2}Sh_x\right)$, when $\lambda = 1.0$, S=0.5, $M = 0.1$, $\beta = K_1 = 0.01$, $\phi_1 = 0.01$, $\phi_2 = 0.1$, $P_r = 6.2$, $\gamma = E_c = R = \delta = Q = 0.1$.

L_e	N_t	N_b	Γ	$Re^{-1/2}Sh_x$
1.0	0.1	0.1	0.1	-0.992260
1.5				-0.614160
2.0				-0.255651
2.5				0.086632
	0.2			-2.968314
	0.3			-4.944367
	0.4			-6.920420
		0.4		0.489779
		0.8		0.736785
		1.2		0.819121
			0.5	-0.600527
			1.0	-0.239409
			1.5	0.050004

4.5.2 Velocity Profile

Analyzing the velocity distribution, is fundamental for a comprehensive understanding of fluid flow and its related attributes. The dynamics of flowing fluids are expected to be influenced by the external forces. One prominent external force in this scenario is the magnetic field. Figures 4.3 to 4.6 illustrate the characteristics of the velocity profile, represented as $f'(\eta)$, in relation to several physical parameters such as the magnetic field parameter (M), volume fractions (ϕ_1, ϕ_2), Maxwell's parameter (β) , porosity parameter (K_1) and the suction/injection parameter (S).

Figure 4.3 illustrates the influence of the suction/injection parameter (S) on the velocity profile $f'(\eta)$ for magnetic parameter $M = 0.1$ and $M = 1.0$. It is observed that the suction/injection

parameter (S) directly contribute to a reduction in the velocity profile. With higher values of S, there is a decrease in both the velocity profile and the boundary layer thickness across the full extent of the boundary layer. Physically, an increase in S results in a greater removal of fluid, which reduces the fluid's momentum near the surface and consequently lowers the overall speed. Additionally, it is noted that the elevated values of the magnetic parameter (M) diminish the velocity of the hybrid nanofluid throughout the flow domain. This reduction is attributed to the Lorentz force, which acts perpendicular to the applied magnetic field and opposes the fluid's motion.

Figure 4.4 demonstrates the compelling results of the velocity profile for stretching/shrinking sheet scenarios. The observations indicate that by positively varying the titanium dioxide volume fraction (ϕ_1), the velocity distribution decreases for the shrinking sheet ($\lambda = -1.0$), whereas it shows an entirely opposite behavior in the case of the stretching sheet ($\lambda = 1.0$).

Figure 4.5 illustrates the velocity distribution as a function of the volume fraction of iron oxide (ϕ_2). By comparing figures 4.4 and 4.5, it is clearly observed that the velocity distribution is significantly affected in the same manner by changes in the volume fraction of both the titanium dioxide (ϕ_1) and iron oxide (ϕ_2). However, it can be observed through these two figures that the velocity profile is more sensitive to the variation in titanium dioxide nanoparticles' volumne fraction ϕ_1 as compared to that due to ϕ_2.

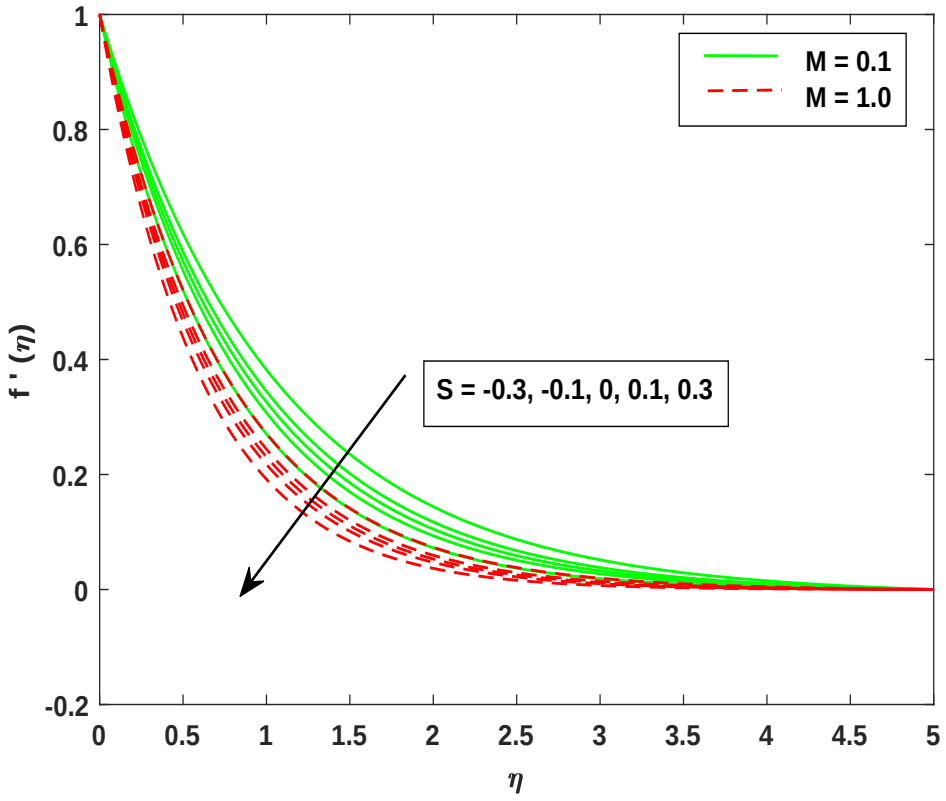

FIGURE 4.3: The distribution of velocity across S when M=1.0 and $M = -1.0$, ϕ_1 =0.01, $\phi_2 = 0.1$, $\lambda = 1.0$, S = 2.0, $\beta = K_1 = 0.01$.

The illustration in Figure 4.6 demonstrates that an enhancement in the Maxwell parameter leads to a noticeable reduction in the velocity profile $f'(\eta)$. Physically, this means that the viscoelastic nature of the fluid creates additional internal resistance during flow. Consequently, the fluid's velocity is reduced as molecular formations develop due to its viscoelastic properties. However, an increment in the porosity parameter (K_1) results in a decline of velocity. In a medium with greater porosity, the larger number of voids raises the resistance, causing a decrease in velocity.

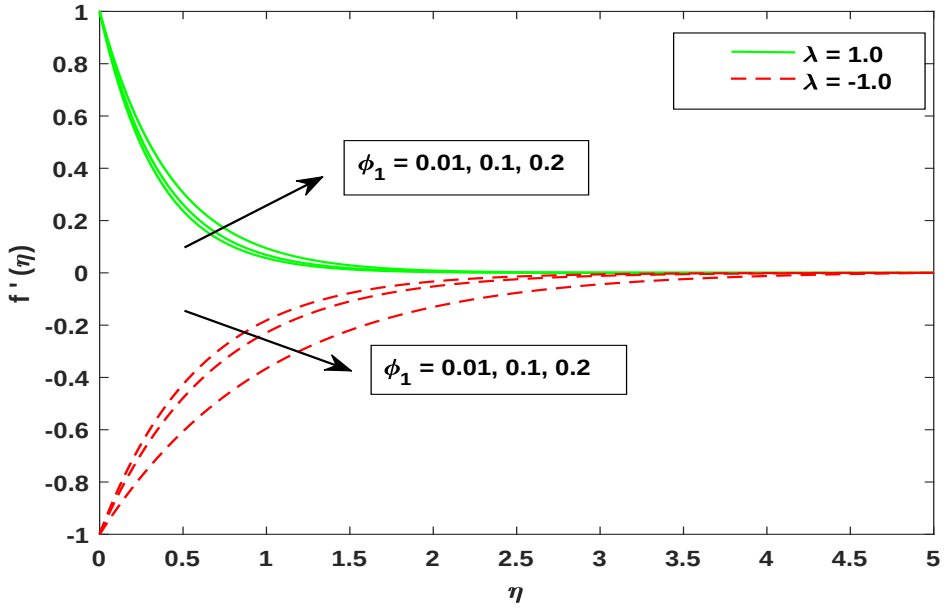

FIGURE 4.4: The distribution of velocity across ϕ_1 when $\lambda = 1.0$ and $\lambda = -1.0$, $\phi_2 = 0.1$, S $= 2.0$, $M = 0.1$, $\beta = K_1 = 0.01$.

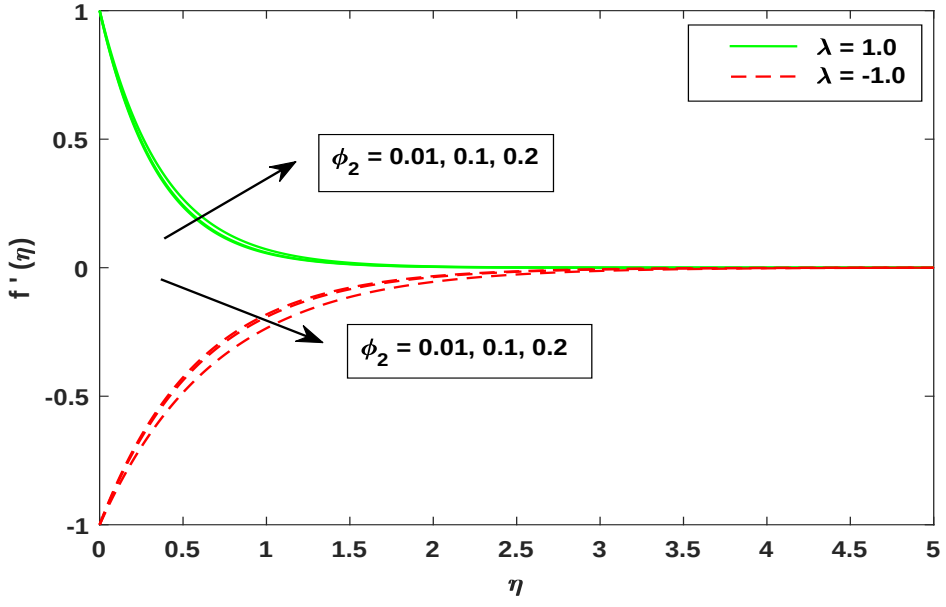

FIGURE 4.5: The distribution of velocity across ϕ_2 when $\lambda = 1.0$ and $\lambda = -1.0$, $\phi_1 = 0.1$, S $= 2.0$, $\lambda = 1.0$, M $= 0.1$, $\beta = K_1 = 0.01$.

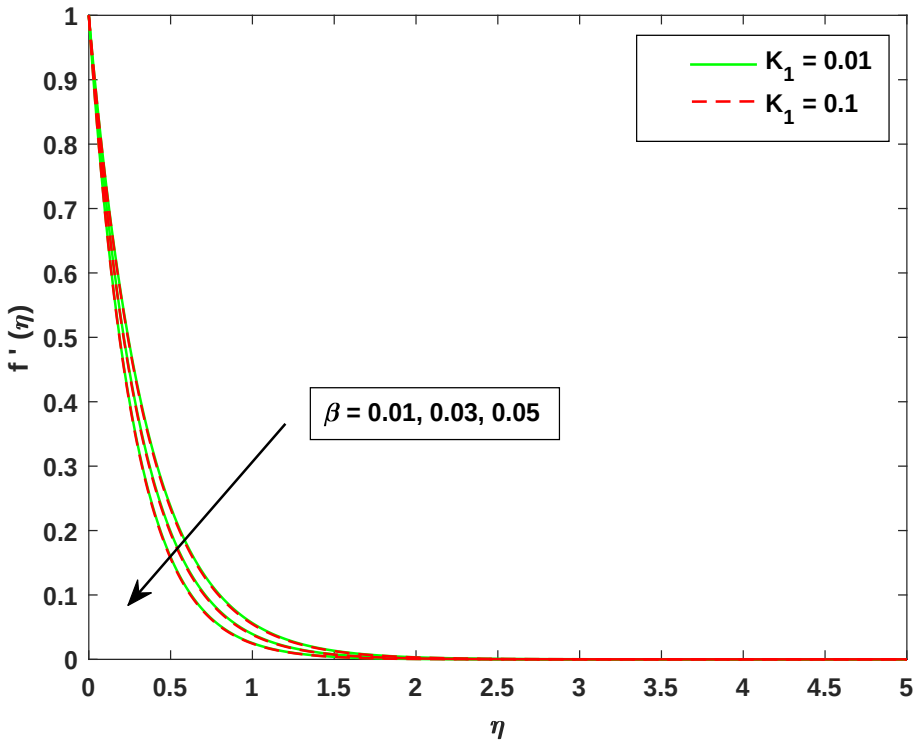

FIGURE 4.6: The distribution of velocity across β when $K_1 = 0.01$ and $K_1 = 0.1$, $\phi_1 = 0.01$, $\phi_2 = 0.1$, S = 2.0, $\lambda = 1.0$, M = 0.1.

4.5.3 Temperature Profile

The temperature distribution $\theta(\eta)$ is presented in figures 4.7 to 4.13, reflecting the significant influence of various thermophysical parameters, including the Prandtl number (Pr), radiation parameter (R), Eckert number (Ec), Cattaneo-Christov parameter (δ) , magnetic parameter (M), volume fractions (ϕ_1, ϕ_2), thermal Slip parameter (γ), heat source parameter (Q) and the suction/injection parameter (S) on the fluid motion, across a stretching or shrinking sheet.

The findings depicted in Figure 4.7 suggest that a greater thermal slip results in lower temperature, while a higher volume fraction contributes to the increased temperatures. This illustrates that an enhanced thermal slip significantly improves the transport of thermal power, especially as the volume fraction of the medium increases. The slip factor, whether concerning velocity or temperature, results from the fluid's thinness. Thus, an noticeable rise in the volume of nanoparticles, which signifies a greater concentration, leads to a rise in the temperature associated with higher values of (ϕ_1), whereas it decreases in response to the thermal slip parameter γ.

The data presented in Figure 4.8 demonstrates that temperature increase for increasing values of the volume fractions (ϕ_2) for iron oxide, Whereas an opposite trend is observed for the thermal slip parameter γ. The thermal slip phenomenon is attributed to the imperfect thermal interaction

occurring between a fluid and a solid surface, leading to a reduced temperature within the boundary layer.

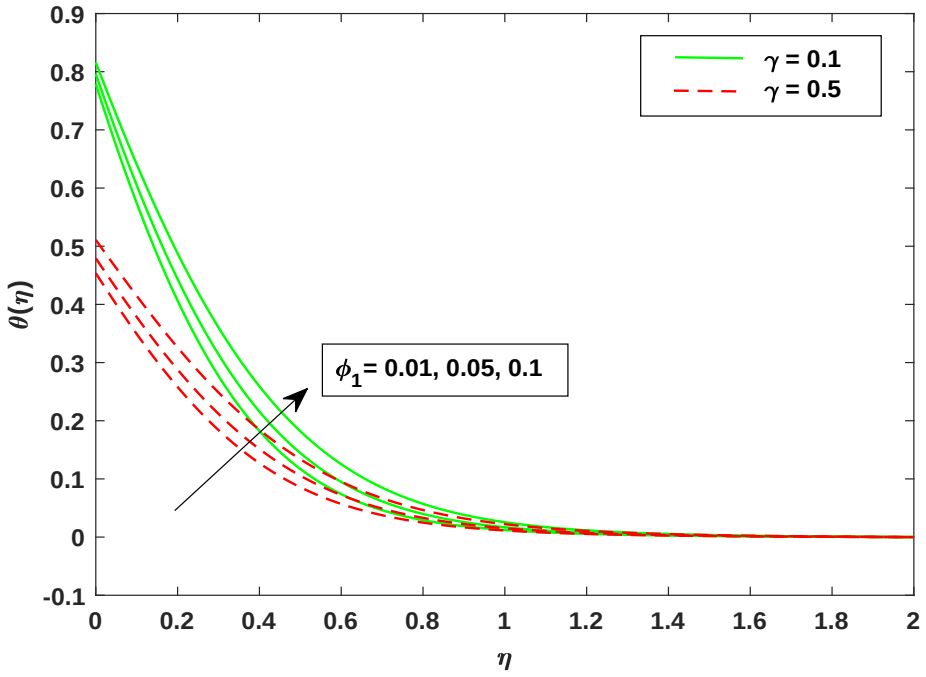

FIGURE 4.7: The distribution of temperature across ϕ_1 when $\gamma = 0.1$ and $\gamma = 0.5$, $\phi_2 = 0.1$, $S = 0.5$, $\lambda = 1.0$, $M = E_c = \delta = Q = R$=0.1, $P_r = 6.2$, $\beta = K_1 = 0.01$.

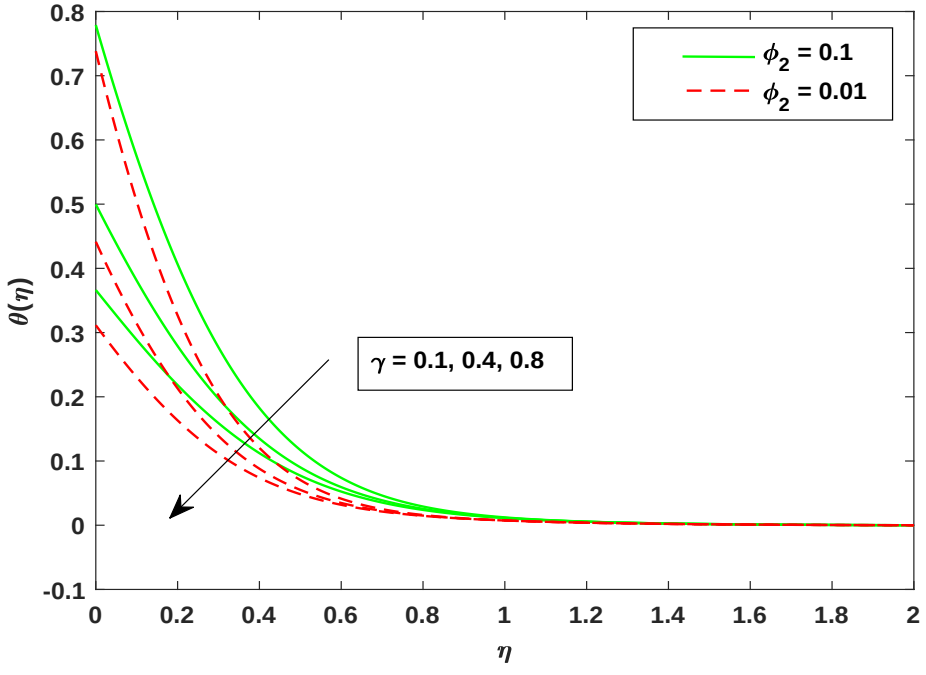

FIGURE 4.8: The distribution of temperature across γ when $\phi_2 = 0.1$ and $\phi_2 = 0.01$, $\phi_1 = 0.01$, S $= 0.5$, $\lambda = 1.0$, M $= E_c =$ Q$=$ R $= \delta = 0.1$, $P_r = 6.2$, $\beta = K_1 = 0.01$.

It is depicted in Figure 4.9 that there is a notable increase in temperature corresponding to higher values of the magnetic parameter (M). Additionally, the temperature continues to rise with elevated values of E_c, which serves as an indicator of frictional heat and the heat contributed by viscous dissipation.

Figure 4.10 demonstrates that a contracting bounding surface ($\lambda < 0$) results in an elevated temperature at all measured points as compared with that for a stretching surface ($\lambda > 0$). The transport of thermal energy within fluid layers is further improved with rising values of the radiation parameter R continue to increase. Figure 4.11 illustrates a consistent decrease in temperature throughout the flow field, with an increased suction observed at the plate.

Figure 4.12 presents the notable influence of δ on the temperature distribution $\theta(\eta)$. When δ=0, the model simplifies to the Fourier's law. An extension of the classical Fourier heat conduction law is proposed, which incorporates a relaxation time parameter to account for an increase in the heat propagation, enabling a more realistic modeling of thermal transport phenomena. The figure shows that the thickness of temperature boundary layer increases as δ rises. In addition, it illustrates that an increase in β corresponds to a higher temperature.

In Figure 4.13, it is evident that an enhancement in the porosity parameter K_1 causes the heat to rise. A porous medium is a material that possesses a network of interconnected pores or spaces within its solid framework, permitting the transmission of fluids or gases. The porosity of a medium has a dual impact on heat transfer rates. Higher porosity promotes heat transfer by increasing fluid penetration and surface area, while a thicker porous layer impedes heat transfer due to increased flow resistance and decreased contact area.

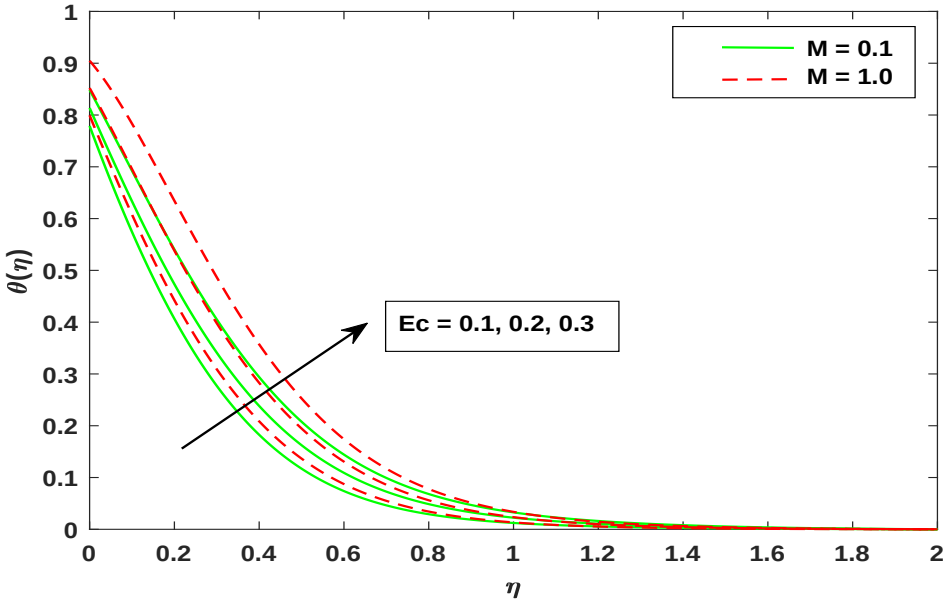

FIGURE 4.9: The distribution of temperature across E_c when M = 0.1 and M = 1.0, $\phi_1 = 0.01$,$\phi_2 = 0.1$, S = 0.5, $\lambda = 1.0$, γ = Q= R = $\delta = 0.1$, $P_r = 6.2$, $\beta = K_1 = 0.01$.

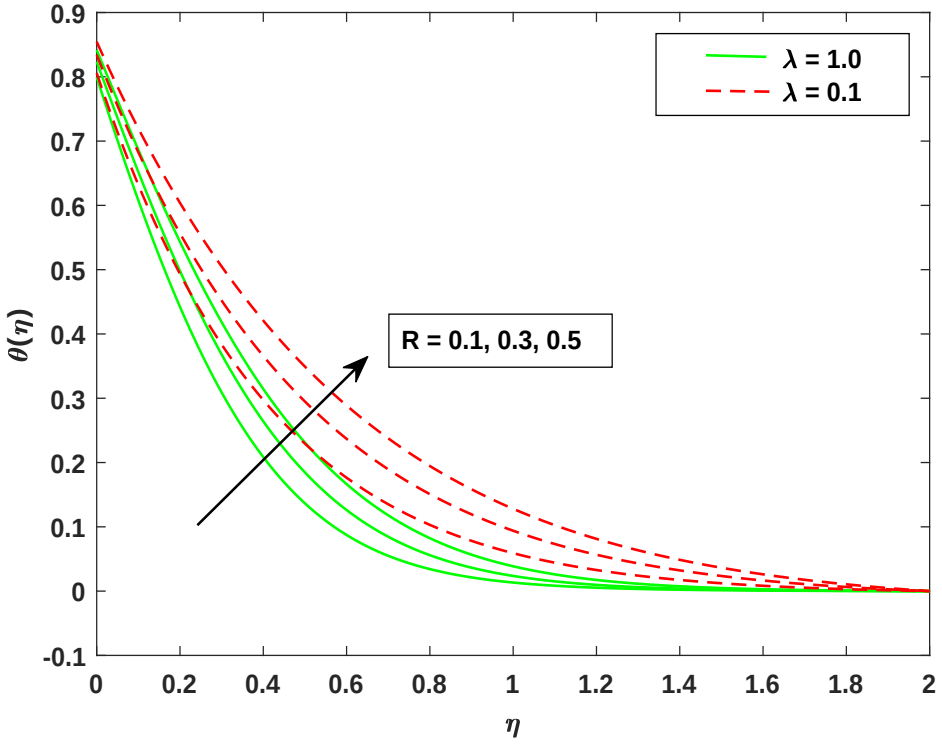

FIGURE 4.10: The distribution of temperature across R when $\lambda = 1.0$ and $\lambda = 0.1$, $\phi_1 = 0.01$,$\phi_2 = 0.1$, S $= 0.5$, M $= 1.0$, $\gamma =$ Q $= \delta = E_c = 0.1$, $P_r = 6.2$, $\beta = K_1 = 0.01$.

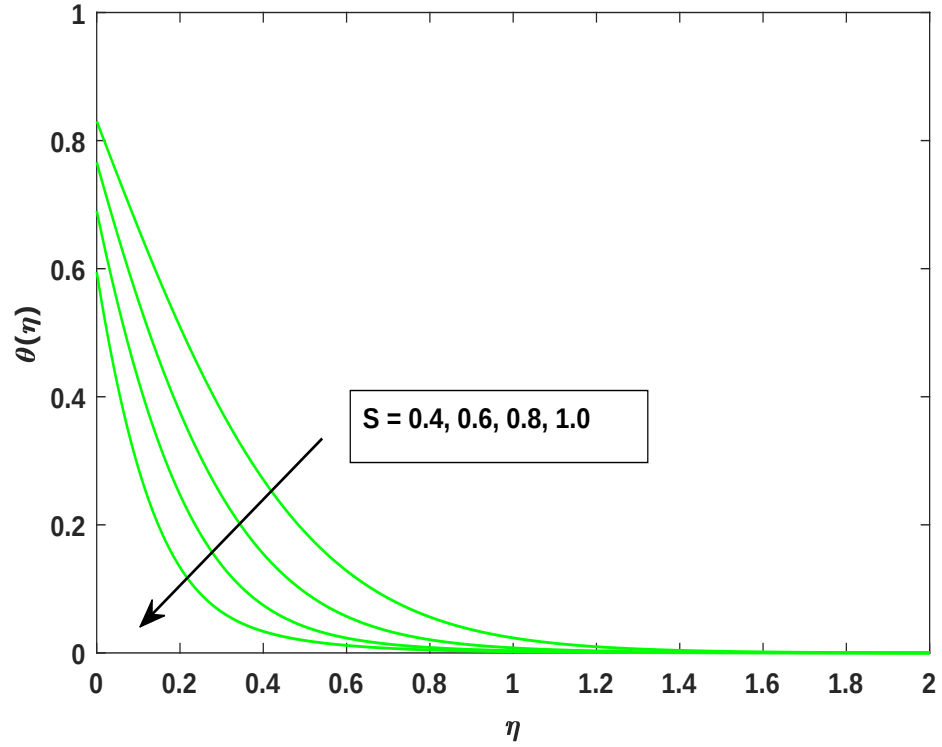

FIGURE 4.11: The distribution of temperature across S when $\phi_1 = 0.01$, $\phi_2 = 0.1$, M $= \lambda = 1.0$, R $= \gamma =$ Q $= \delta = E_c = 0.1$, $P_r = 6.2$, $\beta = K_1 = 0.01$.

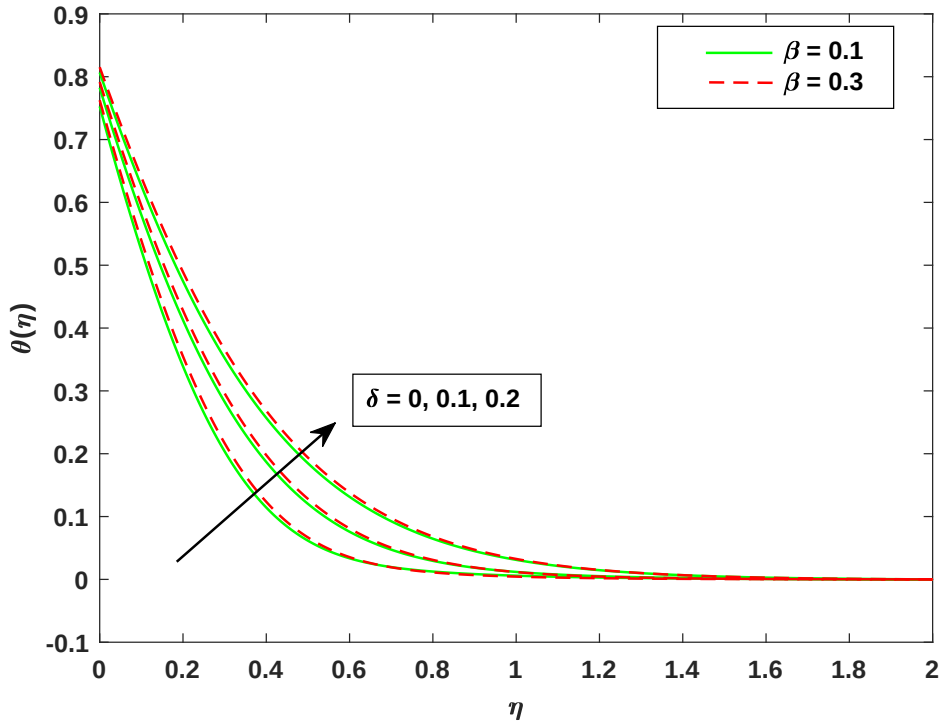

FIGURE 4.12: The distribution of temperature across δ when $\beta = 0.1$ and $\beta = 0.3$, $\phi_1 = 0.01$,$\phi_2 = 0.1$, S $= 0.5$, M $= 1.0$, $\gamma =$ Q$=$ R $= E_c = 0.1$, $P_r = 6.2$, $K_1 = 0.01$.

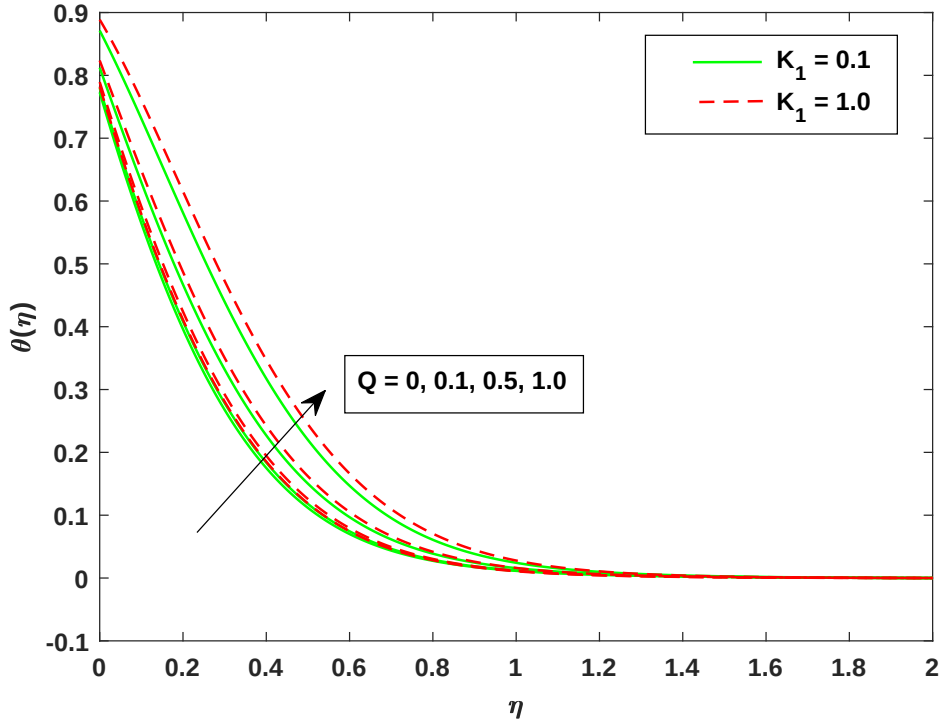

FIGURE 4.13: The distribution of temperature across Q when $K_1 = 0.1$ and 1.0, $\phi_1 = 0.01$,$\phi_2 = 0.1$, S $= 0.5$, M $= 1.0$, $\gamma = \delta =$ R $= E_c = 0.1$, $P_r = 6.2$, $\beta = 0.01$.

4.5.4 Analysis of the Concentration Profile

The nanoparticle concentration in the fluid is a vital determinant of the fluid's properties and its applicability. In particular, nanoparticle-concentration has a profound impact on the thermal and electrical conductivity of nanofluids. Figures 4.14 to 4.17 demonstrate that the concentration distribution of hybrid nanofluid, highlighting the influences of Le, Nt, Γ and Nb.

The movement of small particles in a fluid is influenced by Brownian motion, which arises from the interactions between the particles and the surrounding fluid molecules. The findings illustrated in Figure 4.14 demonstrate that an increase in the Brownian parameter (Nb) leads to an enhancement in concentration profile. Furthermore, an increase in the Lewis number (Le) also causes an enhancement in concentration profile. Although, the Brownian motion does not directly alter the Lewis number, its impact on the transport coefficients can lead to apparent changes in Lewis number behavior, influencing the system's heat and mass transfer characteristics. From a physical perspective, as Nb increases, the random acceleration decreases, which enhances the movement of fluid particles from higher to lower regions.

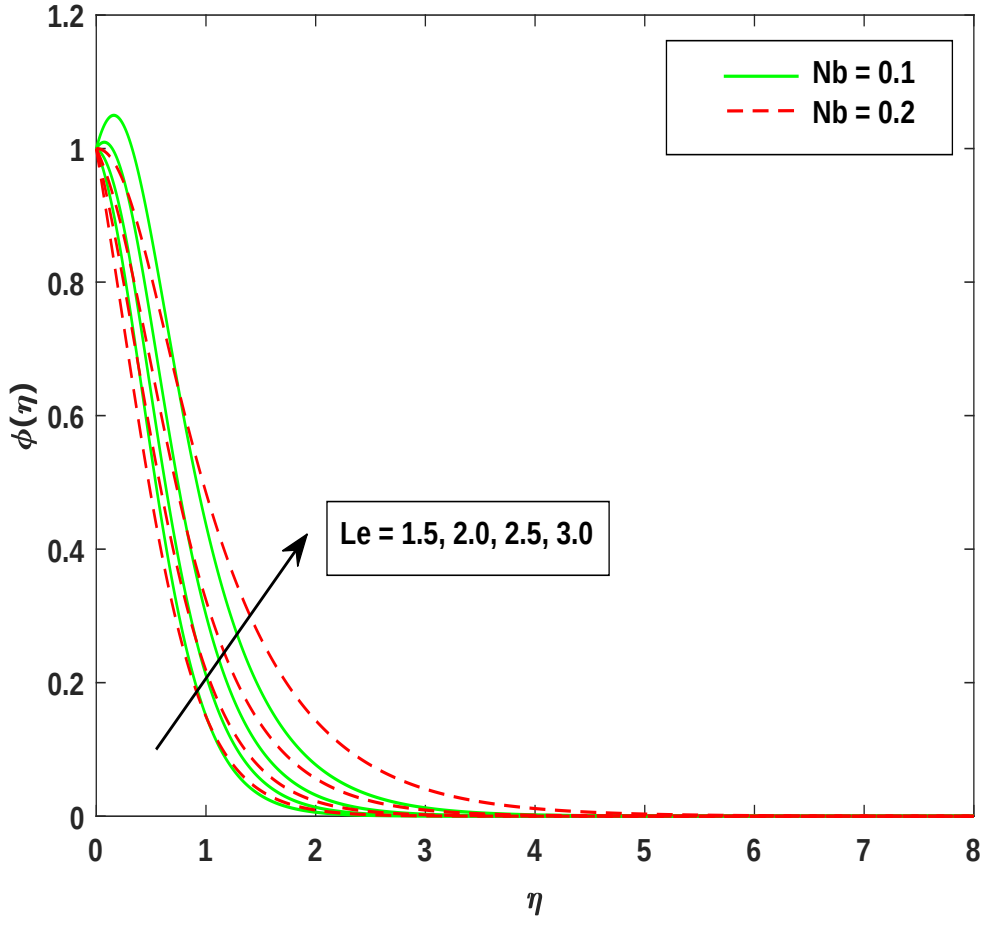

FIGURE 4.14: The distribution of Concentration across Le when $Nb = 0.1$ and $Nb = 0.2$, $\phi_1 = 0.01$,$\phi_2 = 0.1$, $S = 0.5$, $M = \lambda = 1.0$, $\gamma = Q = \delta = R = E_c = 0.1$, $P_r = 6.2$, $\beta = K_1 = 0.01$, $Nt = Nb = \Gamma = 0.1$.

Figure 4.15 indicates that an increase in the thermophoresis parameter (Nt) is associated with a rise in the concentration profile. Thermophoresis is the process by which particles in a fluid are transported from a region of relatively higher temperature to a region of comparatively lower temperature. Increased Brownian motion induces a higher degree of particle fluctuations, resulting in the creation of a concentrated layer near the surface, as seen in Figure 4.15.

As depicted in Figure 4.16, a rise in the Lewis number (Le) results in a decline in the concentration profile. The Lewis number (Le) is a dimensionless parameter that quantifies the ratio of thermal diffusivity to mass diffusivity, describing the interplay between heat and mass transfer in fluid flow. By increasing the thermophoresis parameter (Nt) the more fluctuation become occur and results in a reduction of concentration profile.

Furthermore, Figure 4.17 demonstrates that an increase in the porosity parameter (K_1) enhances the concentration profile. By increasing the chemical reaction parameter (Γ) more fluctuation occur which enhances the boundary layer of concentration profile. A chemical reaction parameter is a defined variable that impacts the reaction rate, mechanism, or outcome. The porosity of a medium has a direct impact on the rate of chemical reaction, as a higher porosity provides more surface area for reactants to interact, leading to increased reaction rates.

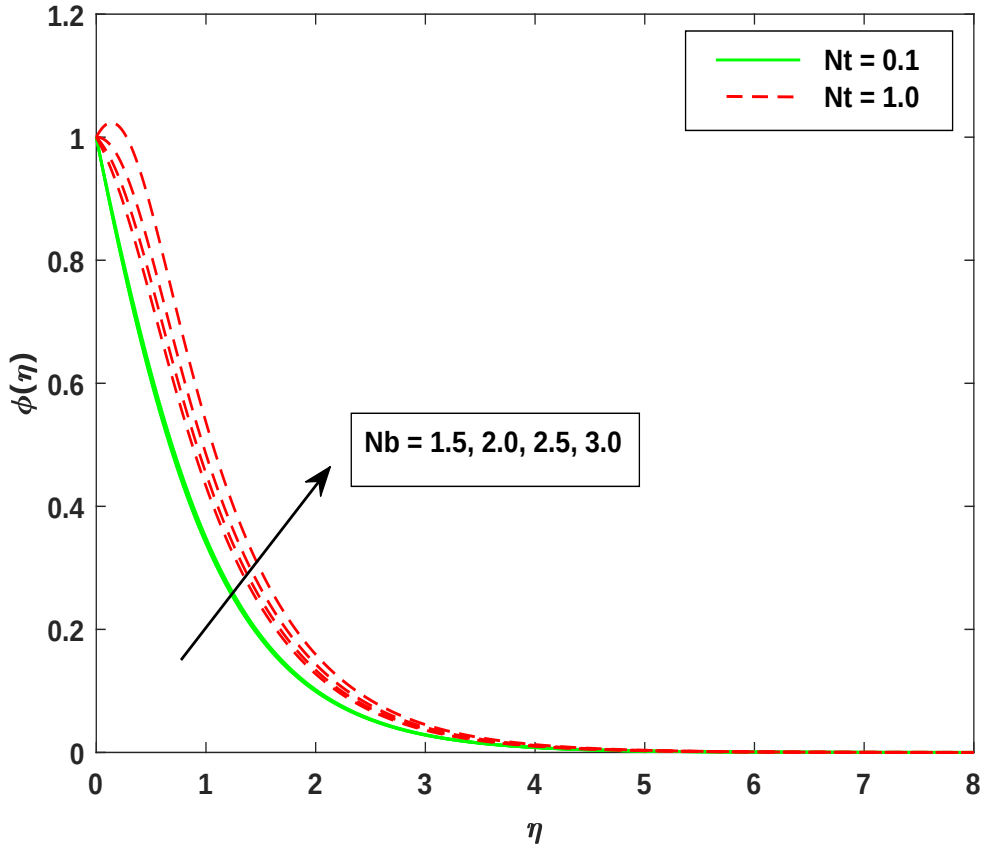

FIGURE 4.15: The distribution of Concentration across Nb when $Nt = 0.1$ and 1.0, $\phi_1 = 0.01$,$\phi_2 = 0.1$, $S = 0.5$, $M = \lambda = 1.0$, $\gamma = Q = \delta = R = E_c = 0.1$, $P_r = 6.2$, $\beta = K_1 = 0.01$, $Nt = \Gamma = 0.1$ and $Le = 1.0$.

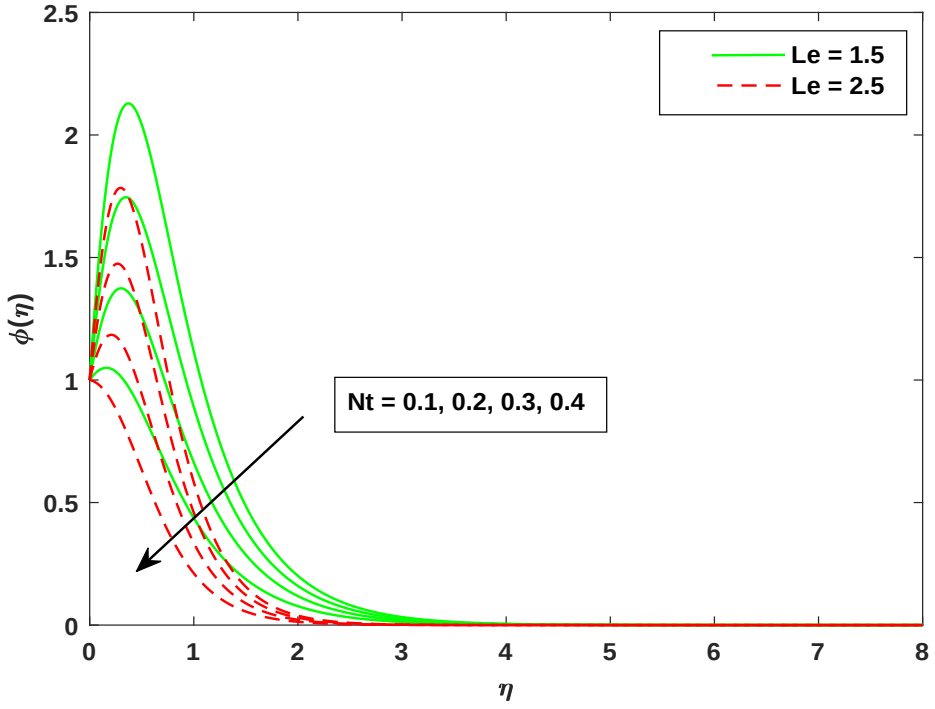

FIGURE 4.16: The distribution of Concentration across Nt when $Le = 1.5$ and 2.5, $\phi_1 = 0.01$, $\phi_2 = 0.1$, $S = 0.5$, $M = 0.1$, $\lambda = 1.0$, $\gamma = Q = \delta = R = E_c = 0.1$, $P_r = 6.2$, $\beta = K_1 = 0.01$, $Nb = \Gamma = 0.1$.

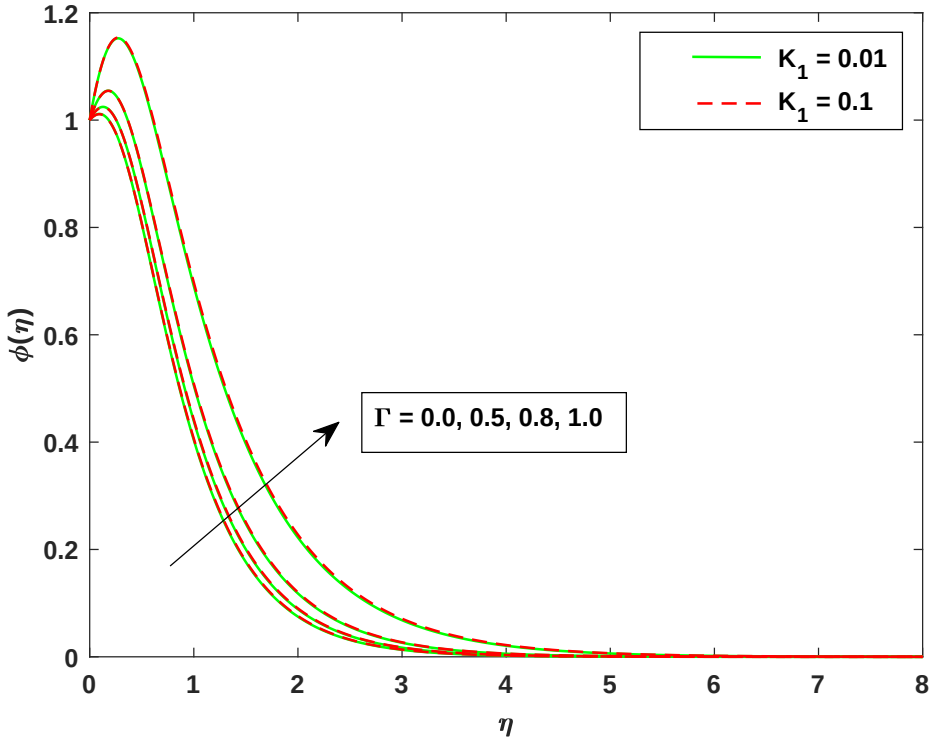

FIGURE 4.17: The distribution of Concentration across Γ when $K_1 = 0.01$ and 0.1, $\phi_1 = 0.01$,$\phi_2 = 0.1$, $S = 0.5$, $M = 0.1$, $\lambda = Le = 1.0$, $\gamma = Q = \delta = R = E_c = 0.1$, $P_r = 6.2$, $\beta = 0.01$, $Nb = Nt = 0.1$.

Chapter 5

Conclusions

This thesis presents a thorough examination of the effects of physical parameters on the velocity, temperature, and concentration profiles of nanofluids in a two-fluid system, specifically focusing on (TiO_2/H_2O) and hybrid nanofluid $(TiO_2 + Fe_3O_4/H_2O)$. The parameters examined include the magnetic field (M), volume fractions (ϕ_1, ϕ_2), Maxwell's parameter (β), porosity medium (K_1), suction/injection parameter (S), heat source parameter (Q), radiation parameter(R), Eckert number (Ec), Cattaneo–Christov parameter (δ), thermal slip parameter (γ), thermophoresis parameter (Nt), Brownian motion (Nb), Lewis number (Le), chemical reaction parameter (Γ) across stretching/shrinking sheet $(\lambda < 0, \lambda > 0)$. The main outcomes of this study are:

- Increased in magnetic field the fluid, velocity dimishes due to Lorentz force while increased in magnetic filed results in a greater temperature distribution.

- When volume fraction of titanium dioxide is increased, there is a corresponding rise in skin friction. This observation is consistent with the boundary layer thinning progression that occurs with an increase in ϕ_1, the volume fraction of titanium dioxide.

- Increasing the thermal slip causes a decline in temperature distribution, while a higher volume fraction leads to an augmentation of it. Hence, it is important to regulate thermal slip to enhance the efficiency of thermal energy transport.

- When we increase the Maxwell's parameter β and porosity parameter K_1, a reduction in the velocity is observed.

- An increase in the Cattaneo-Christov heat flux model δ leads to an elevation in the temperature profile, while a decrease in this parameter results in a lower Nusselt number.

- Moreover, enhancing the parameters linked to Brownian motion (Nb) and chemical reactions (Γ) leads to a noticeable rise in the concentration levels.

- As the Lewis number (Le) and thermophoresis parameter (Nt) increase, the concentration profile shifts upward.

Bibliography

[1] H. Brinkman, "Heat effects in capillary flow i," *Applied Scientific Research*, vol. 2, pp. 120–124, 1951.

[2] A. Tassaddiq, I. Amin, M. Shutaywi, Z. Shah, F. Ali, S. Islam, and A. Ullah, "Thin film flow of couple stress magneto-hydrodynamics nanofluid with convective heat over an inclined exponentially rotating stretched surface," *Coatings*, vol. 10, no. 4, p. 338, 2020.

[3] T. S. Kumar, "Hybrid nanofluid slip flow and heat transfer over a stretching surface," *Partial Differential Equations in Applied Mathematics*, vol. 4, p. 100070, 2021.

[4] A. Asghar, A. F. Chandio, Z. Shah, N. Vrinceanu, W. Deebani, M. Shutaywi, and L. A. Lund, "Magnetized mixed convection hybrid nanofluid with effect of heat generation/absorption and velocity slip condition," *Heliyon*, vol. 9, no. 2, 2023.

[5] S. Zafar, A. A. Khan, S. M. Sait, and R. Ellahi, "Numerical investigation on unsteady compressible flow of viscous fluid with convection under the effect of Joule heating," *Journal of Computational Applied Mechanics*, 2024.

[6] Y. Ouyang, M. F. M. Basir, K. Naganthran, and I. Pop, "Dual solutions in Maxwell ternary nanofluid flow with viscous dissipation and velocity slip past a stretching/shrinking sheet," *Alexandria Engineering Journal*, vol. 105, pp. 437–448, 2024.

[7] A. Ullah, H. Yao, F. Ullah, W. Khan, H. Gul, F. A. Awwad, and E. A. Ismail, "Viscous dissipation and Joule heating effects on the unsteady micropolar fluid flow past a horizontal surface of revolution," *Alexandria Engineering Journal*, vol. 94, pp. 159–171, 2024.

[8] N. B. Khedher, Z. Ullah, M. Alturki, C. R. Mirza, and S. M. Eldin, "Effect of Joule heating and mhd on periodical analysis of current density and amplitude of heat

transfer of electrically conducting fluid along thermally magnetized cylinder," *Ain Shams Engineering Journal*, vol. 15, no. 2, p. 102374, 2024.

[9] S. U. Choi and J. A. Eastman, "Enhancing thermal conductivity of fluids with nanoparticles," tech. rep., Argonne National Lab.(ANL), Argonne, IL (United States), 1995.

[10] J. Buongiorno, "Convective transport in nanofluids," 2006.

[11] R. K. Tiwari and M. K. Das, "Heat transfer augmentation in a two-sided lid-driven differentially heated square cavity utilizing nanofluids," *International Journal of Heat and Mass Transfer*, vol. 50, no. 9-10, pp. 2002–2018, 2007.

[12] T. Hayat, M. I. Khan, M. Farooq, T. Yasmeen, and A. Alsaedi, "Water-carbon nanofluid flow with variable heat flux by a thin needle," *Journal of Molecular Liquids*, vol. 224, pp. 786–791, 2016.

[13] M. Karim, S. Huq, A. Azad, M. Chowdhury, and M. Rahman, "Numerical analysis of thermofluids inside a porous enclosure with partially heated wall," *International Journal of Thermofluids*, vol. 11, p. 100099, 2021.

[14] G. G. Momin, "Experimental investigation of mixed convection with water-Al_2O_3 & hybrid nanofluid in inclined tube for laminar flow," *International Journal of Scientific and Technology Research*, vol. 2, no. 12, pp. 195–202, 2013.

[15] N. A. C. Sidik, I. M. Adamu, M. M. Jamil, G. Kefayati, R. Mamat, and G. Najafi, "Recent progress on hybrid nanofluids in heat transfer applications: a comprehensive review," *International Communications in Heat and Mass Transfer*, vol. 78, pp. 68–79, 2016.

[16] I. Waini, U. Khan, A. Zaib, A. Ishak, and I. Pop, "Thermophoresis particle deposition of $CoFe_2O_4 - TiO_2$ hybrid nanoparticles on micropolar flow through a moving flat plate with viscous dissipation effects," *International Journal of Numerical Methods for Heat & Fluid Flow*, vol. 32, no. 10, pp. 3259–3282, 2022.

[17] U. Mahabaleshwar, A. Vishalakshi, and H. I. Andersson, "Hybrid nanofluid flow past a stretching/shrinking sheet with thermal radiation and mass transpiration," *Chinese Journal of Physics*, vol. 75, pp. 152–168, 2022.

[18] T. Hayat, A. Razaq, S. A. Khan, and A. Alsaedi, "An induced magnetic field utilization for hybrid nanoliquid flow subject to entropy generation," *Journal of Magnetism and Magnetic Materials*, vol. 576, p. 170742, 2023.

[19] K. U. Rahman, Z. Mahmood, S. U. Khan, A. Ali, Z. Li, and I. e. a. Tlili, "Enhanced thermal study in hybrid nanofluid flow in a channel motivated by graphene/Fe_3O_4 and Newtonian heating," *Results in Engineering*, vol. 21, p. 101772, 2024.

[20] A. Jan, M. Mushtaq, and M. Hussain, "Heat transfer enhancement of forced convection magnetized cross model ternary hybrid nanofluid flow over a stretching cylinder: non-similar analysis," *International Journal of Heat and Fluid Flow*, vol. 106, p. 109302, 2024.

[21] B. Singh and S. Sood, "Hybrid nanofluids preparation, thermo-physical properties, and applications: A review," *Hybrid Advances*, p. 100192, 2024.

[22] A. Al-Hadhrami, L. Elliott, and D. Ingham, "A new model for viscous dissipation in porous media across a range of permeability values," *Transport in Porous Media*, vol. 53, pp. 117–122, 2003.

[23] D. Bhukta, G. Dash, and S. Mishra, "Heat and mass transfer on mhd flow of a viscoelastic fluid through porous media over a shrinking sheet," *International Scholarly Research Notices*, vol. 2014, no. 1, p. 572162, 2014.

[24] M. Sheikholeslami, Z. Ziabakhsh, and D. Ganji, "Transport of magnetohydrodynamic nanofluid in porous media," *Colloids and Surfaces A: Physicochemical and Engineering Aspects*, vol. 520, pp. 201–212, 2017.

[25] P. Jordan, A. Puri, and G. Boros, "On a new exact solution to stokes' first problem for Maxwell fluids," *International Journal of Non-Linear Mechanics*, vol. 39, no. 8, pp. 1371–1377, 2004.

[26] J. Zierep and C. Fetecau, "Energetic balance for the Rayleigh–Stokes problem of a Maxwell fluid," *International Journal of Engineering Science*, vol. 45, no. 2-8, pp. 617–627, 2007.

[27] M. Jamil, C. Fetecau, and C. Fetecau, "Unsteady flow of viscoelastic fluid between two cylinders using fractional Maxwell model," *Acta Mechanica Sinica*, vol. 28, pp. 274–280, 2012.

[28] A. Sohail, D. Vieru, and M. Imran, "Influence of side walls on the oscillating motion of a Maxwell fluid over an infinite plate," *Mechanics*, vol. 19, no. 3, pp. 269–276, 2013.

[29] D. Vieru and A. A. Zafar, "Some Couette flows of a Maxwell fluid with wall slip condition," *Applied Mathematics and Information Sciences*, vol. 7, pp. 209–219, 2013.

[30] C. Cattaneo, "Sulla conduzione del calore," *Atti del Seminario Matematico e Fisico dell'Universita di Modena*, vol. 3, pp. 83–101, 1948.

[31] C. Christov, "On frame indifferent formulation of the Maxwell–Cattaneo model of finite-speed heat conduction," *Mechanics Research Communications*, vol. 36, no. 4, pp. 481–486, 2009.

[32] J. Ahmad Khan, M. Mustafa, T. Hayat, and A. Alsaedi, "Numerical study of Cattaneo-Christov heat flux model for viscoelastic flow due to an exponentially stretching surface," *PLOS One*, vol. 10, no. 9, p. e0137363, 2015.

[33] S. Saleem, M. Awais, S. Nadeem, N. Sandeep, and M. Mustafa, "Theoretical analysis of upper-convected Maxwell fluid flow with Cattaneo–Christov heat flux model," *Chinese Journal of Physics*, vol. 55, no. 4, pp. 1615–1625, 2017.

[34] M. G. Reddy, M. S. Rani, K. G. Kumar, B. Prasannakumar, and H. Lokesh, "Hybrid dusty fluid flow through a Cattaneo–Christov heat flux model," *Physica A: Statistical Mechanics and its Applications*, vol. 551, p. 123975, 2020.

[35] H. Waqas, U. Farooq, D. Liu, M. Imran, T. Muhammad, A. S. Alshomrani, and M. Umar, "Comparative analysis of hybrid nanofluids with Cattaneo-Christov heat flux model: A thermal case study," *Case Studies in Thermal Engineering*, vol. 36, p. 102212, 2022.

[36] R. Rajput, *A Textbook of Fluid Mechanics and Hydraulic Machines.* S. Chand Publishing, 2004.

[37] R. Bansal, *A Textbook of Fluid Mechanics.* Firewall Media, 2005.

[38] S. Som, *Introduction to Heat Transfer.* PHI Learning Pvt. Ltd., 2008.

[39] J. N. Reddy and D. K. Gartling, *The Finite Element Method in Heat Transfer and Fluid Dynamics.* CRC press, 2010.

[40] J. Kunes, *Dimensionless Physical Quantities in Science and Engineering*. Elsevier, 2012.

[41] S. Mishra, K. Swain, and R. Dalai, "Joule heating and Viscous dissipation effects on heat transfer of hybrid nanofluids with thermal slip," *Iranian Journal of Science and Technology, Transactions of Mechanical Engineering*, vol. 48, no. 2, pp. 531–539, 2024.